University of Bath

UNIVERSITY OF BATH

PHD

Magneto-elastic processes in polycrystalline ferromagnets

Maylin, M. G.

Award date:
1994

Awarding institution:
University of Bath

[Link to publication](#)

Magneto-elastic processes in polycrystalline ferromagnets

submitted by M G Maylin
for the degree of PhD
of the University of Bath
1994

COPYRIGHT

UMI Number: U602185

Dissertation Publishing

CONTENTS PAGE

ACKNOWLEDGEMENTS

For Luke, Rose and my parents.

PREFACE

The reader's attention is drawn to the following publications which arose as a direct consequence of work carried out in this study.

'The effects of stress on induction, differential permeability and Barkhausen count in a ferromagnet' *IEEE Trans. Mag. November 1993,* Maylin M G and Squire P T.

'Departures from the law of approach to the Principal anhysteretic in a ferromagnet' *J. Appl. Phys. 73, 6, p2948 (1993),* Maylin M G and Squire P T.

The reader's attention is also drawn to the following quotation:

"No part of our subject is more interesting than that which deals with the effects of mechanical stress in altering the susceptibility, the retentiveness, and other qualities of the three magnetic materials"

J A Ewing, 'Magnetic induction in iron and other metals' 3rd edition p393 (The Electrician, 1900).

1. Summary

The magnetic properties of several polycrystalline ferromagnetic materials have been investigated. Changing the external influences such as magnetic field, temperature and applied load within each specimen elastic limit has assisted in understanding the nature of the magneto-elastic interaction in each of the specimens examined. It is shown that there are shared characteristics in the magneto-elastic performance of the tested materials, such that their performance can be explained in terms of common processes.

The experimental observations are discussed in terms of existing theories and magnetic models. It is argued that these are presently not capable of describing the full range of behaviour in these materials. A tentative explanation for the discrepancies is described which may offer the possibility of revising or extending such models.

2. List of symbols and terminology.

2.1. Common symbols used in the thesis.

The symbols used in this thesis are those set out by the Royal Society (1975). When referring to work of other authors, symbols used in their original texts will be altered in order to maintain consistency with this convention.

B, B_s, B_r Magnetic induction, saturation and remanent values, in Tesla.

$\Delta B, \Delta B_{rev}, \Delta B_{irrev}$ Changes in magnetic induction. Reversible and irreversible values.

H, H_σ Applied magnetizing field and stress-induced effective field, in Amps per metre.

$\sigma^{+,-}$ Stress, tensile(+) and compressive(-), in MegaPascals.

λ, λ_s Magnetostriction, saturation magnetostriction.

$\mu, \mu_{rev}, \mu_{irrev}$ Differential permeability, reversible and irreversible components, defined as dB/dH, in Henries per metre.

μ_0 Permeability of free space ($4\pi \times 10^{-7}$ H/m)

T,ΔT	Temperature, changes in temperature, in Kelvin.
p,Δp	Pressure, changes in pressure, in Pascals.
V,ΔV	Volume, changes in volume, in cubic metres.
θ,ϕ	Angles between domain magnetization and applied field or stress, (degrees).
M	Magnetization in Amps per metre
$\chi,\chi_0,\chi_{rev,irrev}$	Susceptibility, initial, reversible and irreversible components, defined as dM/dH, therefore dimensionless.

Conversion factors:

The following conversion factors may be of assistance, as occasionally in the text, it

has been necessary to express concepts in the units used by previous workers:

Magnetic field:- 1 Oersted (c.g.s. unit) = 79.9 A/m (S.I. unit)

Magnetization:- 10^4 Gauss (c.g.s. unit) = 1 Tesla (S.I. unit)

2.2. Terminology.

A certain terminology developed during between 1940-1970, is commonly used in this subject area to denote magnetic processes. This has been used occasionally in the text and although the terms are reasonably self-explanatory for clarity, they are defined below.

H $\bar{\text{H}}$	the application then removal of a magnetizing field.
$\sigma^+ \bar{\sigma}^+$	the application and removal of tension.
$\sigma^- \bar{\sigma}^-$	the application and removal of compression.
H$^\sim$	application of cyclic field.
D	demagnetization through application of a decaying sinusoidal field.
$\sigma^\sim$	stress cycles
DH$\sigma^+ \bar{\sigma}^+$	a process wherein a specimen is initially demagnetized, subjected to an applied field, followed by a single tension cycle.

3. Introduction

The existence of an interaction between magnetic material strain and material magnetic induction has been known for some time. As early as 1842, Joule recorded the elongation of iron bars subjected to an increasing external magnetic field. The inverse relationship, namely that applied load could alter the magnetism of specimens, has been acknowledged for a similar time. Such effects remained of mostly academic interest until the construction of large ferromagnetic carbon-steel structures. Understanding the magnetic properties of ships, greatly influenced by constantly changing ambient fields and stresses, became important during the second world war because of their vulnerability to explosive mines. More recently, attention has been focused on the application of magnetic measurements as a non-destructive technique for the evaluation of stress levels in large structures, especially in the oil industry. Since the original recognition of the stress-magnetism interaction, an understanding of the active processes has been sought in terms of the known magnetic quantities and mechanisms of ferromagnetics. In this section, magnetic concepts relevant to this thesis will be described.

The primary motivation for this work is the need to understand the processes involved in the magnetic instability of constructional steel members. In particular, attention is focused on an alloy steel composition identified under the trade designation 'HY80', comprising 0.2% carbon, 3% nickel. It has not been the objective to draw up a detailed quantitative comparison between the magneto-elastic performance of this material with respect to any other carbon steels. Instead, the effort has been focused

on understanding the general processes at hand in stress-induced induction changes. It will be argued that such processes are not peculiar to any particular specimen or material type. It will be shown that the performance of a range of (polycrystalline) materials can be interpreted in terms of the same or similar mechanisms. In this work, as an aid to understanding these mechanisms, the magnetic properties of several polycrystalline materials are studied. It will be shown that trends in the magnetism-stress interaction are shared by these materials.

Central to this discussion is the concept of magnetostriction. As mentioned, the dimensions of a ferromagnet are seen to change when it is subjected to a change in applied field. The degree of change, that is, the change in specimen strain, is quantified in its magnetostriction constants. Cullity, (1972), identifies two main magnetostrictive effects for a specimen subjected to a changing external field:

(a)   Longitudinal magnetostriction, as commonly demonstrated by the fractional change in length of cylindrical specimens. This dimensional change is seen to occur for the modest fields required to bring a specimen to technical saturation.

(b)   Forced or volume magnetostriction, the continued distortion which occurs at large applied fields when a specimen is taken along its saturate line.

Of these it is the longitudinal magnetostriction which is relevant to this discussion. In referring to this quantity some confusion often arises through the assumed

interchangeability of the terms 'magnetostriction' and 'saturation magnetostriction', the latter quantity being the total strain in taking the specimen from a demagnetized state to magnetic saturation. In this work, care will be taken to distinguish between these two, and unless specified otherwise, the term 'magnetostriction' should be taken as the longitudinal strain associated with a precise applied field or specimen induction value. Because of the hysteretic nature of ferromagnetic materials, the magnetostriction will not be single-valued with field or stress, or field and stress combinations. In the examination of irons and steels, these considerations are of particular relevance. This is partly demonstrated through reference to figures 3.1a and b. In (a) the magnetostrictions along the three principal crystal directions for iron are shown as a function of magnetization from a demagnetized condition. Along an easy, cube edge direction, a parallel applied field will cause a monotonic increase in length. Across the body diagonal, the opposite case is encountered. In figure (b), the magnetostrictions as a function of field for isotropic polycrystalline specimens of the three ferromagnetic elements are shown. Nickel and cobalt demonstrate a monotonic contraction along the applied field axis. However, the performance of iron is complicated by the inversion of the net strain as a function of field, due to the conflicting behaviour of its randomly oriented crystals. It will be shown in subsequent sections that this behaviour can have a marked effect on iron-based specimens' magneto-elastic performance.
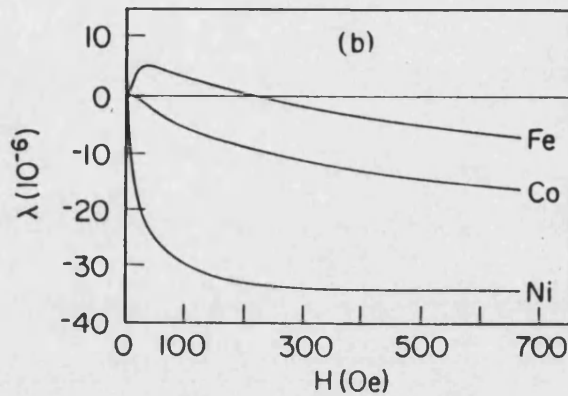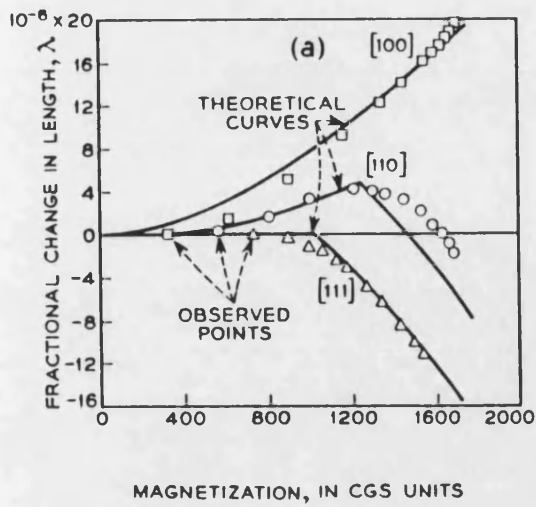
Figures 3.1 (a). (Left). The longitudinal magnetostrictions of iron along the principal crystal directions. (b). The net strain of ferromagnetic isotropic polycrystalline specimens. The inversion of specimen strain (contraction at higher fields) commonly demonstrated by iron-based polycrystalline materials should be noted. (Bozorth, 1951).

Early attempts (Brown, 1949) to explain stress-induced induction changes in specimens have been based solely on the magnetostrictive coupling between the magnetic moments and the crystal lattice. It will be shown in this work that such attempts are not successful for the magnetically complex polycrystalline specimens.

Specimen magnetism in this work is expressed in terms of its induction measured in Tesla's. Under the SI system

$$B = \mu_0 (H + M) \hspace{4cm} 3.1$$

where H, M and μ_0 are applied field, magnetization and permeability of free space (defined in chapter 2). Magnetic measurements on specimens, described in chapter 5, are taken by the inductive technique or 'ballistic' technique discussed in appendix B. Specimen permeability in this thesis is expressed as its 'differential' or 'incremental' value, that is the gradient of its induction-field profile at a precise field location. This is in contrast to the often quoted, dimensionless, 'relative' permeability. In reviewing the works of other authors their original choice of magnetic quantities has been maintained. The change in induction of a material subjected to a varying external influence such as changing field, temperature or load, is envisaged as taking place through magnetic moment rotation and 'domain wall' motion as described in modern magnetic texts (Jiles 1990, Cullity 1972). A domain wall is a boundary region within a magnetic specimen where the magnetic moments associated with each atom possess orientations which gradually change from parallelism to the net moment orientations in magnetic domains on each side of the boundary as a function of distance. This is best described figuratively in figure 3.2. As external mechanisms capable of influencing material magnetism are changed, a domain wall will shift its position rendering a change in macroscopically measured induction for the specimen. Impedances to domain wall motion in the form of 'pinning' sites as described by Néel (1946), are seen to contribute significantly to the hysteretic process as work has to be performed by the external influence to overcome such restrictions to induction change. Overcoming restrictions is considered to render an 'irreversible' change in the macroscopically measured magnetic induction as opposed to 'reversible' changes in which specimen magnetic induction is seen to

return to its initial value if the changing external influence does likewise. Implicit in the work presented here is that it is recognised that specimen magnetic induction changes take place through a combination of reversible and irreversible processes, often occuring simultaneously. How such changes are instigated by stress will become clear in later chapters.
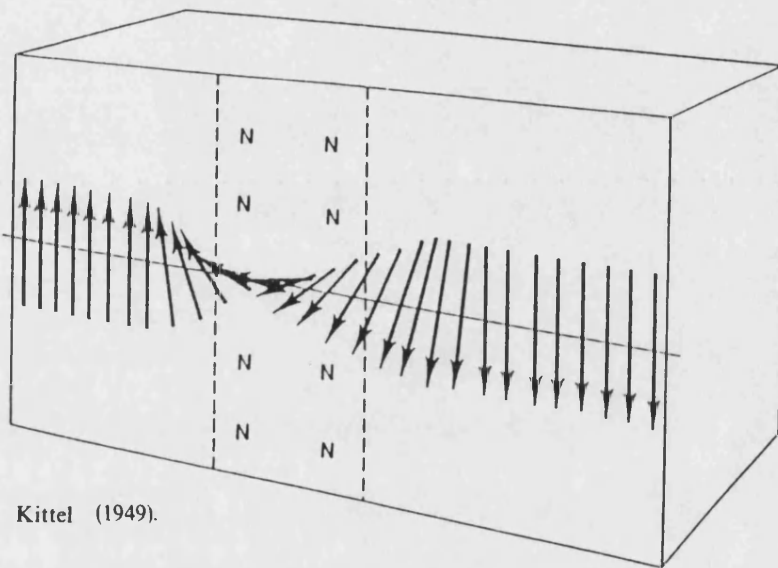
Kittel (1949).

Figure 3.2 The domain wall or boundary is a region where the moment vectors gradually change orientation from the net sense in each adjacent domain. Macroscopically measured specimen induction changes result from the movement of such boundaries through a magnetic material.

In the first part of this study, the work of other authors in the subject area is evaluated in order to provide a platform for the observations and arguments contained here. Experimentally obtained data is then presented and discussed. In the concluding chapters, a modification to the existing view of magneto-elastic processes is suggested and some ideas for future investigations put forward. This will hopefully provide future researchers with input to their own programmes.

4. Survey of progress

An understanding of the complex magneto-elastic behaviour of ferromagnetic polycrystalline materials has been sought since the reports of basic observations in the nineteenth century, (Joule 1842; Ewing 1891). Much of the work conducted in the subsequent decades has been detailed in the German reference text of Becker and Döring (1939), or alternatively the work, (in English), of Bozorth (1951). It is appropriate to base an analysis of modern progress in the area with the seminal work of W.F. Brown (1949). From this work, a chronological survey of developments in the field can be mapped out to the present day. Brown's work signalled the start of the development of theoretical models based on quantities directly related to physical variables such as magnetic susceptibility and the relative proportions of domain wall areas of different types that exist within a ferromagnetic specimen. Historically, investigation into stress-induced induction changes has often been associated with the requirement of gaining insight into the long and short-term magnetic instability of steel structures, especially maritime vessels, (Kittel,1946). The introduction of magnetic techniques for non-destructive evaluation, (N.D.E.), has ensured continued interest in this topic from an engineering view point. Considerable recent work has centred on the provision of an empirical model for stress-induced induction changes based on macroscopically derived quantities. It is hoped that such techniques will be directly applicable to analysis of the engineering data associated with the magnetic performance of structures.

Considering the case of uniaxial load and field applied to iron or steel rods, Brown explored the concept of stress acting as an additional pressure on domain walls in a ferromagnetic polycrystalline material. In this way its action can be equated to that of an additional magnetic field being applied. As such, its effect on specimen induction values is interpreted in terms of the Rayleigh formula, (see appendix C), which allows the shape of the stress-induced induction changes to be predicted in a simple parabolic way. For iron or steel specimens, with their cubic structure, the domain magnetizations lie in directions which are parallel to the cube edges. Domain boundaries in such a specimen separate regions where the domain vectors are perpendicular or anti-parallel, termed 90° and 180° walls. When stress is applied, there is a change in the free energy density, described to second order by,

$$E_\sigma = -C_1 \sigma (\alpha_1{}^2\gamma_1{}^2 + \alpha_2^2 \gamma_2^2 + \alpha_2^3 \gamma_2^3) - C_2\sigma(\alpha_1\alpha_2\gamma_1\gamma_2$$
$$+ \alpha_2\alpha_3\gamma_2\gamma_3 + \alpha_3\alpha_1\gamma_3\gamma_1) \qquad\qquad 4.1$$

where α_i, γ_i are the direction cosines of the domain magnetization and stress axes with respect to the crystallographic axes, (Bozorth 1951). C1 and C2 are constants related to the magnetostriction constants of the cubic material. At regions in the material, the contribution to the energy therefore assumes the values of zero or $\pm C_1\sigma$ depending on the relative orientations of the domains on either side of a domain boundary. Whilst the application of an external field favours growth of domains with magnetic moment vectors closest to its own direction, the action of, for example, tensile stress in carbon steel encourages growth of domains with moment vectors closest to the stress axis. (The inverse argument applies to compressive load). Those

domain boundaries which, when subjected to tension, (positive σ), move in the same direction as that induced by applied field are called $+90°$ walls, those moving oppositely termed $-90°$ ones. Anti-parallel domains separated by $180°$ walls experience no net change in energy, (provided that the domain volumes remain in equal proportion), so motion of these walls under the influence of a load does not contribute to change in the measured induction of the specimen. Examples of these concepts are shown in figure 4.1
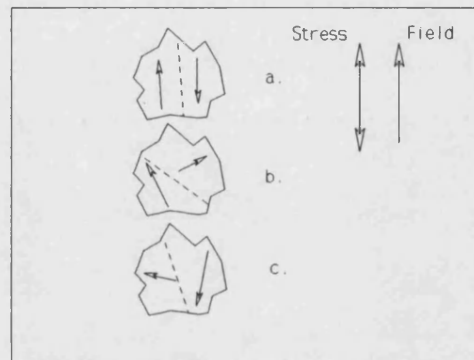
Figure 4.1. Examples of domain orientations in a cubic material in Brown's model. In (a) the imposition of tension will cause equal and opposite changes in the domains leading to a zero net induction change. In (b) tension causes the same motion as the field ($+90°$ wall), the boundary moving to the right. In (c) the tension causes the boundary to move from right to left, opposing the field-induced change ($-90°$ wall).

The process of en-bloc domain moment rotation, a process which is known to be dominant at high fields and stresses is not considered in Brown's model. The net pressure, p, at any domain boundary for a specimen subjected to field and stress is a combination of that induced by field and load, given by

14

$$p=\mu_0 HM_s(\cos\theta - \cos\phi) + \frac{3}{2}\sigma\lambda_s(\cos^2\theta - \cos^2\phi) \qquad 4.2$$

where θ and ϕ are the respective angles between the magnetization in each domain and the applied field and stress. Using the analogy with Rayleigh's law, Brown suggests that the following relationships will apply to the volume displacement of domain walls subjected to an initial magnetizing force from demagnetization (eq. 4.3), and subsequent change in force of opposite sign to the force preceding it (eq. 4.4). (Magnetizing force in this instance can be provided by either field or stress).

$$V = \alpha p + \beta p^2 \qquad 4.3$$

$$\Delta v = \alpha\Delta p + \frac{1}{2}\beta(\Delta p^2) \qquad 4.4$$

Averaged over the whole specimen, Brown's analysis leads to the conclusion that from a point on the initial magnetization curve, the magnetization should increase with tension application but not during its removal. This is represented in figure 4.2. Each group of walls is demonstrated here as behaving quite differently under a field sweep from demagnetization followed by a tension and release cycle. In the first figure the magnetization change shown by 180° walls is seen to be induced solely during the field sweep, arriving at point (a). In the second, the +90° walls are seen to undertake a similar magnetization interval with field, followed by a further increase

with tension, arriving at point (b) during tension application, at (c) during its removal. The -90° walls follow the same field-dictated change followed by a reduction during tension application and an increase during release of stress. As such, tensile cycles cause their magnetization contribution to move between points (b) and (c) on the upper and lower arms. The total magnetization change for the specimen is the summation of these three components. It is on the basis that the magnetization changes are equal and opposite for the two 90° wall types that the change during load release is predicted to be zero.
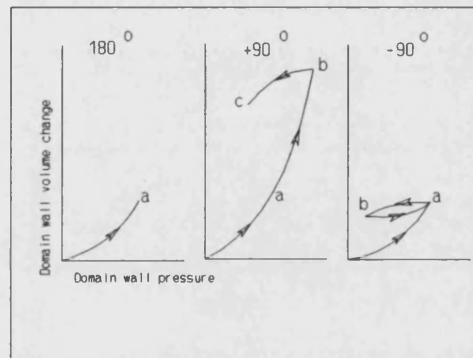
Figure 4.2: Contributions to magnetization changes from the different wall types in Brown's work (1949). In the first figure (left) the 180° walls do not alter their net magnetization contribution during tension cycling. In the second and third figures the contributions from +90° walls and -90° walls are seen to be unequal during the application of a tensile load, (the trajectory ab), yet equal and opposite during release, (the trajectory bc for the +90° walls, ba for the -90° walls).

Using a number of small background fields and tensions, Brown demonstrated the

accuracy of his model compared to experimental data. He concluded the article

with an examination of how the theory may be applicable to the long-term magnetic

instability of ships receiving varying amplitude stresses.

With its strong dependence on the description of domain wall motion in materials

with a cubic crystal structure, Brown's work can be viewed as the most elementary

description of magneto-elastic processess in polycrystalline materials. The necessary

simplifications for the model to maintain its accuracy are that the fields and stresses

applied should not take the specimen outside of the region in which it can be

described by the Rayleigh law.

Significant work subsequent to Brown's included that of Lliboutry (1951) and Brugel

and Rimet (1965, 1966). In 1970, Craik and Wood expanded the discussion by

looking at the properties of several polycrystalline materials subjected to single

tension and compression cycles from points on their initial curves after

demagnetization. In this work the limitations of Brown's theory becomes clear.

Brown's theory in which the roles of tension and compression would be simply

reversed, is seen to be irreconcilable with the observation that even at comparatively

low stresses, the effects of tension and compression are not equal and opposite for all

observations. Initially, this could be seen as a consequence of the unequal areas of

positive and negative domain walls induced by the field sweep. However, the domain

imaging work of Corner and Mason (1964) and Dijkstra and Martius (1953), showed

that stress-induced induction changes are more complicated than could be provided

for in the existing theory. By subjecting Goss-textured silicon-iron specimens to

stress, these workers had shown that massive alterations in the domain patterns of the specimens occurred at very low stress values. It was postulated by Craik and Wood that this was the reason for the observed differences in the comparative magnitudes of the tensile and compressive induction changes. The above works, along with that of Brown, are examined by Faunce (PhD thesis, 1970). This work, along with some published articles from the workers in the same group, (Birss, 1971; Birss, Faunce and Isaac, 1971) provides a summary of the progress at that time. A modified description of magneto-elastic processes was attempted as a consequence of their experimental results. This will be described here.

In Faunce's thesis, the limitations of Brown's work are again highlighted. Whilst it may be useful for fundamental purposes to examine small fields and stresses, the theory was not capable of describing the more varied experimental observations of materials subjected to large domain wall pressures. Furthermore, the implication that compressive loads would simply interchange the roles of the $\pm 90°$ walls was not borne out with the limited available compressive data sets for irons and steels generated before 1971. This indicated a complexity of stress-induced induction changes beyond that expected if one considers the action on the domain wall types alone.

This was explored by Faunce, Birss and Isaac (1971) by examining the stress-induced induction changes from discrete points on initial curves for iron and carbon steels in various states of residual strain caused by either variations in treatment or the level

of carbon. Typical results achieved during the course of their investigations are shown in figure 4.3.

Stress-induced magnetization for an Fe–0·02 wt% C alloy (annealed at 950 °C for 1 h and water-quenched) in a field of (a) 0·5 Oe, (b) 1·0 Oe and (c) 2·0 Oe.
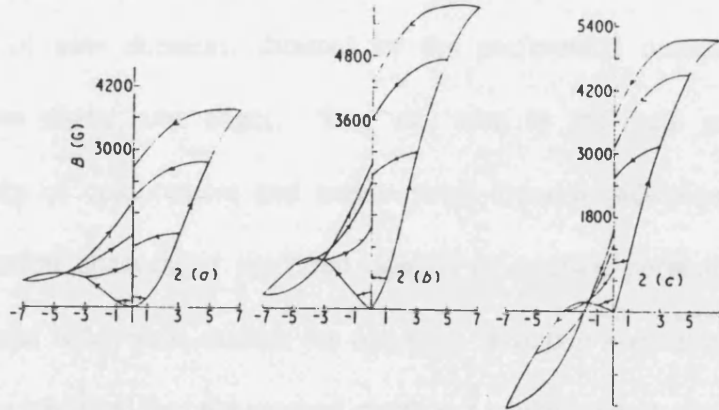
Stress-induced magnetization for an Fe–0·2 wt% C alloy (swaged to produce a 75% reduction in cross-sectional area) in a field of (a) 0·5 Oe, (b) 1·0 Oe and (c) 2·0 Oe.
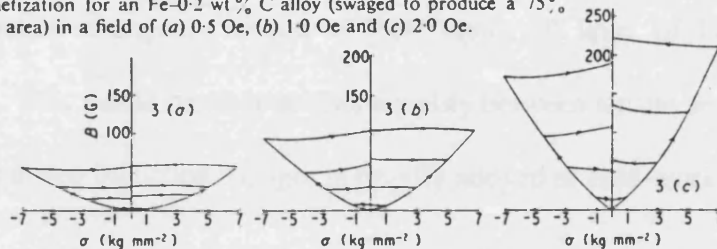
Figure 4.3. Results obtained during the investigations of Birss, Faunce and Isaac (1971).

These results show how the magneto-elastic processes in polycrystalline materials are complicated by treatment and structure, particularly residual strain, and show conclusively how the simplified existing theories could no longer be considered applicable without significant modification. Of particular significance is the approach to symmetrical behaviour for tension and compression for the heavily cold-worked specimen. The main conclusions of these authors are that stress-induced induction changes can be described as occurring by three mechanisms:

19

1. The pressure on $\pm 90°$ domain walls, as suggested by Brown.

2. Large scale changes in domain configuration, involving the nucleation and growth of new domains, dictated by the preferential occupancy of easy directions along cube edges. This was seen as the main reason for the inequality of compressive and tensile stress-induced induction changes, as compression encouraged preferred domain orientation perpendicular to the stress (and field) axis, tension the opposite. Domain nucleation and growth would be inhibited for cold-worked specimens which possess greater resistance to induction change by virtue of their increased level of localised strain centres. This would result in greater equality between tensile and compressive stress-induced induction changes in heavily alloyed or cold-worked specimens.

3. Changes to 'the opposition', (as introduced by Néel), to domain wall movement in the material. In this, Faunce envisaged that the gradient of the wall energy density would be modified by the imposition of a uniform, externally applied load, as discussed below.

The first two processes were seen as accounting for the major qualitative features of the experimental data such as the inequalities of initial B/σ profiles for tension and compression and the pronounced maximum in such profiles often observed of compressive stress-induced induction changes. The third mechanism is based in the domain wall theory of Néel (1946) in which the presence of inclusions and strain variations is seen as being responsible for local fluctuations in the specimen induction.

This is given its classical representation in figure 4.4. The stable condition for a domain wall corresponds to the magnetizing forces being equal to the energy density gradient in the specimen. If the energy gradient changes, as it could during the application of an externally applied load, then the equilibrium location of the domain walls will also change without the need for alterations in domain wall pressure. Conclusive evidence for this process was taken from the work of Yamada (1960), in which irreversible induction changes were initiated from discrete points in the B/H plane through variations in temperature. Increased temperature was seen to change the energy density gradient without alteration of other parameters which could influence domain wall motion. It was of particular relevance that significant irreversible induction changes were only observed during the first temperature cycle, with subsequent cycles producing comparatively small changes. This behaviour could not be explained by the first two proposed mechanisms of induction change.

Figure 4.4. Schematic representation of the variation of energy density throughout a specimen. Such a profile would undoubtably change during the application of load so allowing domain walls to move irreversibly to new equilibrium locations.

By considering this third possible mechanism for stress-induced induction changes the authors realised the fuller complexity of magneto-elastic processes in inhomogeneous media. In particular, the implication that such changes would be dependent on the existing location of domain walls. This in turn implies probable dependence of subsequent stress-induced induction change on the immediate preceding magnetic history. This point should be noted for future reference.

Concluding the discussion on the work of these authors it is worth reflecting on a few points. First, whilst they have itemised three distinct mechanisms for induction change, the point is made that this is for the sake of simplicity, implying that the mechanisms could be related. Second, it will be shown later that by restricting their study to stress-induced induction changes on the initial induction curve alone, they were not able to demonstrate more varied magneto-elastic performance. Finally, whilst their proposed mechanisms are capable of giving a satisfactory explanation of the observations, a quantitative analysis of these complicated processes is very difficult. The ideas put forward do not lend themselves readily to interpretation in terms of the earlier concept of a stress-effective field. It is in this context that the attempts of some of the most recent workers to model stress-induced induction changes using macroscopically derived quantities becomes more understandable.

The contempory workers in the area can be classified into those who have continued with an attempt to describe the effects of stress using the fundamental concepts of domain wall interactions and those who, for engineering purposes, require the numerical efficiency that can be derived from more empirical models. In several

papers, Schneider and co-workers (1981, 1982, 1985, 1992) fall into the former category by continuing the domain wall analysis. Unfortunately, their works are not easily interpreted, partly due to the complexity of the content and partly due to the presentation style. The authors often assume that the reader is well-acquainted with the historically-founded terminology and some advanced concepts which appear to be derived from a wide range of sources. For some of these terms, the reader is referred to chapter 2. Despite these problems, a review of the work is desirable, as it is of particular relevance in this study. In some of the work presented by these authors, it has proved very difficult to follow an argument. Such areas will be highlighted and the most significant results will be presented for reference.

In the Schneider works, an attempt is made to provide a comprehensive explanation of magneto-elastic processes in polycrystalline irons and steels by extending Brown's original model. In order to allow the basic concept of motion of $\pm 90°$ walls to be utilised in explanations of more extensive experimental observations, additional parameters are brought into the formulae. These are centred on:

1.   An extension of the concept of stress-effective field. In the original Brown model, the energy density of a single domain was considered. The effective field or pressure on the domain wall due to stress was then expressed in terms of the

saturation magnetostriction along the easy $<100>$ directions of magnetization. The result was then averaged over all possible domain configurations to calculate the magnetic behaviour of the whole specimen. As an extension to this idea, Schneider and co-workers express the stress-effective field by using the net saturation magnetostriction of the polycrystal:

$$H_\sigma = \frac{3\lambda_s \sigma}{2\mu_o M_s} \qquad\qquad 4.5$$

A typical value for polycrystalline iron is taken at 7 ppm in reasonable agreement with the magnitude calculated in an averaging formula suggested by Callen and Goldberg (1965). In all Schneider's works however there is a significant problem with the polarity of the allocated saturation magnetostriction. Calculations and measurements on irons and steels have proved conclusively that the value is around -7 ppm. This unexplained deviation from the accepted value raises the question of how well founded the model is in the true fundamental magnetic quantities which describe ferromagnetism.

2.   A consideration of the relationship between the magnitude of the experimentally observed stress-induced induction change and the irreversible component of the specimen differential susceptibility. Schneider and co-workers demonstrate quite clearly that the magnitudes of stress-induced induction changes from discrete points show a general increase with increases in the irreversible differential susceptibility.

3. Rules of hysteresis according to Kondorsky, (1941). This gives a phenomenological explanation of ferromagnetic susceptibility. Kondorsky is attributed with the suggestion that upon reversal of the field sweep direction the effective susceptibility at a minor loop point is the value measured at half-way from the field turning point. A possible interpretation of this is shown in figure 4.5. Interpreting the original reference, this may stem from Kondorsky's equation (21) in the referenced work, although no similar graphical detail is given in Kondorsky's original work.
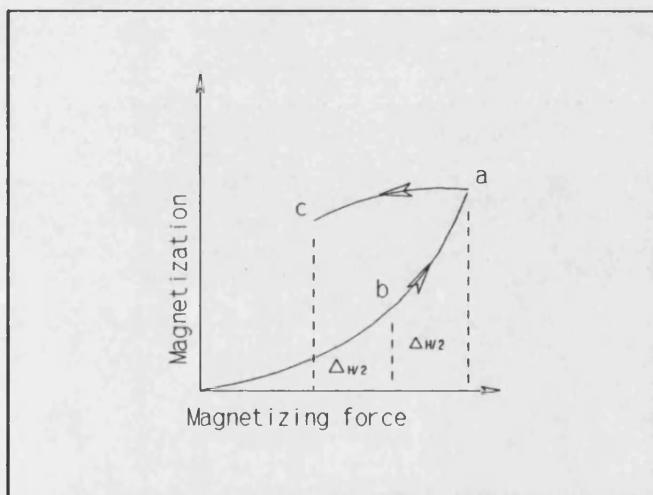

Figure 4.5. Kondorsky's rule. The effective susceptibility at point c is that measured at point b, or in the authors notation:-

$$\chi(\Delta H) = \chi\left(\frac{\Delta H}{2}\right)$$
    4.6

4.   The concept of stress acting in a way that changes the demagnetization field of the specimen. This appears to be attributed to Spano, Hathaway and Savage (1982). In this work the authors demonstrate that over a very small range of stresses the effect of tension on an amorphous ribbon can be expressed in terms of the change in reluctance,

$$\frac{1}{\chi_{eff}} = \frac{1}{\chi_{init}} + \frac{3\lambda_s \sigma}{\mu_0 M_s^2}$$ 4.7

which is analogous to the commonly encountered expression for the change in reluctance with specimen shape anisotropy,

$$\frac{1}{\chi_{eff}} = \frac{1}{\chi_{init}} + D$$ 4.8

with D a function of the specimen shape. Schneider and co-workers adopt this concept as an additional factor in explaining stress-induced induction changes from discrete points.

5.   In the most recent work, the concept of 'saturation anisotropy'. This appears as a scaling factor which models the decrease of stress-sensitivity of iron-based polycrystalline specimens at high induction values. The value is seen to change from 1 to 0 between the Rayleigh region and high induction values. Unfortunately, it is not clear in the latest work how this factor relates to relevant physical variables.

Before reviewing the details of the works presented by Schneider and co-workers, it is worth reflecting on the implications of the foundations of the model. The stress-effective field, expresses how the pressure on $\pm 90°$ walls averages macroscopically. The polarity problem associated with this aspect of the model has already been indicated. It should also be noted that at a particular applied stress level, it is constant for the specimen at any location on its B/H plane if the assumption is made that the relative proportions of domain wall areas stays equal. It will be seen later that this contrasts with a model set out by other workers.

The irreversible susceptibility represents changes in specimen magnetic induction with incremental field steps. As such, as the authors state in their first paper, its inverse, reluctance, could be seen as a quantitative measure of the 'opposition' to domain wall motion, a component of stress-induced induction change proposed by Néel (1946) and Birss (1971). Changes in this opposition, initiated by externally applied load, result in irreversible induction changes of the specimen. In the Schneider model, such changes appear to be accommodated in the 'stress demagnetization' term of point (4) above, allowing the reluctance to increase when compression is applied, the converse for tension. Whilst this is consistent with experimental observations for polycrystalline irons and steels when a net negative polycrystalline saturation magnetostriction is allocated, the concept breaks down when matched against the well-known behaviour of other polycrystalline materials. Nickel, for example has a negative saturation magnetostriction, but its reluctance is observed to increase with application of tension, as evidenced by shearing of its hysteresis loop along the field axis. Materials with positive λ_s are generally observed to increase their

susceptibilities with tension, as evidenced by elongation of their hysteresis loops along induction axes. The authors have adopted the 'stress demagnetization' term directly from that given by Spano and co-workers (1982). In equation (17) of this work, there is an error in the sign of the the stress term. There appears then, to be some problem associated with the polarity of the concept of 'stress demagnetization' when taken outside of the narrow context used by Schneider and co-workers. Despite these uncertainties concerning the physical relevance of some of the model parameters, it should be stated that this work appears to have culminated in an algorithm capable of accurate description of stress-induced induction changes from discrete points.

In their first paper, (1981), Schneider and Semcken examine the results of vibrational stresses on magnetic stability. This is achieved by placing a slender mild steel specimen in a cam-operated device and subjecting it to low level uniaxial field (0-750 A/m) and symmetric tensile and compressive stresses of the order of 10 MPa. This involved measurements of induction changes to a resolution of 5 μT, with overall induction intervals much smaller than those commonly encountered in magneto-elastic literature, typically tens or hundreds of μT. Despite this, it appears that the trends in the results presented are consistent with other reports of larger stresses and induction changes. Some care has been taken to avoid the complexities that arise from the effects of magnetic viscosity at this low level, a complication not so evident when investigating larger stress-induced induction changes.

The important feature of this work is that at these low stress levels the results can be interpreted in terms of the stress-effective field on $\pm 90°$ walls provided that one takes

into account the variations of susceptibility that occur for each wall type. This is summarized in figure 4.6 in which the anticipated paths in the M/H plane of the wall types are described. The authors write the stress-effective field as in (4.5) above. At $\pm$ 10 MPa this is equivalent to $\pm$ 52.5 A/m when the saturation magnetostriction is allocated a value of 7 ppm and the saturation induction of the mild steel, (not specified in the original work), is assumed to be 2 Tesla.
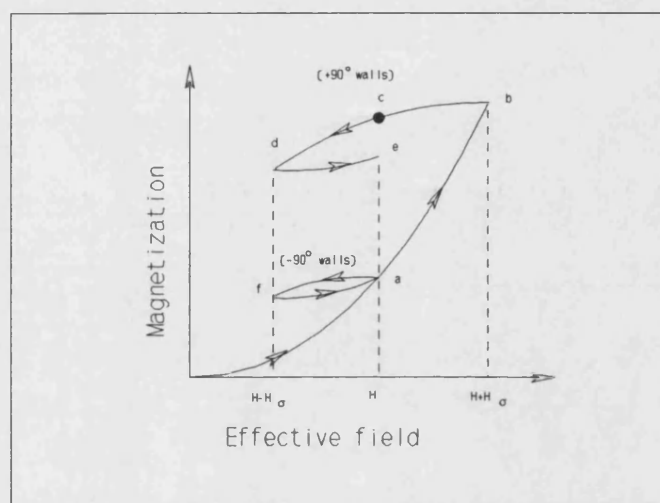

Figure 4.6: Model of magnetization changes undertaken by the $\pm 90°$ wall types for the first symmetrical load cycle. For the initial field sweep, both wall types arrive at point (a). Under tension the $+90°$ walls arrive at point (b), going onto points (c), (d) and (e) respectively, as the tension is released, then compression applied and released. The $-90°$ walls move to point (f) with tension and back to (a) with its release. When compression is applied, they move on to point (b) and continue onto (c), (d), and (e) during the subsequent compression release and second tension cycle. At this stage the actions of the walls with stress are predicted to be almost equal and opposite as the $\pm 90°$ walls describe the loop bcdeb.

29

In the first tension cycle, the $-90°$ walls form a closed loop and do not contribute to the irreversible change in magnetization. By implementing Kondorsky's rule this is

$$\Delta M_{(i)} = \frac{1}{2} f \left(\int_H^{H + H_\sigma} \chi_{irr}(H) dH - 2 \int_0^{\frac{H_\sigma}{2}} \chi_{irr}(H) dH \right) \qquad 4.9$$

where f is the $90°$ fraction of the total domain wall area in the specimen, previously estimated by Brown to be 0.59. For the compressive, or second stage of the symmetric stress cycle,

$$\Delta M_{(ii)} = \frac{1}{2} f \left(\int_H^{H + H_\sigma} \chi_{irr}(H) dH - 2 \int_{-\frac{H_\sigma}{2}}^{H_\sigma} \chi_{irr}(H) dH \right) \qquad 4.10$$

wherein both $90°$ wall types contribute to the net magnetization change. This gives the total predicted irreversible change in the first full combined cycle as,

$$\Delta M_1 = f \chi_{irr} \left(H + \frac{H_\sigma}{2} \right) H_\sigma \qquad 4.11$$

A plot of magnetization change against the irreversible susceptibility evaluated at the effective field, (H + H_o), should give a straight line with slope fH_o which is shown to be true for magnetization changes up to 32 kA/m (ΔB = 40 mT). By using the calculated stress effective field the authors claim this allows f, the fractional area of domain walls, to be derived at 0.61, in close agreement with Brown, although the full details of this estimation are not given. The authors record how the culminative irreversible magnetization change increases with cycle number according to,

$$\sum_{i=1}^{\infty} \Delta M_n = \Delta M_1 \sum_{i=1}^{\infty} \frac{1}{n^2} \qquad 4.12$$

where ΔM_1 is the first full cycle magnetization change. A mechanism for this 'stress-reptation' is not proposed, and it is not inherent in the authors' model. However, the experimental observation that the irreversible magnetization changes decay rapidly with stress cycle number is consistent with many similar observations. The conclusion that vibration cannot therefore instigate long-term magnetic instability is a point worth noting.

On the basis of this work, then, it seems that Brown's model can be extended to describe more complex magneto-elastic processes. Although not given explicitly,the implication from the data presented is that initial inductions up to 0.6 Tesla have been covered, well in excess of the Rayleigh region supposed for the applicability of Brown's model. Inherent in the argument is that the order in which the two stress senses are imposed is not significant, with the attendant suggestion of symmetry of

tension and compression. It is not clear how this fits in with the observation of Birss, Faunce and Isaac (1971) that such symmetry is not often encountered. Indeed even at the comparatively low stress of ± 10 MPa, massive domain re-orientations would have been initiated, as suggested in domain imaging works reported earlier. The state of specimen anneal has not been given however, so it is plausible that a condition of extreme cold-work could have delayed the 'preferential occupancy' discussed by Faunce (1970). Combined with the low loads involved, this would have rendered the stress profiles more symmetric.

In a second work encompassing similar themes, Schneider and Richardson (1982), present more comprehensive experimental data and extend the model to include the effects of 'stress demagnetization' discussed earlier. The free energy per unit volume in a domain in now written to include this effect,

$$F = \frac{3}{2}\lambda_s \sigma \sin^2\theta_\sigma - \mu_0 H M_s \cos\theta_H + \frac{1}{2}\mu_0 D M_s^2 \cos^2\theta_D \qquad 4.13$$

The first term is the magneto-elastic energy, the second the magnetostatic, the third, that associated with the demagnetization field. $\theta_\sigma, \theta_H, \theta_D$ are the angles between the domain magnetization vector and the stress, field and shape axes respectively. The stress effective field is essentially as before, with some modification for experiments conducted on a specimen with field and stress applied orthogonally,

$$H_\sigma = \frac{3\lambda_s(\sigma_\parallel - \sigma_\perp)}{2\mu_0 M_s} \qquad 4.14$$
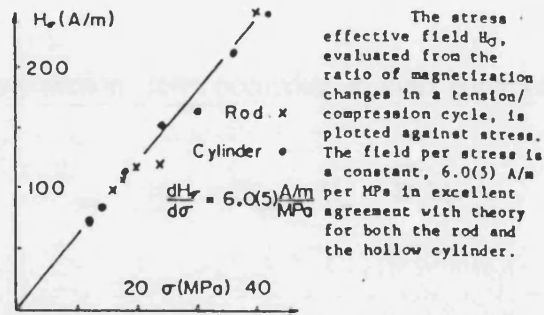
The 'stress demagnetization' terms are written as in (4.7) and (4.8) above. Confirmation of the previously indicated polarity problems comes from the fact that the positive λ_s assigned to the steel allows the 'demagnetization factor' to decrease in compression according to their equation (4);

$$D_{eff} = D + \frac{3\lambda_s \sigma}{\mu_0 M_s^2} \qquad 4.15$$

which is not consistent with experimental observation. It seems appropriate to simply state the main points of this and subsequent works, (1985, 1992), without much further analysis of the model foundations. In this second work (1985) these are,

(i).   That the stress-effective field shows linearity with load as shown in figure 4.7. This is shown for a rod specimen for which field and stress are uniaxial and a cylindrical specimen for which they were orthogonal.

(ii).   That stress applied perpendicular to field is equivalent to that applied uniaxially of the opposite sense i.e. $\sigma_{\parallel} = -\sigma_{\perp}$.

This second point is consistent, at least qualitatively, with data that will be presented in this study.

H. (A/m)

200

Rod x

Cylinder •

100

$\frac{dH_r}{d\sigma} = 6.0(5)\frac{A/m}{MPa}$

20 σ(MPa) 40

The stress
effective field H$_\sigma$,
evaluated from the
ratio of magnetization
changes in a tension/
compression cycle, is
plotted against stress.
The field per stress is
a constant, 6.0(5) A/m
per MPa in excellent
agreement with theory
for both the rod and
the hollow cylinder.

(Schneider and Richardson, 1982)

Figure 4.7: In Schneider's model the stress-effective field is seen to vary linearly with loads up to 40 MPa for uniaxially and orthogonally applied field and stress.

In two further works, Schneider and Charlesworth (1985), and Schneider, Cannell and Watts (1992) continue their model through to describing an increasing range of stress-induced induction changes. The final work is based on the same ideas of stress-effective field, Kondorsky's rule and stress 'demagnetization', with an additional term introduced to allow for the measured decrease in stress-induced induction changes at higher fields. This is termed the 'stress-anisotropy' factor, an unfortunate terminology as it does not seem to be related to the conventional use of the term 'anisotropy' as a statement of inequality of directional properties. As mentioned previously, there does not appear to be any direct correspondence between this quantity and a realisable physical variable.

The 'stress-demagnetization' term occurring in their equation (4),

$$H_i = H_{app} + H_\sigma - D_\sigma M \qquad \text{4.16}$$

(with H_i as the internal field at a sample domain wall) is again expressed as,

$$D_\sigma = \frac{3\lambda_s \sigma}{\mu_0 M_s^2} \qquad \text{4.17}$$

With a positively assigned magnetostriction, this should imply a monotonic increase in demagnetization factor with tension, converse for compression. This prediction is, however, is apparently contradicted by the authors' figure (1) shown below (figure 4.8), in which the experimentally observed change in the reluctance is seen to increase linearly with compression and suffer an inversion in tension. This inversion, interpreted in terms of residual stress is claimed to be a reflection of the Villari process. This is not predicted by the 'Spano demagnetization' and no explanation is given for it. In a cited work (Veksar et al 1975) the authors highlight the shift in the inversion of permeability with changes of residual stress in rail steel but do not suggest a mechanism in terms of fundamental magnetic quantities. It is worth noting at this stage (for subsequent discussion) that no dependence of λ_s on stress forms any part of the analysis being presented by Schneider and co-workers.
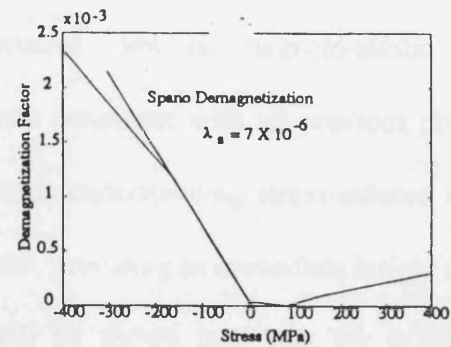
Stress demagnetization factor as a function of
stress for a mild steel.

Figure 4.8. In the work of Schneider, Cannell and Watts, (1992) the variation demagnetizing factor induced by stress is measured as increasing with compression and suffering an inversion with tension. It is not clear how this relates to the modelled 'stress-demagnetization' of their theory.

In conclusion of the commentary on these works the following points should be made. Despite some uncertainties associated with the model foundations it appears that a computerized algorithm is now capable of correctly predicting stress-induced induction changes in irons and steels. Schneider and co-workers appear to be isolated in their attempts to continue the model based on the works of Brown, Lliboutry and Birss, with no other contemporary workers attempting a rigidly fundamental approach. The complexity of the formulae they have advanced to describe magneto-elastic processes is mostly a reflection of the inherent complexity in those processes themselves.

It is understandable then, that other workers have taken a somewhat different approach in a model that is based partly on fundamental quantities, partly on empirically derived rules. In several works, Jiles, Atherton and co-workers, have

36

presented an alternative view of magneto-elastic processes based largely on experimental evidence consistent with all previous observations. This represents a significant step towards understanding stress-induced induction changes. The model is conceptually clearer, providing an immediate insight into magneto-elastic processes. Unfortunately, it will be shown later that the existing format is not capable of describing all features of stress-induced induction changes.

The bases of the model are laid out in several papers written from 1983 onwards and many of the concepts are presented in the recent introductory text by Jiles (1991). Central to the model is the suggestion that the principal anhysteretic curve represents the minimum energy configuration on the B/H plane, and is considered to be the curve that would be described in the absence of obstructions to domain wall motion. This was originally set out in the work of Jiles and Atherton, (1983). In this, the authors describe how, for materials showing a classical hysteresis loop shape, the anhysteretic curve is described by the modified Langevin or Weiss function,

$$M = M_s \coth \left(\frac{\mu_0 m(H + \alpha m)}{kT} \right) - \frac{kT}{\mu_0 m(H + \alpha M)} \qquad 4.18$$

profiles for which are shown in figure 4.9.
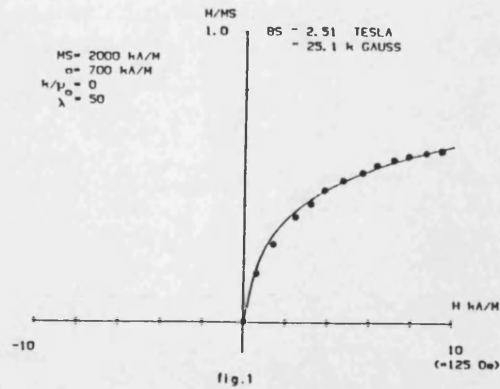
Solutions of equation 1 for various values
of the parameters. The equation is expressed
in the form, $\dfrac{M}{M_s} = \coth\left(\dfrac{M+\lambda H}{a}\right) - \left(\dfrac{a}{M+\lambda H}\right)$.
The solutions represent the anhysteretic
curves.

Figure 4.9. Graphical interpretation of equation (4.18), the Weiss formula. Such a profile is thought to represent the locus of points described by a specimen containing no impediments to domain wall motion. (Jiles and Atherton, 1983)).

In the Jiles-Atherton model, defects and inhomogeneities in a specimen are seen to give rise to a resistance to domain wall motion by virtue of their ability to 'pin' domain boundaries at locations in the body of the material. Jiles and Atherton consider that such defects are the main contributors to hysteresis and go on to modify the Weiss formula by the addition of an extra energy loss term. In the authors' own notation, their equation for a hysteresis model is,

$$M = f\left(\frac{M + \lambda M}{a}\right) - k\frac{dM}{dB_e} \qquad\qquad 4.19$$

where,

$$\frac{\lambda}{a} = \frac{\mu_0 m}{kT},$$ 4.20

$$\frac{1}{a} = \alpha\mu_0\frac{m}{kT},$$ 4.21

$$k = \frac{dE_{loss}}{dM}$$ 4.22

Here, λ does not represent specimen magnetostriction, but is used as an effective field scaling parameter, the inverse of α. The first term in equation 4.19 is then the Langevin function and in the second term, k is the work per unit change in magnetization required to release domain walls from their pinned sites. E_{loss} is the total energy lost in overcoming the domain wall pinning. In this model of hysteresis, a uniform distribution of pinning sites each of energy equal to the average pinning site energy is assumed. B_e (= H + αM) is the effective field in a ferromagnet as proposed by Weiss. Figure 4.10 shows two hysteresis loop profiles generated by this equation. Modification of parameter k is seen to increase specimen coercivity, consistent with experimental observations.
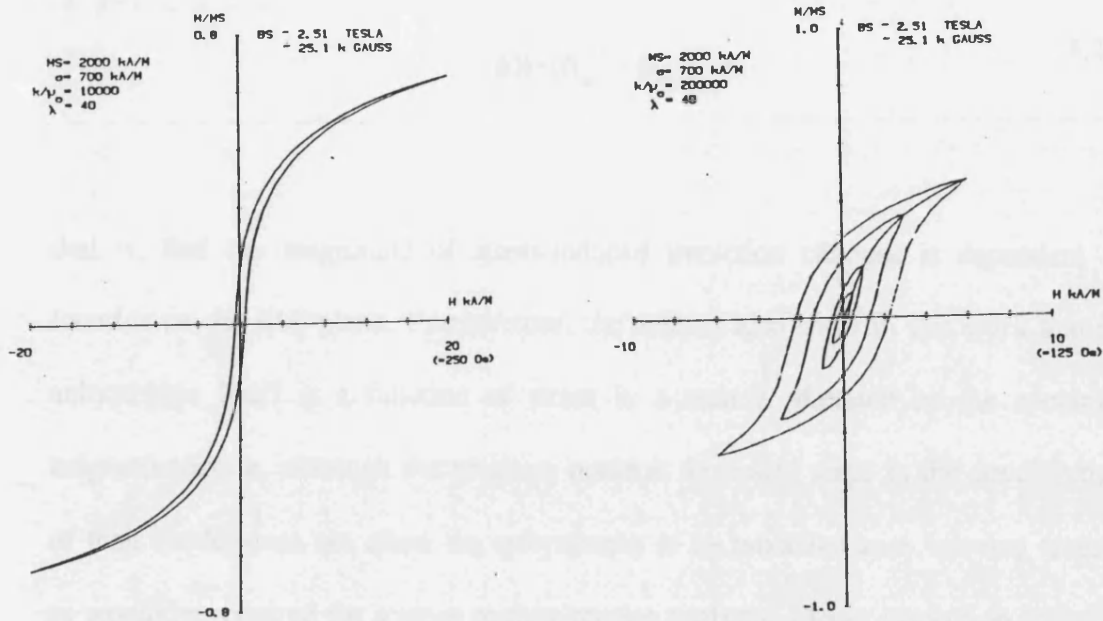
Figure 4.10. Hysteresis loop profiles generated by the Jiles-Atherton model
of ferromagnetic hysteresis. Increasing the value of the pinning coefficient
'k' is seen to enhance modelled coercivity. (Jiles and Atherton, 1983).

In work published simultaneously, the authors go on to describe how the model can
be extended to accommodate the effects of stress, (1983). Experimental observations
presented in this work show that the anhysteretic curve is approached during
stress-induced induction changes of either sense from initial curve and major loop
points, as shown in figure 4.11a. As the 'global' equilibrium condition for the
specimen this seems intuitively correct and using the example of a 1% manganese
steel subjected to a single tension cycle at multiple points along its initial induction
curve, the authors show that the magnitude of the stress-induced induction change
follows the interval between the respective locations of the initial curve and the
corresponding (zero stress) anhysteretic curve, as shown in figure 4.11b. This leads
the authors to suggest the following general relationship,

$$\Delta B \propto (B_m - B_{init})$$

that is, that the magnitude of stress-induced induction changes is dependent on *location* on the B/H plane. Furthermore, the authors also show in this work that the anhysteretic itself is a function of stress in a manner dictated by the specimen magnetostriction, although the progress made at this early stage in the development of their model does not allow the anhysteretic to be modelled as a 'moving target', as would be required for a more comprehensive analysis. Closer inspection of figure 4.11b reveals that whilst there is obviously some relationship between stress-induced induction change magnitudes and relative locations on the B/H plane of the initial and anhysteretic inductions, there is some indication that the match is not perfect. This point will be brought out in work contained in this thesis.
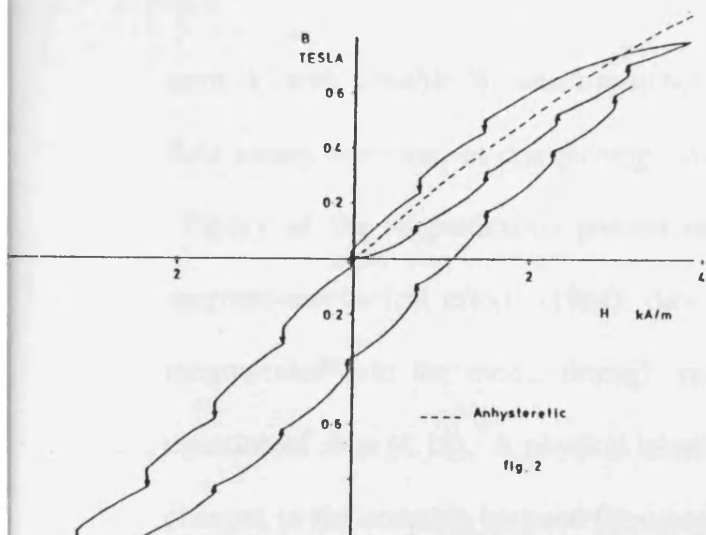
Changes in flux density with a single stress cycle of 140 MPa tension at various different points around a hysteresis loop.
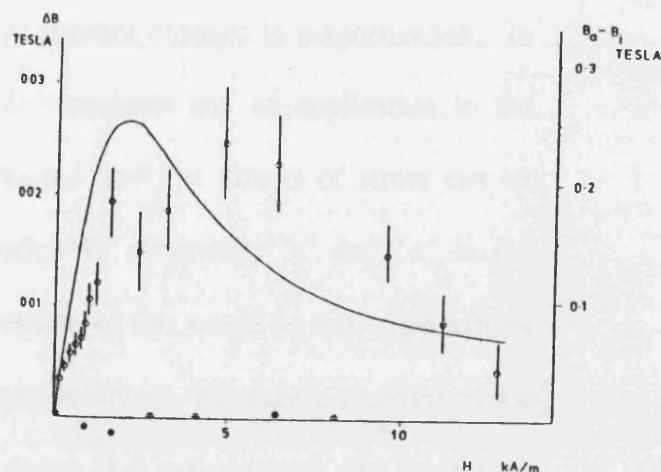
Changes in flux density with a single stress cycle of 140 MPa tension at various points. Open circles are from the initial magnetization curve, closed circles from the anhysteretic magnetization. The solid line is Ba(H) - Bi(H).

Figures 4.11 a & b. (Atherton and Jiles, 1983). In (a), the results of a single tension cycle to 140 MPa at various points on the initial curve and major loop show that the anhysteretic curve (dotted line) is approached in these magneto-elastic processes. In (b) (right), the magnitude of the induction change along the initial induction curve is compared with the difference between original induction value and corresponding anhysteretic location. According to the Jiles-Atherton model these are proportional, (see equation 4.23).

In subsequent works, (1984,1986), Jiles and Atherton build on the foundations of the theory. In essence, the main features of their model do not change significantly in these works, but alternative presentations of concepts and some additional ideas help to refine the model. For brevity, the main points will be mentioned here. First, as a simple correction to the earlier presentations the authors find it necessary to alter the equation of state which defines the classical sigmoid by prefixing the impedance

42

term 'k' with variable 'δ' which switches from +1 to -1 dependent on the previous field sweep direction, so that pinning always opposes changes in magnetization. In 'Theory of the magnetization process in ferromagnets and its application to the magneto-mechanical effect' (1984), they discuss how the effects of stress can be incorporated into the model through variation of parameters 'a' and 'α' in the equation of state (4.18). A physical interpretation of this would be that stress affects changes in the coupling between ferromagnetic moments, although a mechanism for this is not proposed by the authors. It is shown that experimental and theoretical initial and anhysteretic curves can be matched through suitable choice of parameters 'a', 'k', and 'α' as shown in figure 4.12. It appears to be the case though, that such comparison is optimised for the case of compression. Whilst the authors record the experimentally-determined variation in the anhysteretic profiles with tension, no attempt is made to model these over their field range. This is undoubtedly due to the complications arising from processes associated with the Villari reversal in which the magnetization at high fields in tension is seen to decrease relative to the zero stress value, as shown in figure 4.13. It is the case that the hysteresis model proposed at this stage does not have the capability to handle this particularly complex behaviour of iron-based specimens.
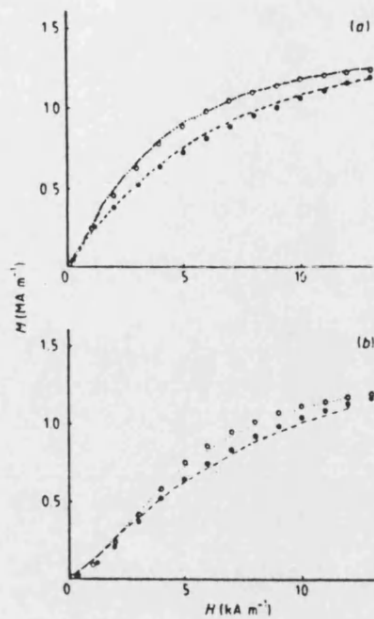
Figure 4.12: (Jiles and Atherton, 1984). The experimental anhysteretic and initial curves at zero stress and 200 MPa compression are matched theoretically through suitable choice of values for a, k, and α. In (a) appropriate zero stress values are a=3750A/m, α =.0033: values at 200 MPa are 4750 A/m and 0.00379 respectively, (k=0). In (b) these parameters hold their respective values with the introduction of the impedence term k=2.787x10^9 successfully modelling the hysteretic behaviour.
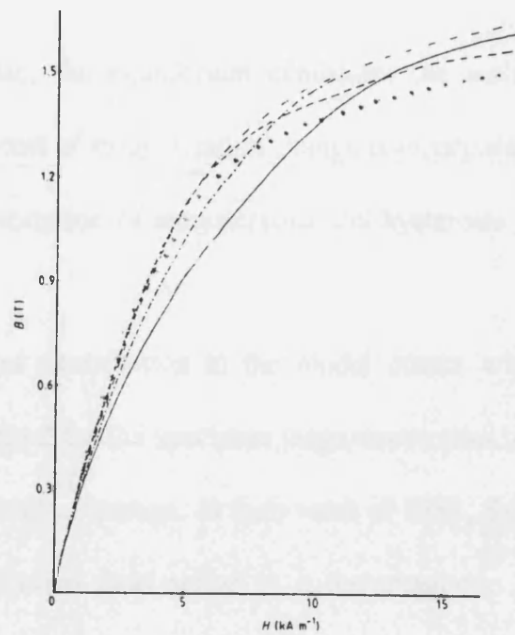
Experimental anhysteretic curves at different levels of stress for sample A.
——, 200 MPa compression; – · – · –, 100 MPa compression; – · · – · · –, zero stress; – – –,
100 MPa tension; · · ·, 200 MPa tension.

Figure 4.13. (Jiles and Atherton, 1986). Experimentally determined iso-stress anhysteretics. The 200 MPa tensile profile should be noted for its relative reduction at high field values. This 'Villari effect' proves difficult to model using the model formulae inclusive in work up to 1986.

With this in mind, the model is seen to undergo further development from 1986 onwards. The significant points are mentioned here. First, there is the recognition that both irreversible and reversible processes are of importance in stress-induced induction changes. According to work by Globus and Duplex (1966, 1969, 1970), reversible magnetization changes can be attributed to domain wall bowing between pinned sites, irreversible ones to domain wall displacement through a specimen. In the Jiles-Atherton model, one can envisage domain walls held at discrete pinning sites bowing in one sense when the magnetization value is less than the corresponding anhysteretic and in the other when the magnetization is above the anhysteretic value.

45

At the anhysteretic, the equilibruim condition, the walls would be planar. The reversible component of magnetization change is incorporated into the model to allow more accurate description of anhysteretics and hysteresis loops.

A more significant contribution to the model comes with the recognition of the important role played by the specimen magnetostriction in dictating the form of the reversible component of change. In their work of 1988, Sablik, Burkhardt, Kwun and Jiles state the effective field active in a ferromagnetic in terms of an additional 'stress-effective' field,

$$H_{eff} = H_{app} + \alpha M + \frac{3\sigma}{2\mu_0}\left(\frac{d\lambda}{dM}\right)$$

4.24

where the stress term, involving the derivative with respect to magnetization of the bulk magnetostriction, is derived from thermodynamic identities. This is in stark contrast to the more commonly encountered single domain effective field formula involving the saturation magnetostriction used by Schneider and co-workers. Incorporated into the hysteresis model, this allows a fuller description of the experimental trends of iso-stress hysteresis loops and anhysteretic profiles. In particular, it is the inversion of sense of the magnetostriction derivative which relates directly to the relative reduction of magnetization values at high fields and stresses. In this way the Jiles-Atherton model can successfully describe the Villari process, provided of course, that the specimen bulk magnetostriction is previously measured or known.

Iso-field stress-induced induction changes can be conveniently separated into reversible and irreversible components, as shown by Atherton, Rao and Schönbächler, (1988). This is demonstrated in figure 4.14. The irreversible component, measured by the net change at the end of a stress cycling sequence, will, according to the model, have a magnitude dictated by location on the M/H plane relative to the equivalent anhysteretic location. The reversible component of change is measured by the magnitude of the 'closed loop' magnetization changes observed in the specimen after (usually) several cycles. It is observed experimentally that this has a form dictated by the magnetization derivative of the magnetostriction. Atherton, Rao, De Sa and Schönbächler, (1988) have shown that a relationship between the reversible component of stress-induced induction change and the reversible component of magnetostriction can be predicted from thermodynamics. The stress-effective field formula of equation (4.24) predicts the alteration of the anhysteretic curve as being dependent on the magnetization derivative of the total bulk magnetostriction term. It seems that some continued work may be necessary to clarify the real dependence of the reversible component of stress-induced induction change. This will be the subject of some work presented here.

*
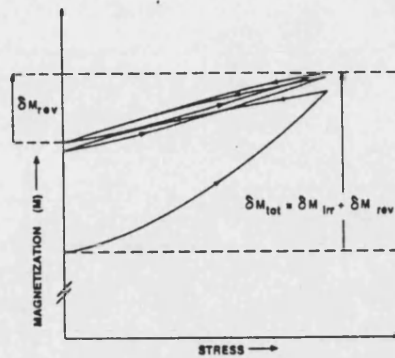
Figure 4.14. In work presented by Jiles, Atherton and co-workers, stress-induced induction changes from discrete points within or around a hysteresis profile can be separated into reversible and irreversible components. The magnitudes of such changes are dictated by specimen magnetostriction and location on the M/H plane respectively. (Atherton, Roa and Schonbachler, 1988).

In recent work, Atherton and Vi Ton (1990) have investigated the applicability of the empirical model to magnetic histories more complicated than those discussed in earlier works. By separating the stress-induced induction changes observed from minor loop points into reversible and irreversible components, they have revealed some discrepancies between theory and measurement. Irreversible magnetization changes are expected to allow the specimen to approach the principal anhysteretic with stress cycling. In some cases on minor loops, these authors have found this not to be the case. This aspect of the model will be investigated at some length in this study.

In summary then, there are two significant yet different approaches to solving stress-induced induction changes in available literature which are of primary interest to this study. On the one hand an attempt has been made to develop the wall-type analysis initiated by Brown. On the other is the provision of a relatively new empirical model. It will be the objective of this work to confirm the basic experimental observations and through generation of new data, investigate the applicability of the models where possible.

For completeness, it should be mentioned that stress-induced induction changes in steels has been investigated on a wider basis than indicated above. Some workers, (Pitman (1990)), have presented their own experimental work as a confirmation of the Jiles-Atherton empirical model. Others (Langman (1990,1983), Tanner (1989)), have generated data for purposes associated with non-destructive evaluations, but have not attempted a modelling solution. There is of course, a plethora of information concerning the stress-dependence of the magnetic properties of electrical steels, (e.g. Stanbury (1989, 1982), Shirkoohi and Moses (1990), Moses (1979)), and it is of interest to attempt to interprete many of these observations in terms of the models discussed here. Many of the aspects of stress-induced induction changes in carbon steels are not exclusive to this class of materials and are shared across all magnetic materials, as shown by Saito, Yamamoto and Ueda (1991) in their investigations of the effects of stress on amorphous specimens. In examining the specific case of stress-induced induction changes in steels and other polycrystalline specimens, it is worth bearing in mind that an attempt is being made to describe magnetic processes which are common to most, if not all ferromagnetic materials. Aspects of

magneto-elastic behaviour which are peculiar to a particular specimen are often the result of some impediment to the normal expected ferromagnetic performance, usually associated with the manufacturing process, i.e. carbon content, anisotropy induced through texture or residual strain. By examining a range of polycrystalline materials in this work, it is hoped that a general pattern of stress-induced induction changes will emerge across all the materials studied, implying the active processes may be universal in the ferromagnetic class.

5. Experimental details

5.1. *Specimens and their preparation*

This study is motivated by the need to understand the stress-related magnetic behaviour of the structural steel classified commercially as "HY80". Accordingly, this material, in a number of forms or preparations, features predominantly in the data. It has been observed though, (Craik and Wood 1970), that the stress-induced induction changes in several polycrystalline specimens have certain shared characteristics. In order to expand on this observation and aid the current investigation, several other polycrystalline materials have been studied. These are Nickel, Silicon-iron and Iron, as for HY80, in a number of forms.

5.1.1 HY80

The composition of this material, analysed by spark discharge emission spectroscopy (S.D.E.S.) is compared in table A to some recognized standards, (Smithells 1982). Some uncertainty in the precise designation, particularly with the less prominent constituents, is indicative of the plethora of existing compositions and assignments. Other consistent designations include ASTM A372(6), MIL-S16216 (plate), MIL-S-21952 (bar), MIL-S-22664 (shapes), MIL-S-23009 (forgings), MIL-S-2441 and UNS specifications K31820 and J42015 ('Metals and alloys in the UNS numbering system' 3rd edition 1983). Material preparation involves a quench and temper process, which leads to a stable 'spheroidized' martensitic structure. All specimens used in this study were cut from a two inch section rolled sheet, obtained

51

direct from the Raivenscraig plant. For a more complete discussion of the metallurgy the reader is referred to appendix A.

During the course of this study, a specimen, the surface of which was electropolished using a solution of acetic acid and chromium tri-oxide, (Tegart, 1959), was observed to show by optical micrograph, the characteristic martensitic lath-type structure with large impurities evident as surface features. A Scanning Electron Micrograph (courtesy of Dr. G. Fourlaris, School of Materials, Leeds University) shown below, confirms this on a clearer scale (1mm = 10μm). The randomised orientation of the material crystals, indicate that any anisotropies dictated by material fabrication are unlikely in the as-cast condition. This would be the case for both mechanical and magnetic results, although it should be borne in mind that subsequent treatments i.e. welding, may mean that this condition does not always hold on structural members.
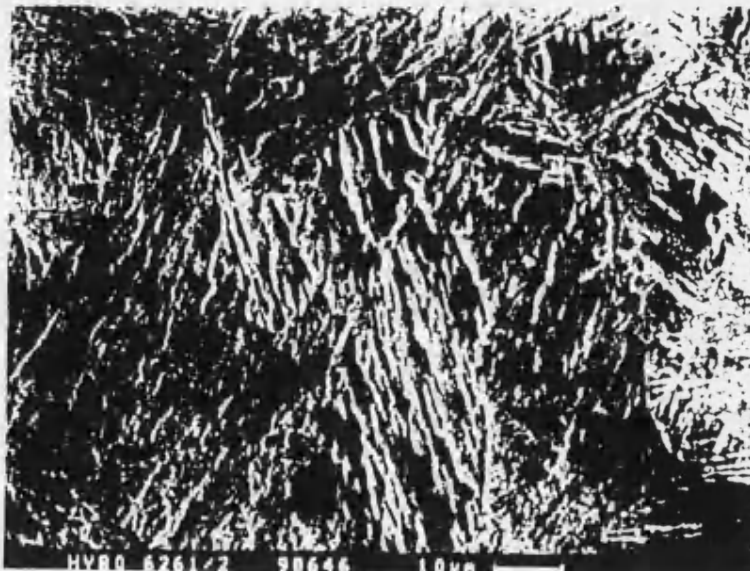
ELEMENT	S.E.D.S	ASTM A543	UNS K42338
Carbon	.15% wt.	.18%	.23%
Nickel	2.66%	2.25-3.25%	2.6-4.0%
Molybdenum	.39%	.45-60%	.45-.6%
Manganese	.31%	.4%	.4%
Silicon	.28%	/	.2-.35%
Titanium	<.01%	/	/
Chronium	1.38%	1.0-1.5%	1.5-2.0%
Sulphur	<.01%	/	<.04%
Phosphorous	<.01%	/	<.035%
Copper	.02%	/	/
Vanadium	.01%	<.03%	<.03%

Table A. Composition for HY80, according to various sources

ELEMENT	SHEET	TUBE
Mn	3000 ppm	<800
Si	<800	<200
C	<800	<200
P	<400	<200
S	<500	<150

Table B: Iron composition specifications

Figure 5.1 shows the results of tensile tests to failure for six specimens cut at three mutually orthogonal directions from the as-received block, (two each). All specimens show the double-yield profile characteristic of materials of this type. Whilst full mechanical isotropy is not an obvious conclusion from such results it is true to say that the lack of any marked difference in the curves suggest reasonable constancy of properties. There is no conclusive recognizable trend within the results for the specimens used. The high elongation specification of 17% and typical minimum yield specification around 590MPa (ASTM 543) are demonstrated in this figure.

Figure 5.2 gives the X-ray diffraction analysis for an electropolished specimen. The trace is predominantly that which can be expected for α-iron.

For magnetic studies, HY80 specimens have been investigated in the following forms.

(i)   HY80(1), cut along the rolling direction, in the roll plane.

(ii)   HY80(2), cut orthogonal to the rolling direction but in the rolling plane.

        Both of these specimens are for uniaxial field and stress tests, shown in figure 5.3 Compressive stressing of these thin samples was achieved through use of a Tufnol support along the length of the specimens.

(iii)   'Bi-axial' cylindrical samples, subjected to orthogonal field and stress, shown in figure 5.3.

(iv)   Various specimens for longitudinal magnetostriction measurements.

Samples have been measured in the cold-worked and vacuum-annealed conditions.
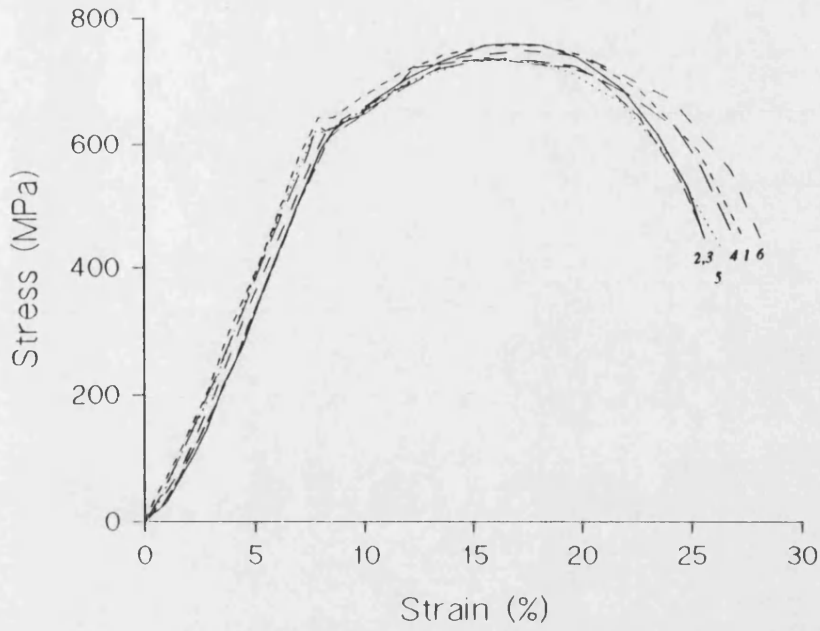
Figure 5.1: Tensile tests to failure on mutually orthogonal HY80 specimens, (engineering stress). 1,2: Parallel to roll direction. 3,4: Perpendicular to roll direction. (All in roll plane). 5,6: Perpendicular to roll direction and plane.
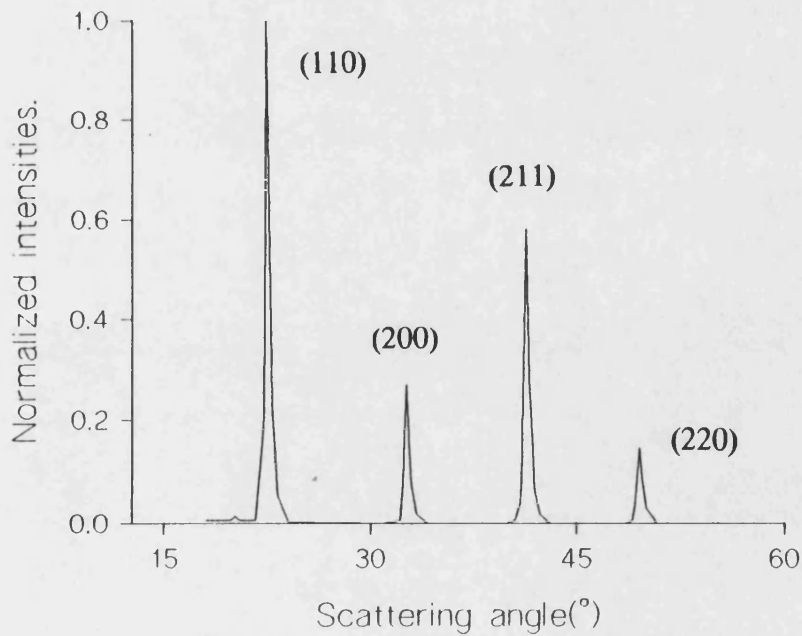
Figure 5.2: X-ray diffractometer trace for HY80.

5.1.2 Iron specimens

The following, variable purity, iron specimens have been investigated. Again these have been measured in both annealed and cold-worked conditions.

(i)   Fe(1), iron sheet cut along roll direction,

(ii)   Fe(2), iron sheet cut perpendicular to the roll direction,

These specimen shapes are shown in figure 5.3. Purity for the as-received sheet is specified by the supplier, (Goodfellows), at 99.5%, with compositions given in table [B]. These specimens lend themselves most readily to uniaxial field and tensile stress studies.

(iii)   Iron tube, 200mm long, 10mm outside diameter, 9.5mm inside diameter. The purity is specified at 99.8%+ by the same supplier. This grade of material is typically used as a magnetic shield. The composition is given in table B. This sample was used because it lent itself most readily to compressive studies.

5.1.3 Nickel

The Nickel sample shown in figure 5.3 has been investigated in the annealed and cold-worked conditions. This specimen is most suitable for uniaxial field and tensile

stress measurements. A purity level of 99.99% is specified by the suppliers (Advent Ltd.).

5.1.4 Silicon-Iron

Electrical steel sheet has been subjected to uniaxial field and tensile tests. Specifications, (courtesy of Orb Electrical Steels Limited, Newport, Gwent), were given as 'Hi-B, 27 MOH'. Specimens were cut from the as-received sheet at 130mm x 8mm x 0.3mm.

Magnetic investigations with the techniques discussed in the following sections are hampered by two conflicting requirements. On the one hand samples should be sufficiently sturdy to allow reasonable compressive loads to be applied without buckling. On the other, short, thick specimens are not appropriate for magnetic measurement by this technique as they possess high demagnetizing factors which lead to uncertainties in the effective field acting on the sample. One consequence of this is the increase in externally applied field required to reach magnetic saturation. For a fuller discussion the reader is referred to standard texts, (Bozorth,1951).
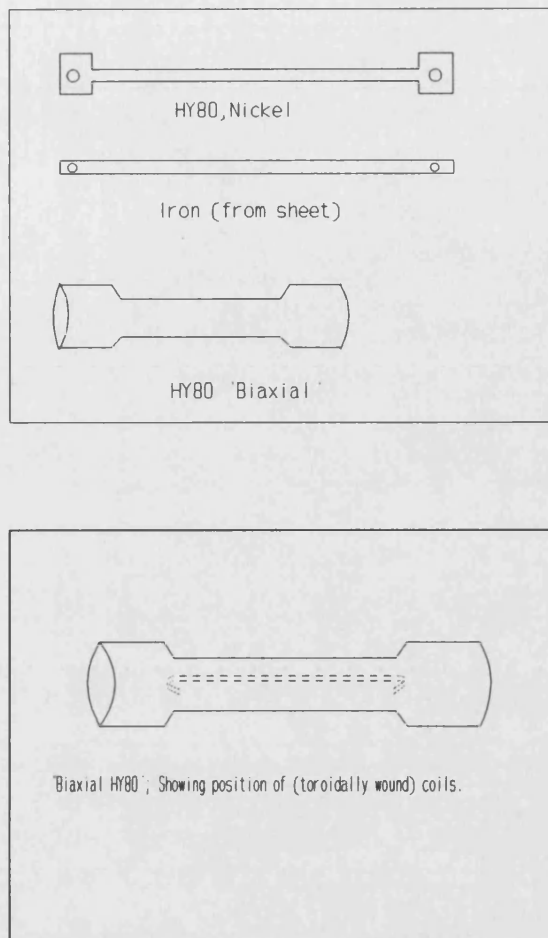
Figures 5.3: Specimens for magnetic tests. Uniaxial: HY80 was cut with a central section at 130mm x 2.5mm x 0.7mm. Nickel was cut at a similar shape with a central section at 115mm x 2.5mm x 0.5mm. Iron specimens were cut from the sheet at 145mm x 3mm x 0.5mm. The biaxial HY80 specimen had toroidally-wound induction and field coils (65 thin gauge induction turns, 15(10 amp) field turns: shown schematically in the lower diagram), so that these quantities were measured perpendicular to the stress axis. The specimen central section measures 9.2mm outside diameter, 8.5mm inside, length 80mm.

5.2   *Measurements and associated instrumentation*

The main measurements undertaken on the specimens of 5.1 can be broadly categorised as:

i.   B/H: the measurement of specimen induction with varying applied field at constant stress.

ii.   B/σ: the measurement of specimen induction with varying applied load at constant field.

iii.   B/T: the measurement of change in induction with varying temperature.

iv. λ/H: the measurement of specimen magnetostriction with varying field at constant stress.

v.   Barkhausen count: the measurement of the high frequency RMS search-coil voltages associated with discrete, irreversible specimen induction changes.

In the following sections the instrumentation and relevant experimental techniques used will be explained. The associated processes of specimen demagnetization and production of 'anhysteretics' will also be described. The complete experimental system is shown in figure 5.4.

Figure 5.4: General experimental arrangement.
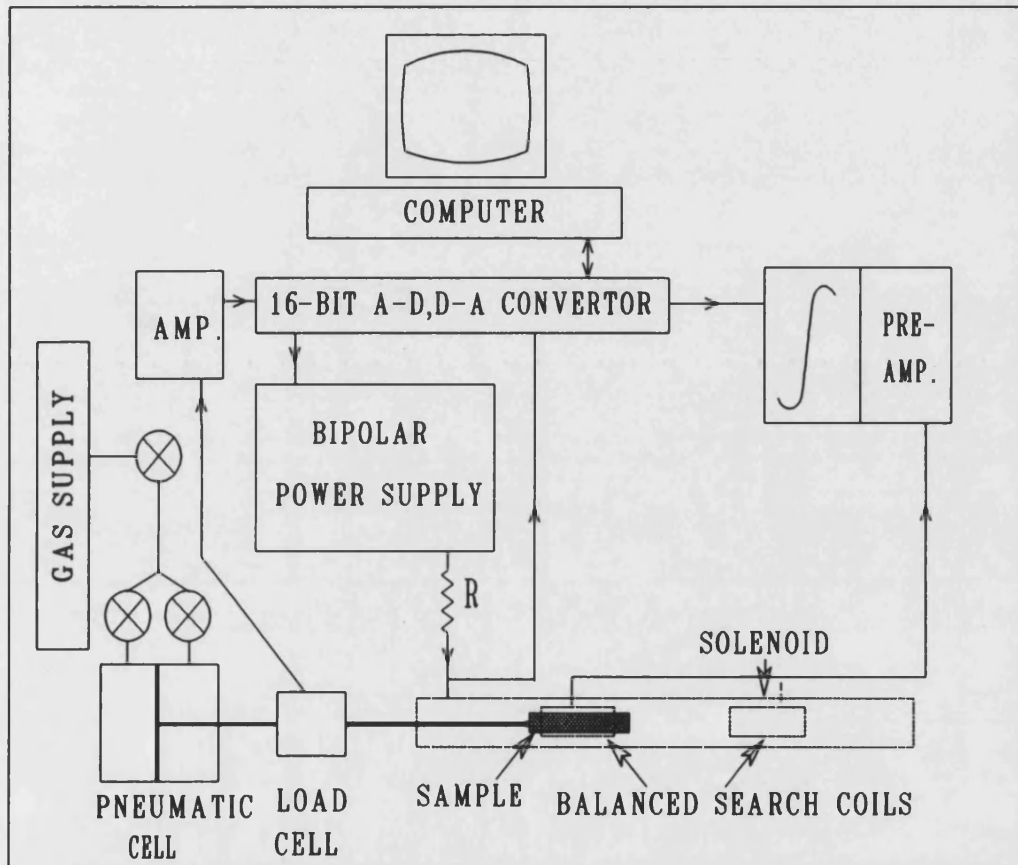
5.2.1 B/H measurements

With limited exceptions, specimen induction changes measured in this work are obtained using the 'ballistic' technique, (Squire et al 1988). This includes the use of two counter-wound multi-turn search coils, (approximately 10,000 turns each), placed equidistant from each end and in the bore of, the magnetic field generating solenoid, as shown in figure 5.4. The specimen is placed inside one search coil and inductions measured by integrating the combined output from the search coils as the field is swept. For a fuller description of this measurement principle, the reader is referred to appendix B. It is important to realise that such a technique does not give an immediate measurement of specimen absolute induction values, but 'changes' in induction. Absolute quantities can only be derived from changes from known conditions, i.e. saturation or demagnetization.

The rest of the B/H measurement system consists of the solenoid power supply and current shunt, the search coil balance network, pre-amplifier and integrator, and a 16 bit ADC/DAC (analogue to digital/digital to analogue convertor) data station, interfaced over the IEEE bus to the controlling BBC computer. BASIC software routines implement all automatic control functions and data acquisition associated with the B/H measurement sequence. The hysteretic data can be presented on screen and saved on disk for later retrieval or conversion to a graphic software package.

The magnetic field generating solenoid consists of four co-axial copper windings connected in parallel. At 758 turns per meter and with a maximum power supply

current of 10 amps, calculated peak fields of 7,580 A/m are achieved in this study. The field homogeneity from one end of the solenoid to the specimen position is shown to high resolution in figure 5.5. Measured using the axial axis of a 3-axis fluxgate magnetometer at the low field values of 175 A/m, the indicated field uniformity is ±0.4 A/m, (±0.2%), over typical specimen lengths of 130mm centred around 50cms from the solenoid end. At the peak field of 7580 A/m this scales as a spread of ±15 A/m along the specimen length. The background field around the sample location was measured at 0.5±0.1A/m which was compensated for in magnetic measurement processes. A background variation of ±0.1 A/m is small compared to the inhomogeneity of the solenoidal field across the specimen. Bipolar currents to the solenoid are controlled remotely over the interface to a resolution of 1 part in 32768 and measured directly across a 0.1 ohm constantan series shunt to the same resolution. The high temperature stability of this item, (+/-40 ppm/°) and the control mechanism, indicate that fields to a reproducibility of better than ±1 A/m should be regularly obtainable for typical (±3 degrees) temperature variations in the environment. The field stabilities at the sample position, with the power supply at 0 amps, 1 amp and disconnected, are shown in figure 5.6, over a typical measurement time of four minutes, again measured using the fluxgate. The data sets represent the totality of the field uncertainty measurement, as they include the fluxgate, its associated wiring and the data acquisition stage. It is evident that the applied field associated noise is larger than the general background level but clearly maintained within ±1 A/m. On this basis, use of magnetic shielding, whilst desirable, was not considered essential at all times for short duration experiments when set against the convenience of easier sample access. During induction

measurement sequences, the fluxgate magnetometer was intermittently observed to assess the stability of the background field.
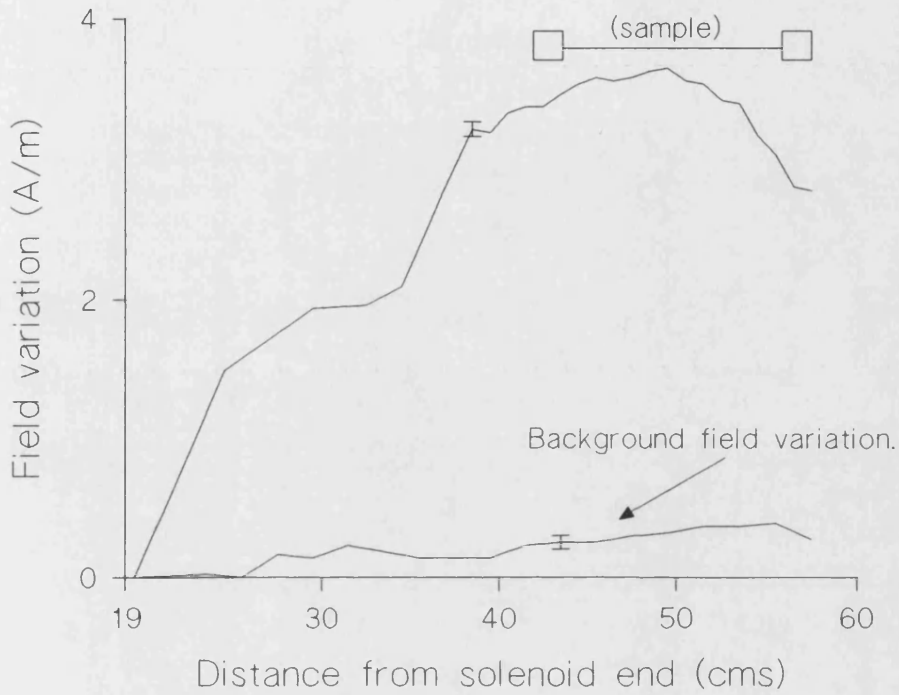
Figure 5.5: Field homogeneity against distance from the solenoid end at 175A/m. The curve represents the combination of the solenoid and background field, (also shown), contributions. Specimen mid-points are at 50 cms.
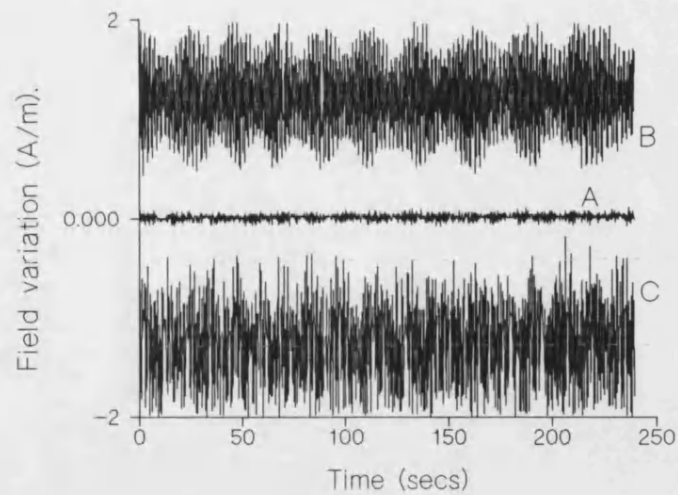
Figure 5.6: Field stability at sample location. A: Background noise (power supply off). B: Power supply on, zero amps. C: 750 A/m applied field. Profiles off-set from zero for clarity.
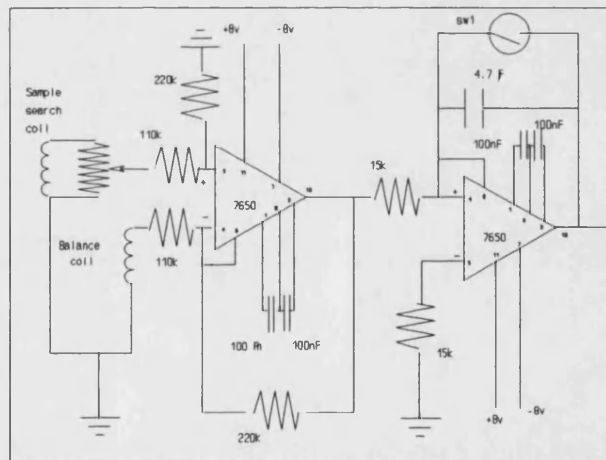
Figure 5.7: Combined balance circuit, pre-amplifier and integrator assembly.

The balance circuit, differential pre-amplifier stage and integrator assembly used for the measurement of specimen inductions are shown in figure 5.7. In combination with the data acquisition ADC, the mechanism can be operated in two ways. In the

first, the nulling reset switch, (sw1) across the integrator can be reset at the end of

each data acquisition step of the ADC and the measurement stored at the computer.

In the second, the data station can be set to acquire a continous stream of data at a

maximum rate of 20 msecs per datapoint and the data stored in its 2 kbyte buffers for

later retrieval. In this mode, more appropriate for monitoring comparatively rapid

events, the integrator null switch is reset at the start and end of each data acquisition

process. This second mode of operation has been used predominantly for

measurements. It is an acknowledged problem that output drift is inherent with

hardware integrators, although a linear drift correction is often found to be adequate

during the data analysis. Figure 5.8 shows the departure from linearity of a corrected

integrator drift measurement, acquired on the 0.1v range, (32768 bits = 0.1v), of the

data station. This measurement again represents the totality of the induction

uncertainty as it includes the search coil plus an iron, (Fe(2)), specimen held at a

constant field in the search coils. (Directly converted, this represents an induction

uncertainty within ±0.2mT under the specific measurement conditions). It is evident

then, that a combination of drift and the field instability sets the limit on the

available magnetic moment resolution for measurements in this mode. Induction

resolutions are dictated by specimen size and differential permeability and are

generally observed to be between ±0.15 and ±4mT. Figures 5.9a and b, show the

gain for the amplifier over large and small inputs. Linearity to within ±0.5% of

mean gain is evident for input signals over 10 μ volts, with larger uncertainties at

very low levels contained within ±10%. (The associated larger errors here are a

reflection of the uncertainty in the calibration process). In normal operation the

pre-amplifier sees the full range of these input signals.
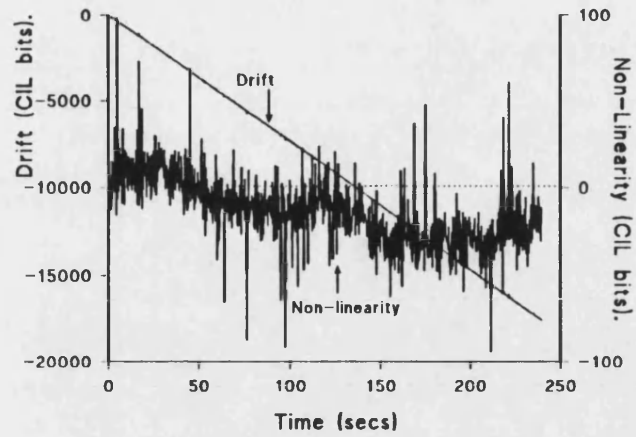
Figure 5.8: Integrator drift against time. The departure from linearity is indicated on the right-hand scale. Specimen (Fe(2)) in situ., field held constant.
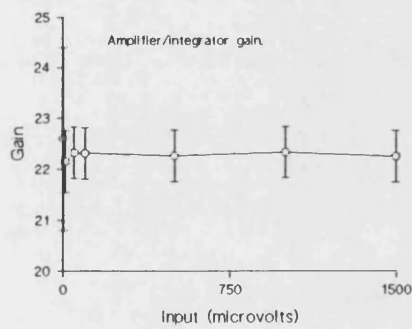
Figure 5.9a:Pre-amplifier gain.
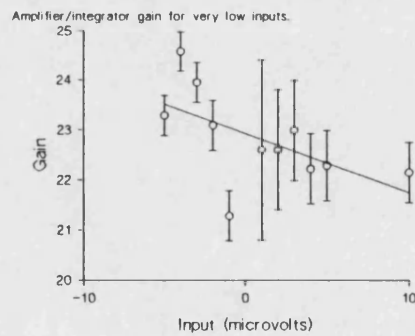
Figure 5.9b: Gain for very low inputs.

66

The CIL data station, (supplied by Control Interfaces Limited), consists of differential analogue input channels with three sensitivity ranges, $\pm 10v$, $\pm 1v$, $\pm 100mv$. These take the various instrumentation outputs from around the system and resolve them to 15 bit resolution, (32768 units). One $\pm 10v$ analogue output drive is used to control the power supply delivered current, as previously mentioned, over ± 32768 bits. Another is used to set the integrator null switch. In continous acquisition mode, 2000 data points can be stored across all inputs at the maximum and minimum rates of 10msecs and 0.54secs per data point. For multi-channel use, data acquisition is simultaneous across all channels such that for the commonly used two channel techniques of this study (B/H, B/σ ,B/T), this translates to 20msecs and 1.08 secs per point, or acquisition time spans ranging from 10 seconds to 9 minutes.

Figure 5.10 gives a typical B/H profile obtained by this system. The measurement technique, controlled through the software, involves,

i	Specimen demagnetization as described in section 5.2.6.
ii	Open integrator null switch. (Default condition closed).
iii	Start analogue acquisition at desired rates and ranges.
iv	Ramp fields over desired intervals.
v	Reset field to zero (if required). Close integrator switch.
vi	Retrieve data from station buffers.
vii	Apply linear drift correction: VDU screen plot.
viii	Store on floppy disk, if required.

Typically, the acquisition and storage of a full B/H profile requires around two minutes. During the course of the study it has been occasionally more fruitful to modify the above routine to allow real time display of the acquired induction results, especially in long duration measurements. The above technique is, however the dominant one. The raw data stored is converted to its physically meaningful parameters through later manipulation.
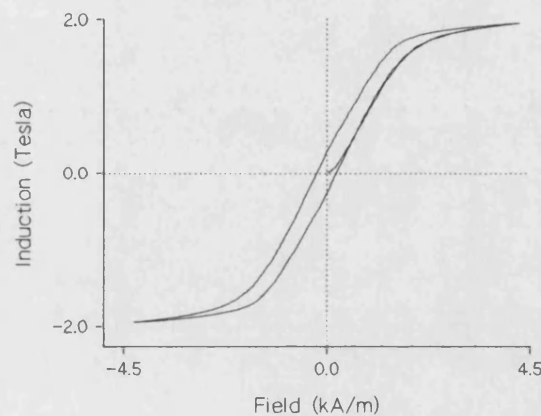
Figure 5.10: Typical hysteresis loop profile. (Iron tube, under compression).

B/H measurements have been performed on the 'biaxial' HY80 specimen by a different method. With this specimen, the field and the stress can be imposed in orthogonal directions through use of coils wound longitudinally (toroidally) along the specimen sides, as shown in figure 5.3. This applies to both the field generating coil and the induction-measuring search coil. In this technique it is not possible to cancel the field-generated emf, (electro-motive force), through use of a balancing

68

counter-part, although this can be shown to be a small contribution. Set against this is the beneficial absence of demagnetizing fields which are present in the uniaxial specimens. B/H measurements are conducted in a similar fashion, the induction and field values obtained from a knowledge of the specimen dimensions and the number of respective windings.

5.2.2 B/σ measurements

To allow specimen loading, the stress-insert shown in the experimental general arrangement (figure 5.4) was constructed. This is shown in more detail in figure 5.11. The assembly is constructed from low magnetic permeability components throughout, and designed such that it sits within the bore of the existing magnetic field solenoid, allowing the specimen to maintain its nominal location.
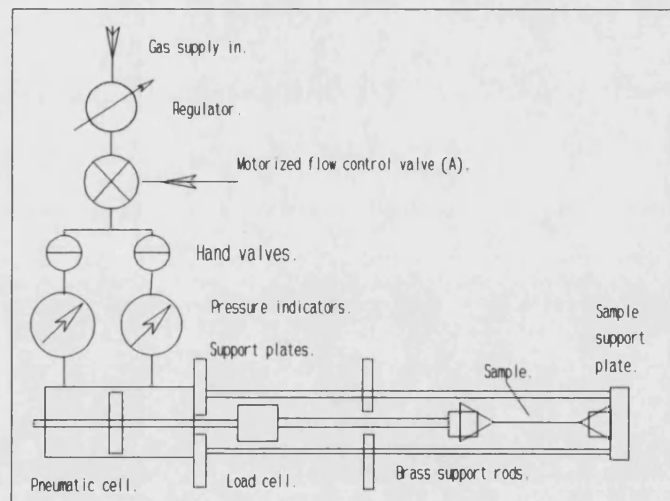
Figure 5.11: Mechanism for providing specimen tensile or compressive loads.

The stress-insert operates by pneumatics, in common with systems used by other researchers in this area, (Schönbachler and Atherton, 1988). Co-axial and external to the solenoid, a dual-action pneumatic cell is supplied with compressed nitrogen or air, to either compartment, from a regulated gas source through a series of manual and automatic valves. The force generated is imparted to the specimen by an extension to the thrust rod, joined at the in-line load cell (supplied by RS components Ltd. (RS 645-811)). Load release can be implemented through either equalling the gas pressures on each side of the pneumatic cell or by isolating the active section and allowing pressure reduction through gas loss at bleads at the cell. Specimens are braced at each end within the insert with their search coil mounted on the insert support struts. In this way specimens can be subjected to single or multiple tension or compression cycles.

Specimen stress levels are calculated from a knowledge of the specimen cross-sectional area and the level of the applied load. Two types of stress-related measurements are of interest in this work. In the first, the load is held constant by application of the desired gas pressure to one side of the pneumatic cell, whilst the general field-induction profiles are obtained. These experiments yield useful information concerning the changes in the sigmoid shape with compressive or tensile loads, quantified by variations in remanent, coercive and maximum induction values, as well as changes in the permeability of the material. Such information features prominently in N.D.E. (non-destructive evaluation) studies (Langman, 1990). Second, and more predominant in this work, the induction changes observed with the application of stress at constant background field from discrete points within and

around a specimen hysteresis loop have been measured. Such measurements are of interest when considering the long term magnetic instability of structures. In each measurement type, the output from the load cell is amplified and relayed to one analogue input channel of the data station and a digital voltmeter, so that values can be either automatically or manually recorded.

The active components for the force measurement are the load cell and its amplifier. The cell consists of four strain gauges arranged in a "Wheatstone" bridge configuration. The low drift, linear amplifier, (RS 435-692), is specifically designed for strain gauge measurements, set up in this circuit for a calibration $2mV \equiv 1$ Newton as indicated in the linear load/output profile of figure 5.12. The inherent stability of the devices far exceed the stability that can be achieved during an iso-stress measurement as indicated in figure 5.13. This data shows the force stability in Newtons that is measured at the load cell over a period of four minutes at both zero load and 250 Newtons, shown for comparison on the same axes. Some settling of the mechanism as the full load is achieved is indicated by a small decline in the force soon after it is established. For the specimen used in this experiment, a change of one Newton represents a stress drift of 0.5 MPa. As this was one of the smallest section samples used in the study, it is indicative of the worst case stress uncertainty. It is evident that sample loads can be known to a precision of $\pm 0.1N$, with stabilities falling within the range $\pm 0.5N$ over time periods considered quite long compared to normal measurement conditions.
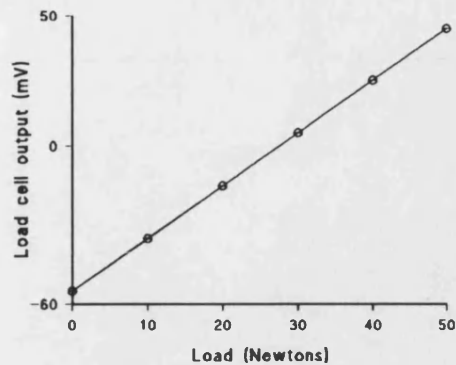
Figure 5.12: Load cell output calibration
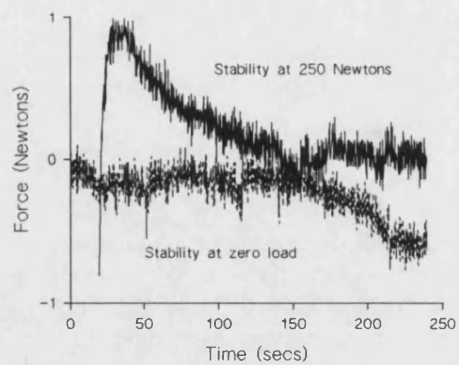
Figure 5.13: Load cell and stress-insert stability.

For the dynamic stress measurement, the quickly varying loads are measured simultaneously with specimen induction changes. The operational techniques for data acquisition mirror the B/H process with load replacing field as the applied variable. A typical measurement sequence would include:

i   Demagnetize the specimen, (section 5.2.6).

ii   Choose the software option which allows collection of B/H data. Instigate data collection and arrive at the field/induction value of interest through the appropriate field sweep intervals. Hold the field constant.

iii   V.D.U. plot. Record the data.

iv   Choose the software option which allows collection of B/σ data. Instigate data collection and operate the relevant valves in the gas handling circuit, (either manually or automatically), in order to subject the specimen to the desired stress levels or cycles.

v   V.D.U. plot. Record the data.

72

Contained within this process are the options of measurement interval, rate and sensitivity. Figure 5.14, shows a typical data set for the above process. The specimen is seen to start in the demagnetized condition and arrive at a point close to positive remanence through the appropriate field sweep intervals. The field is then held constant whilst the specimen is subjected to a single tension and release cycle shown, for convenience, on the same axes and on the same induction scale. It is interesting to observe in this data set how the material absolute induction value changes significantly with the application of tension in a sense consistent with that of the previous field sweep. This will be expanded upon in section 6.
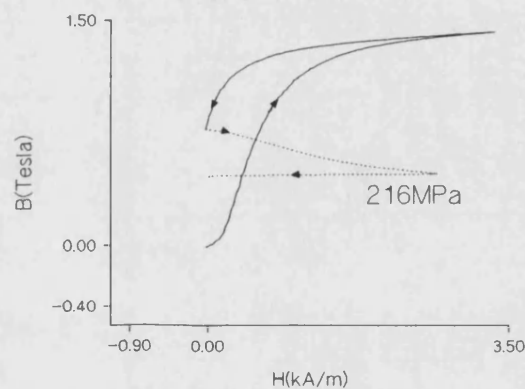
Figure 5.14: Typical B/σ profile from a major loop point for HY80(2).

During this study the effects of changes in the rate of application of stress were also investigated. This involved controlling and measuring the applied stress rate of change to the best precision available. Manual control of the gas handling system was abandoned in favour of the finer control allowed by use of the stepper-motorized gas inlet valve shown in figure 5.11, driven by an analogue output channel of the

73

data station and the relevant software commands. For the longest duration induction measurements undertaken in this study, the voltages induced in the specimen search coil became very small. Under these circumstances it was found more appropriate to use the fluxgate magnetometer to measure the specimen near field and cross-calibrate it against known induction changes as measured by the integrator system. This applied solely to the case of constant field, variable stress or variable temperature measurements, the so-called B/σ or B/T processes. In this mode of operation the output from the magnetometer forms the 'induction' input to the data acquisition system. The CIL would be prompted into either acquiring a stream of data (allowing a nine minute maximum duration of the experiment) or into point acquisition, depending on the time period of the stress interval. The later option was used when full load was reached in times greater than nine minutes. For reference, the investigations into the influence of varying the rate of application of stress to specimens did not reveal any consistent variation in the accompanying induction changes. For stress application rates in the range from 0.03 MPa/s to 20 MPa/s measured induction variations fell within the general uncertainty levels. Consequently, the results of such tests are not reported in this thesis.

5.2.3 *B/T measurements*

The effects of changes in temperature over the range 7°c to 80°c on specimen magnetic behaviour have been investigated. This has involved measurement of the overall hysteresis loop parameters as a function of temperature, as well as a study of the induction changes that can be observed of specimens from discrete points within

or around their B/H profile. Uniaxial specimens of HY80 and iron have been examined in this way.

The specimen is held in its usual location by the stress-insert attachments within the solenoid and specimen search coil. Temperatures above ambient are achieved by passing currents, up to a maximum of 1.5 amps, through a tightly wound, non-inductive, 30 swg, (Standard Wire Gauge), constantan heater placed in intimate contact along the length of the specimen. Specimens below ambient have featured less prominently in the investigation. They have been achieved by use of a Peltier cooling stage thermally anchored between the specimen and an aluminium heat sink. Forced convection near the sample area improved the base temperature achieved in this way. During separate tests, energizing either the constantan heater or the Peltier unit was not observed to have a measurable effect on the local field, although some magnetic component within the Peltier stage was observed to give rise to a small d.c. field offset.

Specimen temperatures are measured by the output from a copper-constantan thermocouple. This is wired in a re-entrant manner along the sample length on the opposite side to the heater and placed in contact with the specimen near its mid-point. The whole assembly is shrouded in a combination of P.T.F.E tape and Kapton sheet to limit heat loss to the immediate environment. As with the B/σ measurements, data collection mirrors the B/H process but on this occasion, temperature replaces field as the applied variable, the thermocouple emf forming an input to one of the data station analogue input channels.

Along with the iso-thermal hysteresis loops, the induction changes from discrete points are of interest. For this, a measurement sequence would include,

i   Demagnetize the specimen, (section 5.2.6).

ii   Instigate data collection and arrive at the required B/H values. Hold the field constant.

iii   V.D.U. plot. Record the data.

iv   Instigate data collection of temperature and induction. Energise/de-energise the heater/cooler in order to subject the specimen to the desired temperature intervals.

v   V.D.U. plot. Record the data.

Figure 5.15 shows a typical result obtained by changing the temperature of an iron specimen after arrival at a major loop point near the coercive field.
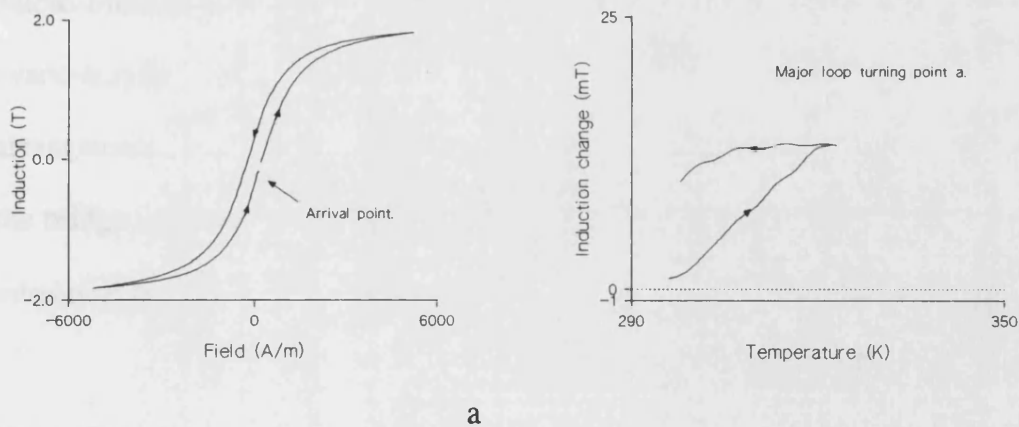
Figure 5.15 a & b:Induction change induced by increasing the temperature from a major loop point for Fe(2). a. Arrival at major loop point. b. Induced change.

76

5.2.4 λ/H, (magnetostriction), measurements

Magnetostriction measurements have been performed on several uniaxial-type specimens. Two measurement technique methods have featured in this work. In the first case, specimen changes in length have been measured using a fibre-optic dilatometer system described elsewhere, (Squire and Gibbs, 1987). This high-precision technique, specifically designed for amorphous ribbons, allows unrestricted sample strains to be measured to better than 1 part in 10^8 with minimal preparation. During the earlier stages of the study, magnetostrictions of several specimens were obtained in this manner.

This technique does not easily lend itself to alteration of applied variables such as stress or temperature, as the specimen is required to remain undisturbed within the optical system. For this reason specimen magnetostrictions have also been acquired using more traditional, strain gauge, measurements. Strain gauges, (supplied by Micro-Measurements Inc.), are bonded to the surface of the samples using cyano-acrylic (super-) glue. The gauge forms one arm of a Wheatstone bridge arrangement in the usual manner for such measurements. The amplified output from the bridge is fed to an analogue input channel of the CIL with acquisition techniques mirroring those of B/H but with strain as the measured variable.

Using this technique, it has proved possible to measure magnetostriction for uniaxial samples whilst placed within the current experimental rig. Magnetostriction measurements have then been made as a function of field at various levels of stress
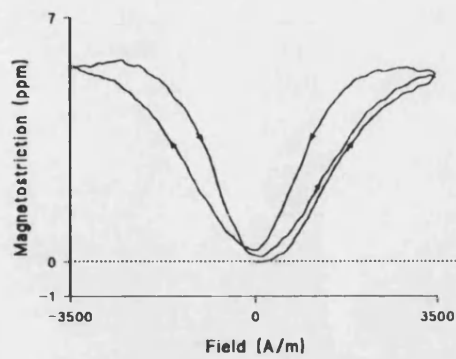
(a)
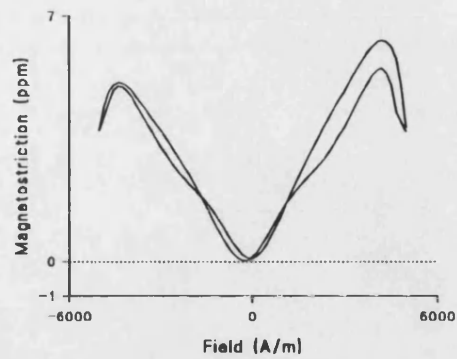
(b)
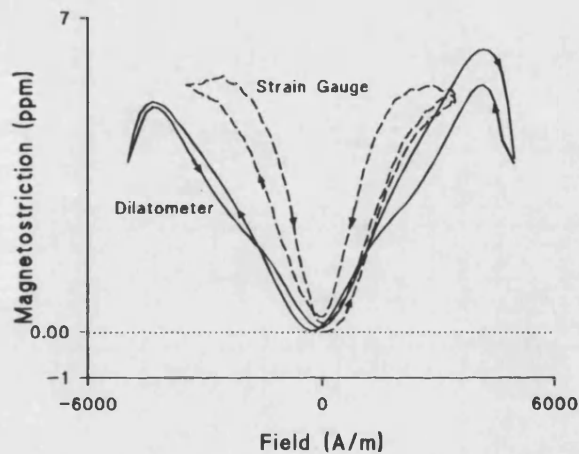
(c)

Figure 5.16 a, b & c: Comparison of zero stress magnetostriction profiles obtained from Fe(2) using (a) strain gauge and (b) dilatometer techniques. The dilatometer test shows how polycrystalline iron demonstrates (relative) contraction at high fields. The strain gauge method yields a slightly noisier result. In (c) the profiles are plotted on the same axes for reference.

and temperature. Figure 5.16 shows a typical strain against field profile for Fe(2) taken around its hysteresis loop from demagnetization and compares this to the equivalent data from the fibre-optic dilatometer. Some degradation of the quality of

the result obtained from the strain gauge technique is offset by the convenience and wider allowable variation of applied parameters.

5.2.5 *Barkhausen count*

The discrete induction changes that occur at the finest levels in a ferromagnet during variation of an externally applied variable can be quantified through acquisition of the high frequency components in the measuring device, (Jiles 1989). In this study, these changes have been monitored by collection of search coil voltages in the frequency range 100 Hz to 100 kHz, the acquired RMS voltage being fed to the relevant analogue channel of the data station. The magnitudes of the RMS voltages are dependent on the rates of change of the applied field or stress so that comparative studies must constrain these within close limits. Field-induced Barkhausen noise has been acquired at different iso-stress conditions using a field sweep rate of 330 A/m/s. A limited number of stress-induced Barkhausen data sets were examined but are not reported in this thesis.

5.2.6 *Demagnetization processes*

At room temperatures, specimen demagnetization can be achieved through either large mechanical shock or by subjecting to an initially large, but gradually decaying, sinusoidal external field. Both processes are accepted as producing a randomized moment direction within the body of the material. A truly disordered state of the ferromagnetic domains is difficult to achieve, so one has to decide an acceptable level

of demagnetization for engineering and measurement purposes. It is worth noting at this stage that whilst it is generally accepted that a good demagnetization process has the effect of largely erasing the previous magnetic history, a macroscopically measured zero state may not be defined by a unique domain configuration and as such may not always give are producible start condition. Such a condition is more likely to be satisfied at a positive or negative saturation state. Some results of chapter 6 will add weight to this argument, with the discussion of section 6.2.2.3, (figures 6.39) describing excursions to saturate conditions and the impact of this on subsequent magnetic history.

In this study, sample demagnetization has been achieved by subjecting specimens to decaying oscillatory fields. This involves the imposition of an initial field large enough to bring the sample to either saturated condition (in this case usually the maximum available power supply current), and the gradual reduction of this field to zero as it oscillates through all positive and negative values. An oscillation frequency of 1 Hz with a step interval of 20 A/m, (from a peak of 7580 A/m), allowing demagnetizations within seven minutes was found acceptable for this work.

The efficiency of the process can be measured in two ways. First, the symmetry of the hysteresis loop taken from demagnetization can be measured to the best available resolution of the instrumentation. With care taken to adjust the zero point to take into account any long term shifts in the background fields, demagnetizations to within $\pm$ 1 mT would be typical of demagnetization reproducibility for the uniaxial specimens.

Second, it is widely accepted that stresses within the elastic limit imposed on a perfectly demagnetized specimen will not produce any change in net induction as the initially randomized moments align parallel and anti-parallel to the stress axis, (Cullity, 1972). Any observed induction deflection can then be taken as a measure of the inefficiency of the demagnetization process. This second method has proved useful in this study. Figure 5.17 shows the very small change in induction that has been observed of uniaxial specimen HY80(2) subjected to tensile stress after a demagnetization process. The observed deflection is indicative of the degree of difficulty associated with producing a perfectly neutral state.
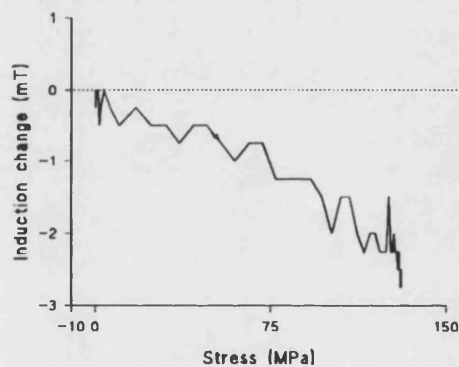
Figure 5.17: Induction deflection observed from HY80(2) after a demagnetization process.

5.2.7 *Anhysteretic curve production*

The anhysteretic curve represents the B/H profile that would be described by a specimen which had no obstructions to domain wall motion, (Cullity, 1972: Atherton and Ton, 1990), effectively the equilibrium condition for the range of applied background fields. Accordingly, the state may be achieved in a similar fashion to the

demagnetized state, namely the imposition of mechanical shock or decaying sinusoidal field in the presence of a constant offset field. The field variation technique has been employed in this study.

Each anhysteretic curve has been achieved by the point-by-point measurement of the final induction-field co-ordinate produced by the oscillatory process, with the decaying field settling at the desired background value. These points are calculated from their measured distances from the known positive and negative maximum induction values taken as the specimen is subsequently swept through its B/H profile. This proves to be a lengthy process, with the generation of a complete iso-stress anhysteretic profile taking several hours. Figure 5.18 shows the zero stress curve generated for the biaxial HY80 specimen.
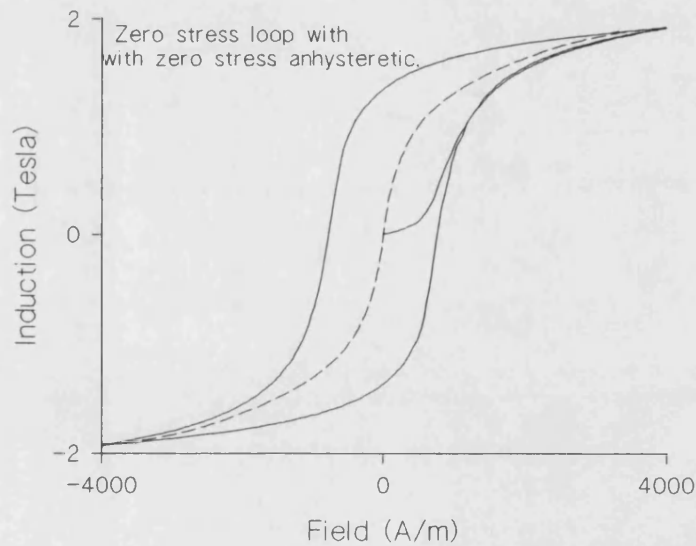
Figure 5.18: Typical anhysteretic (dashed) curve produced for biaxial HY80.

6.   Results and discussion

6.1   *General magneto-elastic characteristics: Iso-stress hysteresis loops*

As discussed in chapters 3 and 4, the changes observed in the magnetic properties of a material when acted upon by a load can be described, (in part), in terms of the magnetostriction constants for that material. In polycrystalline specimens, an averaged value of the magnetostrictions in the three principle crystallographic directions, as described by Callen and Goldberg, (1965), can be used as a guide to the expected bulk magnetostrictive constant in isotropic materials. It is worth bearing in mind though that texture, where introduced during material fabrication or treatment, can have the effect of distorting this value.

Specimens which possess a net positive magnetostriction behave (in part) in an opposite fashion under stress to those showing a negative net magnetostriction. This point is drawn out figures 6.1-6.2. The magnetostriction of the polycrystalline nickel specimen, measured on the fibre-optic dilatometer, is observed to be negative throughout the field range, a maximum value of around -34 ppm comparing well with tabulated data at that field. The behaviour of the overall hysteresis loop, shown in 6.1b indicates a shearing of the sigmoid along the field axis with increasing tension. A decrease in both the remanent and maximum inductions is accompanied by an increase in the coercive field, as shown in figures 6.1c and 6.1d.
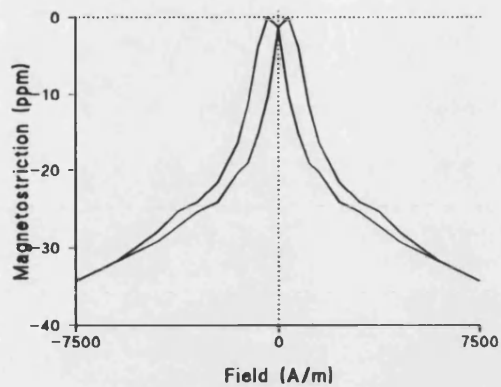
a
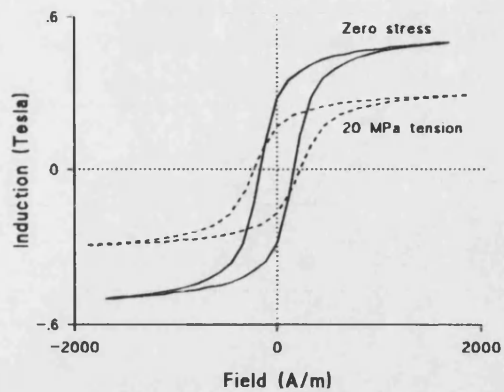
b
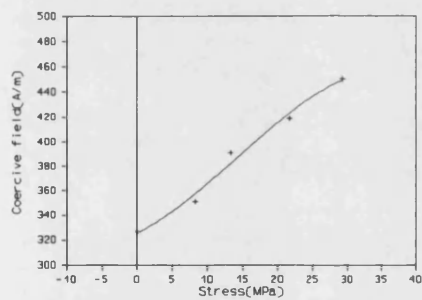
c
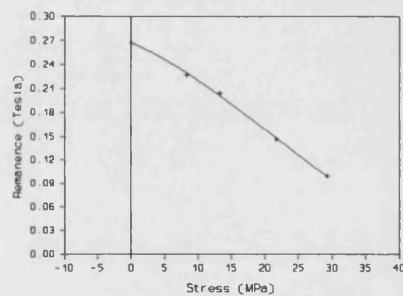
d

Figures 6.1 (a): (Top left) Polycrystalline nickel magnetostriction. (b): (Top right) Performance of the iso-stress hysteresis loops in tension. c: Change in coercive field with tension. (d): (Bottom right) Change in remanence with tension.

In contrast to this, the behaviour typical of polycrystalline, positively magnetostrictive materials is demonstrated in figures 6.2. HY80 possesses a positive magnetostrictive

84

profile throughout the most of the available field range when in the cold-worked condition. Shown in figure 6.2a are the magnetostriction versus field profiles for the HY80(1) specimen in cold-worked and freshly annealed conditions. The changes in the sigmoid for this material in the cold-worked condition are marked by increasing remanent and decrease coercive values with increasing tension for the range of fields used. The reverse trends are observed for this specimen in compression. These points are demonstrated in figures 6.2b and 6.2c.
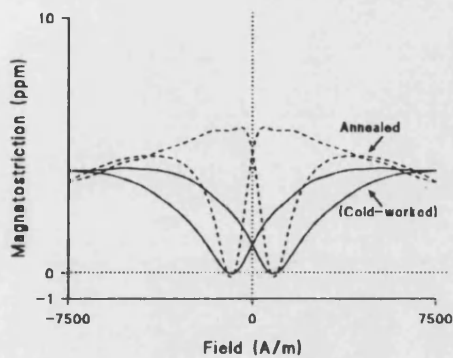
a
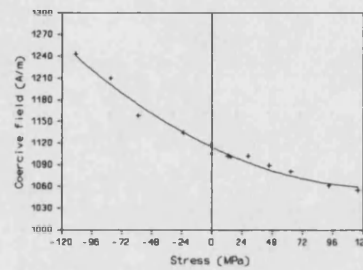
b
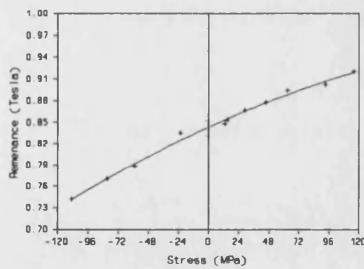
c

Figures 6.2 (a) Magnetostrictions (HY80(1)) shown for cold-worked and annealed state. (b) Coercivity against stress. (c) Remanence against stress.

85

The sense of the iso-stress change in the induction parameters agrees with that reported by other workers in this area (Pitman, 1990). Changes in the stress sensitivity of these parameters are observed for various states of cold work for a particular material. This implies that the results shown in the above figures for nickel and the martensitic HY80 are not intrinsic material characteristics but largely a reflection of the state of anneal. One of the prominent features in this respect for iron-based materials is the presence of the Villari reversal, the process in which the net magnetostriction is driven to negative values. The field at which this occurs is known to be stress sensitive, (Cullity, 1972). Compression has the effect of increasing the field required to instigate the reversal, with tension giving the opposite effect, large enough tensions being capable of driving the magnetostriction to a wholly negative value for all fields. Cold-worked specimens are most likely to be in a state of residual compression, a condition which renders the measurements shown in figures 6.2b and 6.2c characteristic of positively magnetostrictive materials over the whole of the available field range.

After an annealing process, the allowed relaxation of the internal stresses gives rise to a magnetostriction profile for HY80(1) consistent with that expected of iron-based specimens. Whilst the applied fields of figure 6.2a are not large enough to cause an overall contraction of the annealed specimen, the change in the sense of the differential magnetostriction for fields greater than 6000 A/m is indicative of the

earlier onset of the negative-going trend.

For completeness, it is worth noting the magnetostriction of one of the iron specimens. Fe(2) in the as-received state (prepared directly from the delivered sheet), is observed in figure 6.3 to show some relative contraction at high fields without the need for an annealing process. This may be a reflection of a less rigourous preparation than HY80, producing less cold-working. The specimen is simply cut from the as-delivered sheet as compared to the grinding and milling preparations required for the HY80. Alternatively, it may be a reflection of the lack of localised internal strains which, in the case of HY80, result from the quench and temper process. Some of the magneto-elastic characteristics shown for Fe(2) sheet in the next section are consistent with the negative-going magnetostriction at high fields.
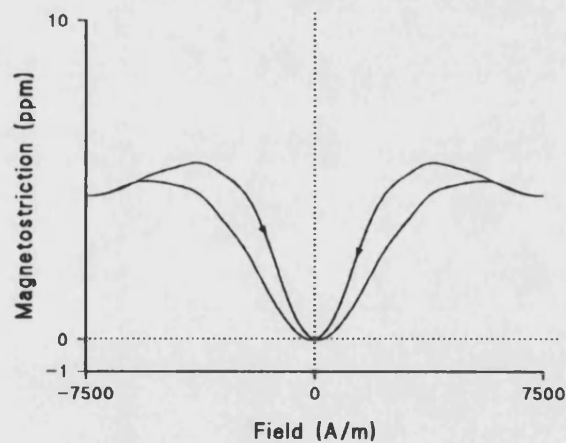
Figures 6.3 Magnetostriction profile for polycrystalline iron (Fe(2)).

87

A fuller study of available data indicates significant variation in the reported magnitude of the stress sensitivity of the coercive fields in polycrystalline specimens. In principle one may expect that, for magnetostrictive materials, the increased anisotropy induced by stress should increase the reverse field necessary to return the induction value to zero. The experimental observation of a decreased coercive field with tension in experiments with co-axially applied field and load on iron and steel would appear to be in contradiction to this. It is important to note though, that stress acts on both the processes of domain wall motion and moment rotation. For iron and steel data presented here, it seems likely that reduced coercive fields in tension, (converse for compression), are associated with complexity in domain wall motion processes. Using an illustration of the effects of tension on a 180° wall, Garshelis (1993), has suggested that a decreased coercive field in tension is a result of the lower fields required to allow domain walls to break free from their various pinned sites as the more favourable domain aligns even closer to the field direction as stress is applied. Associated reduction in moment orientation dispersion is also seen to act to reduce coercive field, so explaining the non-monotonic change with compression. Whilst a comprehensive argument for the observations is not yet complete, it is clear that such processsess, where they exist, must counter the stress-induced anisotropy. In the materials of this work, such effects are indeed dominant.

Finally, the iso-stress hysteresis loops for the bi-axial HY80 specimen are shown in figure 6.4. The large cross-section ($9.29mm^2$) of this specimen restricts the available loads to a maximum of ± 50 MPa. Nonetheless, this is sufficient to observe the general change of the sigmoid with tensile or compressive forces. Remembering that

in this specimen the field and induction coils are wound orthogonal to the field axis, one can see that the roles of tension and compression are effectively reversed compared to the observations of the uniaxial specimens. This point should be borne in mind when viewing some of the data for this item in the subsequent sections.
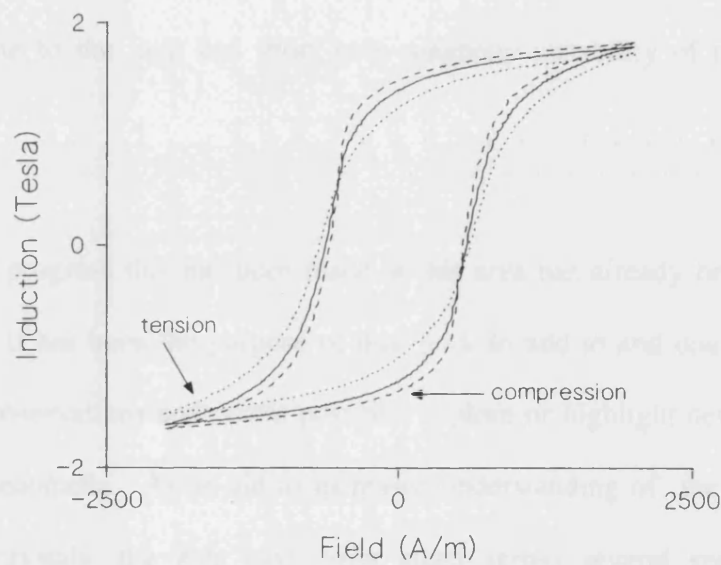
Figure 6.4: Biaxial HY80 iso-stress profiles at zero and 50 MPa tension and compression.

6.2 *Iso-field stress-induced induction changes*

Studies of induction changes observed from discrete points within or around the specimens' magnetic profile feature predominantly in this work. As described in section 5, this involves taking a chosen specimen through a known magnetic cycle and then changing the applied stress from zero as the field is held constant. It is hoped that data collected in this manner will allow increased understanding of the processes which contribute to the long and short term magnetic instability of materials and structures.

The significant progress that has been made in this area has already been discussed in chapter 4. It has been the purpose of this work to add to and confirm existing experimental observations and where possible, explore or highlight new or hitherto unexplained phenomena. As an aid to increased understanding of the mechanisms active in polycrystals, the data have been taken across several specimens and materials. For convenience and clarity, the observations reported here are separated into those made from relatively simple and those made from more complex magnetic histories.

6.2.1 *Simple magnetic histories: induction changes from initial curve and major loop points*

6.2.1.1   Initial curve behaviour across several polycrystalline samples

In order to demonstrate some of the general characteristics of stress-induced induction changes observed from discrete points within specimen induction-field profiles, it is perhaps convenient to start with the example of the uniaxial nickel specimen taken to points along its initial induction curve. The material was received in a mechanically hard condition. As the magnetic properties of nickel are highly dependent on the mechanical state, after the specimen was cut from the as-received sheet, it was annealed at 1100°c in a purifying atmosphere of hydrogen gas. This renders the specimen both mechanically and magnetically soft, suggesting that domain wall motion through the specimen will be less restricted than for the cold worked state. Unfortunately, it proved difficult to maintain this highly annealed state, such that in common with many recorded observations on nickel specimens, the data reported here is for a specimen slightly cold-worked through handling. This is not expected to alter the main qualitative features of the results.

The magnetostrictive constants for the three crystallographic directions for nickel are of comparable magnitudes and all negative. This simplifies the magneto-elastic behaviour in two ways. First, the characteristics will not be greatly distorted by any anisotropies introduced during the sheet rolling or subsequent treatments. Second, the

so-called 'inverse' magnetostrictive (or inverse Joule) effect will not be complicated

by the polarity changes which can be observed of iron-based materials. As such the

specimen can be expected to demonstrate the processes involved in stress-induced

changes in polycrystalline materials in their simplest form.

In figures 6.5 and 6.6 the specimen is originally demagnetized. It is then taken to the

point of interest on the initial induction curve through the relevant field sweep, the

field being held constant as tension is applied and released, either singly or by

multiple cycles. In figures 6.5, the induction changes observed through single tension

and release cycles at increasing field values are shown. In this data set, which closely

resembles that of Craik and Wood (1970), some important principles are

demonstrated. It is immediately apparent that the net result of the stress cycle is a

significant (irreversible) alteration of the start induction value. Secondly, the

magnitude of the net change is dependent on the original location on the initial

induction curve. This is observed to rise to a maximum and then decrease to almost

zero at the highest field values such that the final stress-induced change is almost

closed i.e. 'reversible,' in character. In figure 6.6 the results of three tension and

release cycles from a point on the initial curve show that the large irreversible shift

in the induction is largely taken up in the early stage, with the third cycle giving an

almost closed 'reversible' induction change. (The second tension cycle in figure 6.6

shows the induction change from the end of the first cycle change. Likewise for the

third and second cycles). These results are consistent with the observations of the

workers discussed in chapter 4 (e.g. Schneider and Semcken, 1981), although their

data is predominantly for iron-based materials.
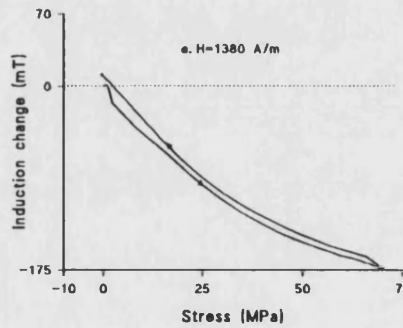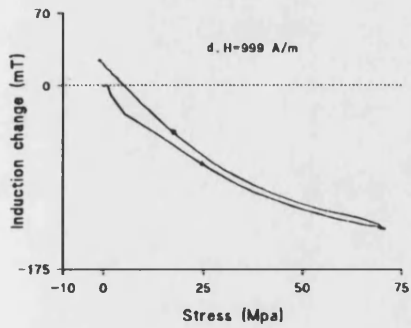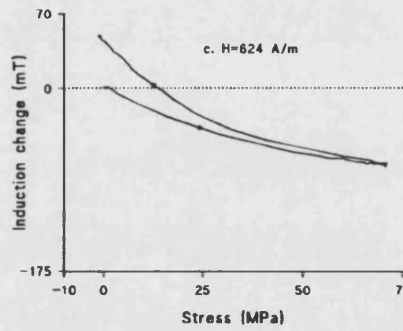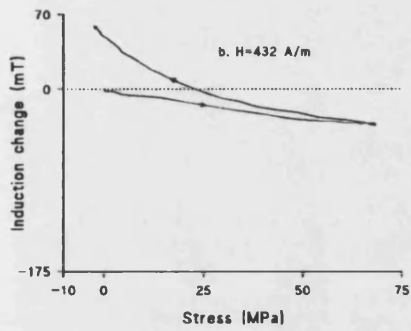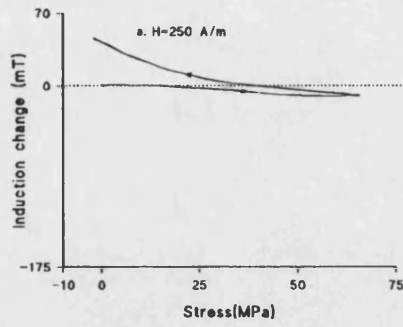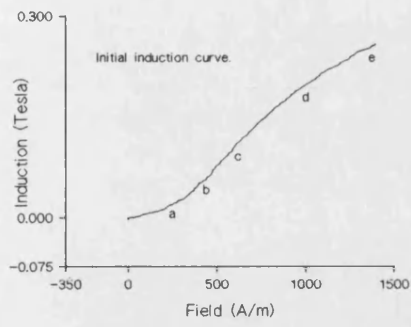
Figure 6.5: Nickel subjected to a single tension and release cycle at increasing fields along its initial induction curve.
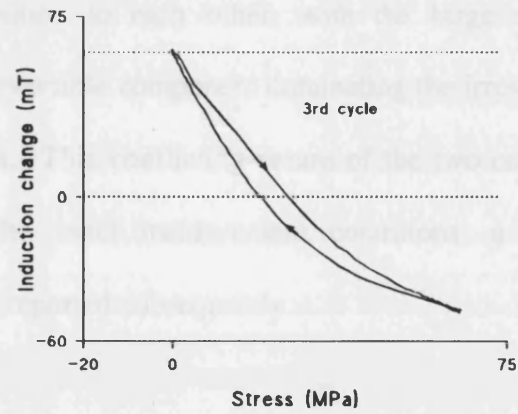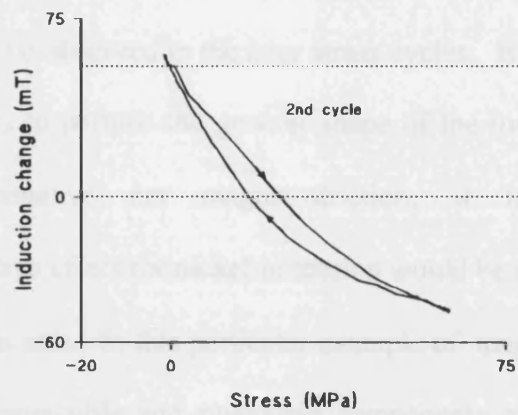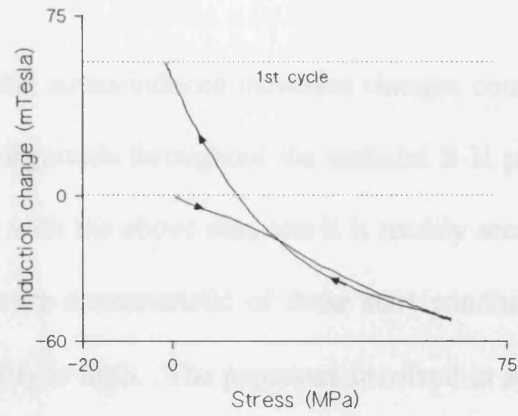
Figure 6.6: Nickel under multiple tension and release cycles from 500 A/m on initial curve (post-demagnetization), between points (b) and (c) in figure 6.5.

94

It can be concluded that stress-induced induction changes comprise two components, which may vary in magnitude throughout the material B-H plane. In the controlled conditions associated with the above data sets it is readily seen that large irreversible changes in induction are characteristic of those start conditions where the material differential permeability is high. The processes involved in such a change are active for the early stress cycles. The so-called 'reversible' component of stress-induced induction change can be observed in the later stress cycles. It is present at the earlier stages, acting such as to perturb the general shape of the induction change profile. Because of its negative net magnetostriction, it is expected that an inverse-magnetostrictive effect for nickel in tension would be a reduction in induction value along the tensile axis. In this particular example of magneto-elastic processes, it is seen that the irreversible and reversible components of the overall induction change act in opposition to each other, with the large negative-going inverse magnetostrictive or reversible component dominating the irreversible one during the application of tension. This conflicting nature of the two components of change is a consequence of the exact measurement conditions, a point which will be demonstrated in data reported subsequently.

The processes evident in the stress-induced induction behaviour of the nickel specimen can be observed in the other polycrystalline specimens, with the qualification that the relative magnitudes and senses of the active components can be different. HY80(2) was given a sub-critical (600-650°c for 3 hours) vacuum anneal, whereby residual stresses induced in specimen preparation are removed yet gross

metallurgical changes in the steel are minimized. This produced the main magnetic characteristic shown top right in figure 6.7. Following demagnetization by the usual process, it was then subjected to multiple compression and release cycles at points along its initial induction curve to yield the induction-stress profiles shown for points (a) to (e). The reader's attention is drawn to the fact that because of the large range of induction changes encountered in these measurements, the profiles can only be meaninfully represented on different axes scales. For clarity the second and third stress cycles are omitted from the plots. In each case, the closed loop which represents the fourth compressive cycle induction change is shown in its correct relative position along the induction axis. The fundamental mechanisms of an irreversible component, greatest in magnitude where the specimen permeability is high (near point (c)), and a reversible component measurable from the last compressive cycles are again evident, although the behaviour of the steel differs from that of nickel in two distinct ways. First, as the net magnetostriction for this specimen is positive for the range of fields and stresses presented, a reversible component which reduces the total induction value is seen in compression as opposed to tension for the nickel specimen. Second, the relative magnitudes of the reversible and irreversible components are such that with the full load applied, it is only at comparatively high field values, where the irreversible component diminishes, that the negative induction-driving mechanism dominates. These results, with their large, significant irreversible changes are a clear indication of the inadequacy of any induction-stress models which attempt to predict changes solely in terms of the magnetostriction constants. Such 'stress-effective' field treatments fail on two counts. First, such modelling procedures cannot accommodate these large irreversible
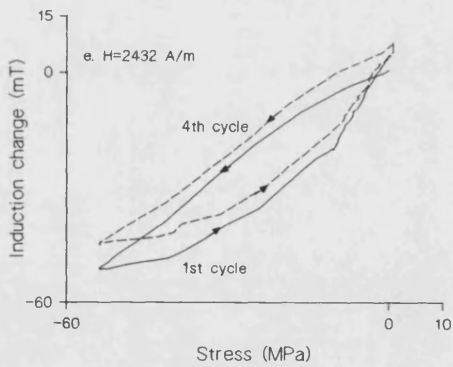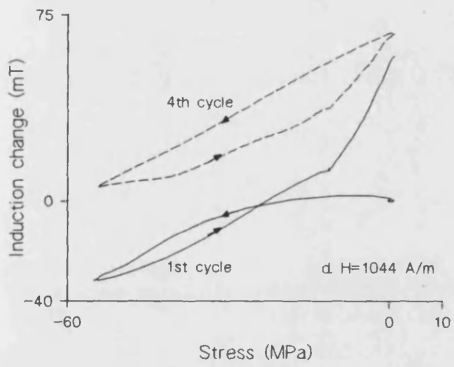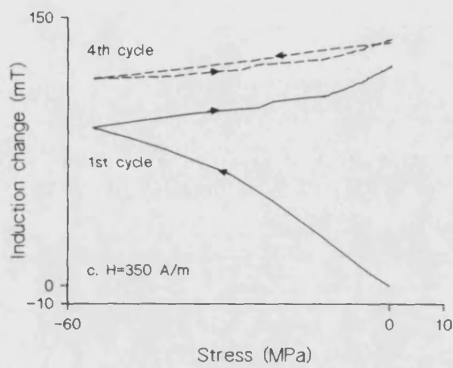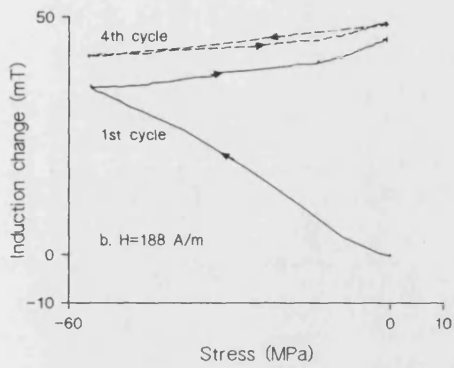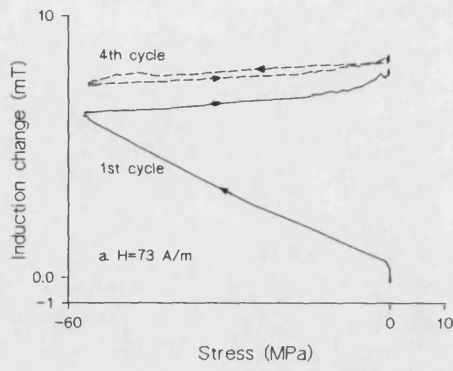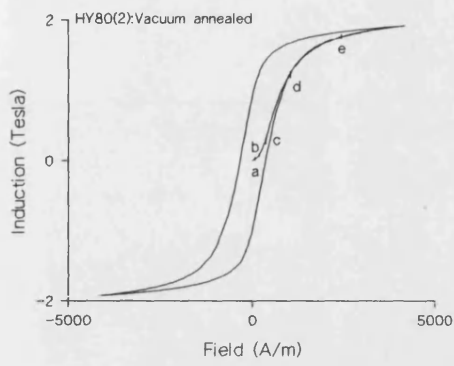
Figures 6.7 (Top left): Vacuum annealed HY80(2): main magnetic hysteresis loop. Induction changes with compressive cycles at indicated points on the initial induction curve are as indicated. For clarity, only the first and fourth induction changes are shown.

97

processes. Second, any attempt to describe the reversible component using only the saturation magnetostriction values in the traditional 'effective field' formula is also inadequate, as such a technique starts with the assumption of a constant value for the stress effective field (as contained in the works of Schneider and co-workers 1982, 1985). The data clearly show that the magnitude of the reversible component of induction change is a sharply changing function of the initial location on the B/H plane.

It can be shown, however, that the reversible component of induction change is intricately linked with the field-dependent average magnetostriction value for the specimen. In figure 6.8a the magnitude of this component is plotted against applied field for the data shown. In 6.8b the zero stress magnetostriction profile taken from demagnetization over a larger field range using the strain gauge technique clearly shows that the relationship between λ and the magnitude of the reversible component is not simply one of direct proportionality as suggested by 'effective field' formulae involving either the saturation or field-dependent magnetostrictions. The magnitude of the reversible component of induction change is observed to be highly field dependent, possessing a maximum at around 1600 A/m on the initial induction curve. In the equivalent field range, the specimen magnetostriction is observed to be wholly positive and not indicating relative contraction within 6000 A/m. For reference, figure 6.8c shows how the magnetostriction varies as a function of induction. In figure 6.8d the differential of magnetostriction with respect to induction is plotted as a function of induction along with its initial magnetostriction curve. Comparing this

98

to the next figure (e), in which the reversible component is plotted against absolute induction value, it is apparent that the profiles possess similar characteristics. This suggests that a description of the magnitude of the reversible change in terms of the differential magnetostriction will give a more satisfying result than descriptions using saturation magnetostriction or the field-dependent bulk value. This has been suggested by Sablik and others (1988). The relationship between $d\lambda/dB$ at zero stress and the reversible component magnitude is however, complicated by the stress-dependence of the magnetostriction. This may go some way towards explaining why the shapes of the profiles of figure (d) and (e) are slightly dissimilar. As explained in chapter 4, it is known that compressive loads force magnetostrictions to increasingly positive values, so it could be argued that this data indicates that this stress dependence should be accounted for in attempting to model the reversible component of induction change. The irreversible component of induction change taken for the HY80(2) specimen along its initial induction curve is shown for reference in figure 6.8f. This is observed to peak assymetrically at field values close to the peak in the material permeability along the initial induction curve.
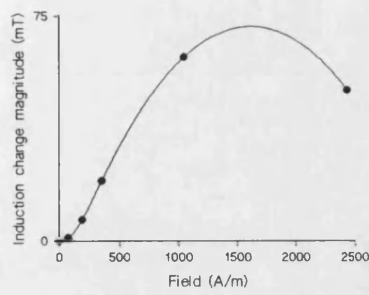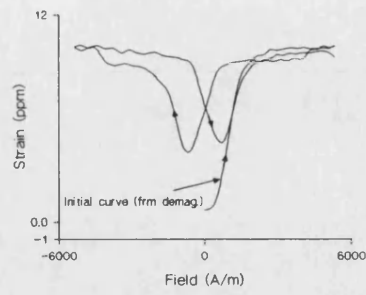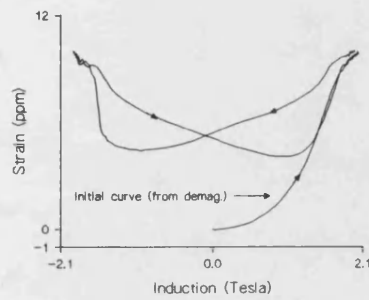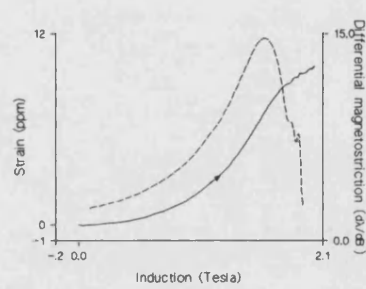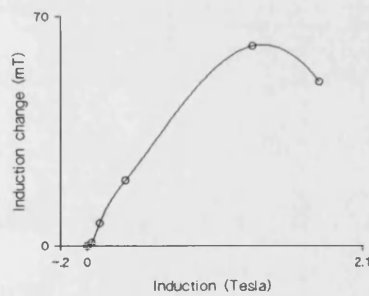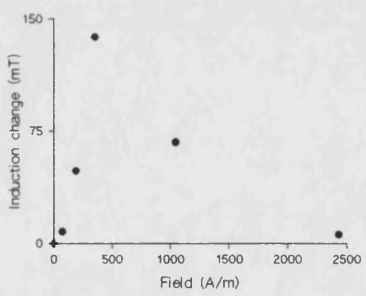
Figures 6.8a. Reversible component of induction change for HY80(2) along initial induction curve. b. Strain over a larger field interval. c. Strain against induction around the hysteresis loop. d. Differential magnetostriction (dλ/dB, broken line) plotted with the initial magnetostriction curve. e. Reversible induction change as a function of induction along the initial curve. f. Irreversible induction change for HY80(2) along its initial curve.

100

In the above data sets, an exact analysis of the apparent correspondence between the magnitude of the irreversible component of stress-induced induction change and the material permeability is hampered by the demagnetizing fields associated with the specimens. Use of the biaxial HY80 specimen overcomes this problem so allowing a more accurate determination of such a relationship. For a full description of this specimen the reader is referred to chapter 5, figures 5.3. The zero stress magnetic characteristic for the biaxial specimen, in cold-worked form is shown in figure 6.9. At the indicated locations along its initial induction curve the specimen has been subjected to a single tensile and compressive stress cycle to 50 MPa, the results of which are shown on the same scales in figures 6.10a-f. Trends similar to those observed of the HY80(2) uniaxial specimen are seen, with the roles of tension and compression reversed as the stress and field axes are perpendicular in these experiments. At all stages along the initial induction curve, tensile-induced changes are seen to be significantly smaller than compressive ones. In earlier works (Faunce, 1970) the converse of this effect was observed in specimens subjected to uniaxial field and stress. Such inequality was deemed then to be an inherent property of the process, but as will be demonstrated later this is an artefact of the exact measurement conditions. In each case the induced change is seen to go through a maximum at a field value close to the material permeability peak.
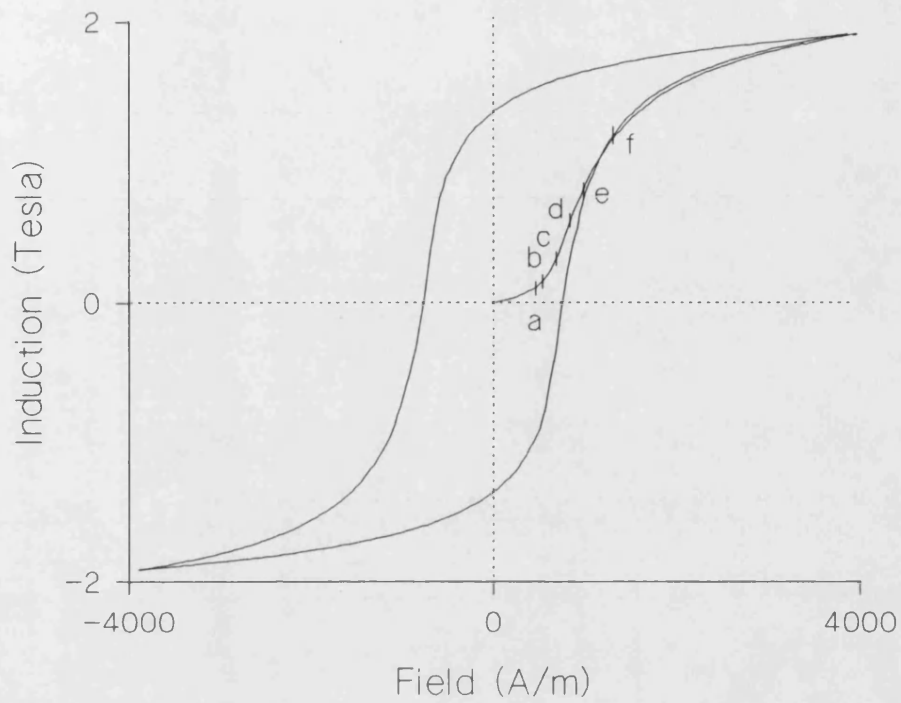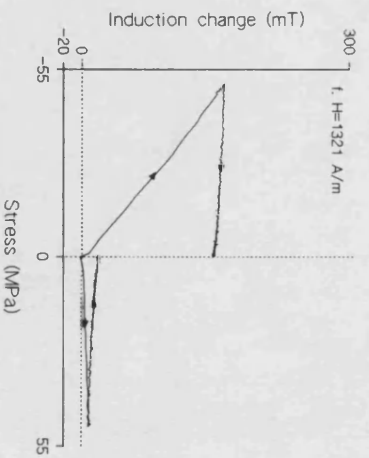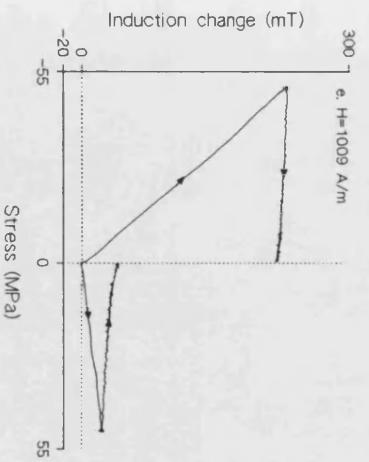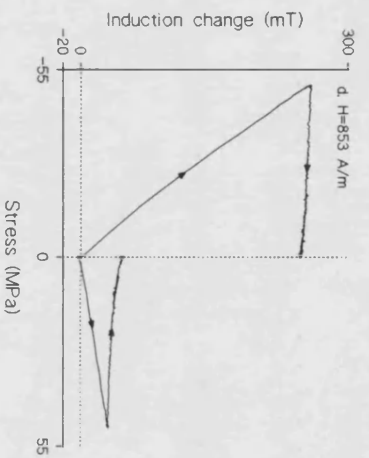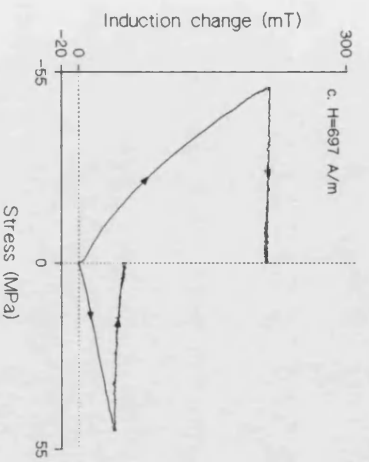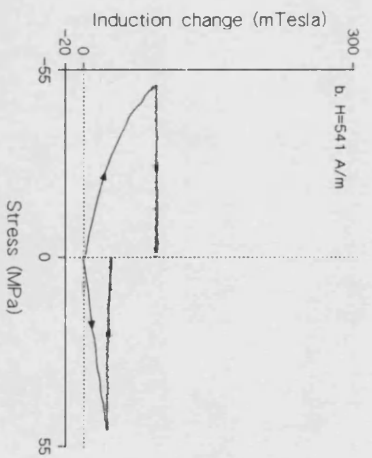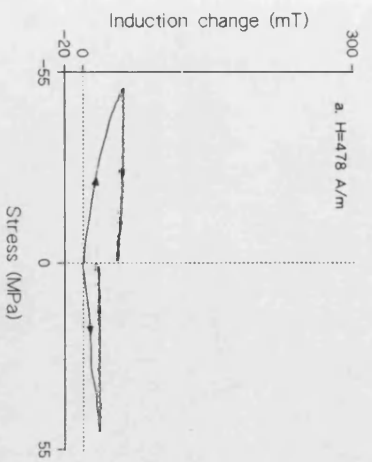
Figure 6.9: Biaxial HY80 specimen hysteresis loop from demagnetization.

Figures 6.10 a-f:Biaxial HY80 specimen subjected to single tension or compression cycles at points along its initial induction curve.

105

This is explored further in figure 6.11. The tensile and compressive induction changes are plotted on the same axes along with the material differential permeability, dB/dH. Close examination indicates that the compressive peak lies very close to the specimen differential permeability peak, whilst the lower tensile maximum appears to be shifted laterally along the field axis. Combined with the inequality of the tensile and compressive irreversible changes, this shift poses an additional problem in attempting to predict the magnitude of such changes. It has been suggested by other workers (Jiles-Atherton 1983, Schneider 1981), that the magnitude of the irreversible change of a tensile or compressive cycle will be proportional to the differential permeability at the onset of the stress process. (More precisely, the irreversible component of the differential permeability has been proposed as the prime indicator of subsequent stress-induced induction changes. In the material under investigation here, it can be shown that the reversible component is often a negligible correction in the range of fields studied). The (irreversible) permeability represents the rate at which the field is able to release domain walls from their pinned sites. As Brown (1949) and others have pointed out, stress acts as an additional pressure on domain walls, so it seems reasonable to conclude that the magnitudes of stress induced changes will be greatest where the greatest release from pinning sites has been instigated by the previous field sweep. To a first approximation this assumption is correct, but as figure 6.11 indicates, some modification of this idea is necessary to accommodate the mismatch which occurs between the differential permeability profile and the irreversible induction change profile as indicated by the lateral shift in tension shown in the figure. Data will be presented subsequently which demonstrate that such shifts also occur in compression.
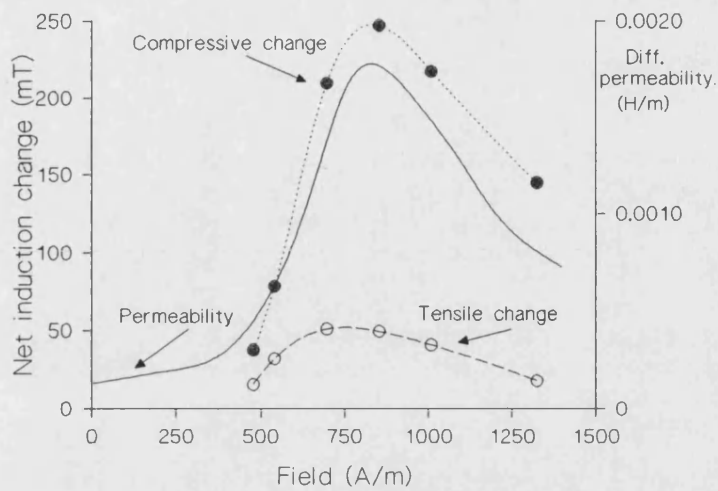
Figure 6.11: Tensile and compressive net induction changes from points along the initial induction curve for biaxial HY80. The differential permeability is shown as the solid line.

For completeness, the behaviour of HY80(1) (cut from a direction orthogonal to HY80(2) but in the same (rolling) plane) from a point along its initial induction curve is recorded. The micrograph (section 5.1.1,) for the steel indicated a martensitic structure which can be expected to show negligible mechanical or magnetic anisotropy. This is borne out to some extent by the data contained in figures 6.12a and b. The specimen is in the fabricated (non-annealed condition) producing the hysteresis loop of figure 6.12a. In 6.12b. the results of multiple tension or compressive cycles from the same point on the initial induction curve indicate magneto-elastic performance similar to that of HY80(2). The reversible components for each stress set are again shown in their correct relative positions along the

107

induction axis, with the intermediate cycles omitted for clarity. For the range of fields and stresses used in the collection of these data, the material net magnetostriction remains wholly positive, giving the expected 'inverse' characteristics of an increase of induction value with application of tension, with the reverse for compression, with magnitudes of the same order.
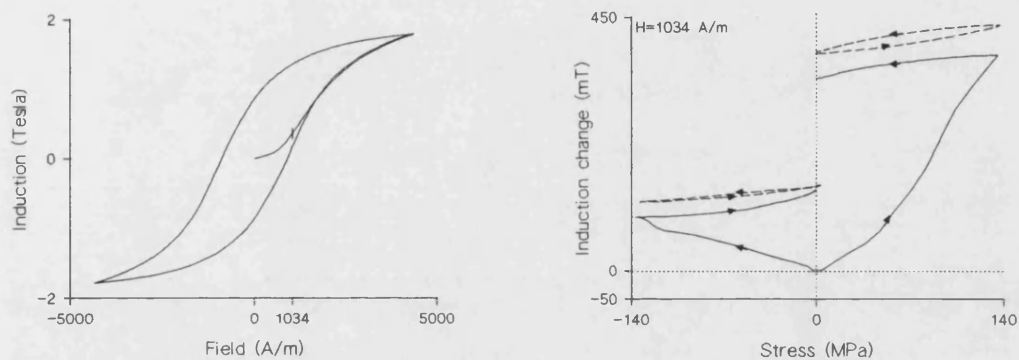
Figures 6.12   a.   Main hysteresis loop for HY80(1) (not annealed), from demagnetization. b. The results of compressive and tensile stress cycles from the same point on the initial induction curve.

Finally, data for the induction change observed for the iron tube specimen from a point along its initial induction curve reveals an interesting departure from some of the above behaviour. In the as-received form this specimen has been drawn along its cylinder axis. In this drawn condition it is likely to provide evidence of the magneto-elastic complexities that can arise from material texture. Figure 6.13 shows, in the usual manner, the induction changes observed during compressive cycles from a point on the initial induction curve. The intermediate induction changes are again omitted for clarity.
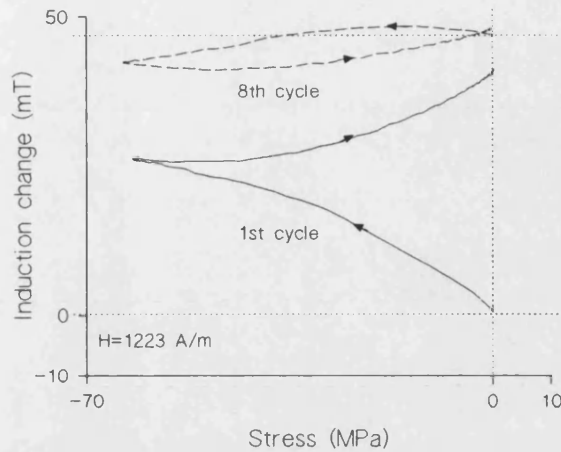
Figure 6.13. Induction changes observed of the first and eighth compression cycles on the iron tube specimen from a point on its initial induction curve. The slight positive going trend in the early portion of the eighth cycle is evidence of texture induced in the drawing process.

Whilst the general trends in magneto-elastic behaviour are consistent with those observed for the other iron-based materials listed so far, the slight positive-going trend of the induction profile during the eighth (reversible) cycle is not. For the range of fields and stress applied in this particular study, one might expect that the reversible component should at all times exhibit an induction decrease. Such a peculiarity can be best explained in terms of magnetic anisotropy induced during the material drawing process. For this to be correct, there must be a preferred crystallographic orientation ($<111>$) along the cylinder axis, because as detailed in chapter 3, this would be the only possibility for the material to show a positive induction change with compression on this axis. Reduction of texture is a process often associated with release of residual strain through thermal annealing. The peculiarity reported here is not unique to the initial induction curve and it will be

shown in the next section that such peculiarity is absent from induction changes observed for this specimen in the freshly annealed condition.

6.2.1.2 *Induction changes from major loop points and the significance of the principal anhysteretic*

In many studies of magneto-elasticity, significant attention has been paid to the variations in induction that occur from the material initial induction curve without full consideration of the restrictions this imposes on subsequent magnetic performance. In uniaxial experiments on positively magnetostrictive materials, this has led to the erroneous conclusion that compressive loads always produce smaller irreversible changes than tensile ones. A fuller understanding of the processes at hand has come from the investigations into the effects of stress from points along the materials' main hysteresis loops, (Jiles and Atherton, 1984). From such studies a consistent picture of stress-induced changes has emerged, with considerable progress made towards the provision of an empirical model for describing these effects, as discussed in chapter 4.

Shown in this section are general characteristics of stress-induced changes around the hysteresis loops which supplement those in the previous section, along with results upon which the Jiles-Atherton empirical model is based. These include measurements of the anhysteretics under iso-stress conditions for the principle materials of the investigation.

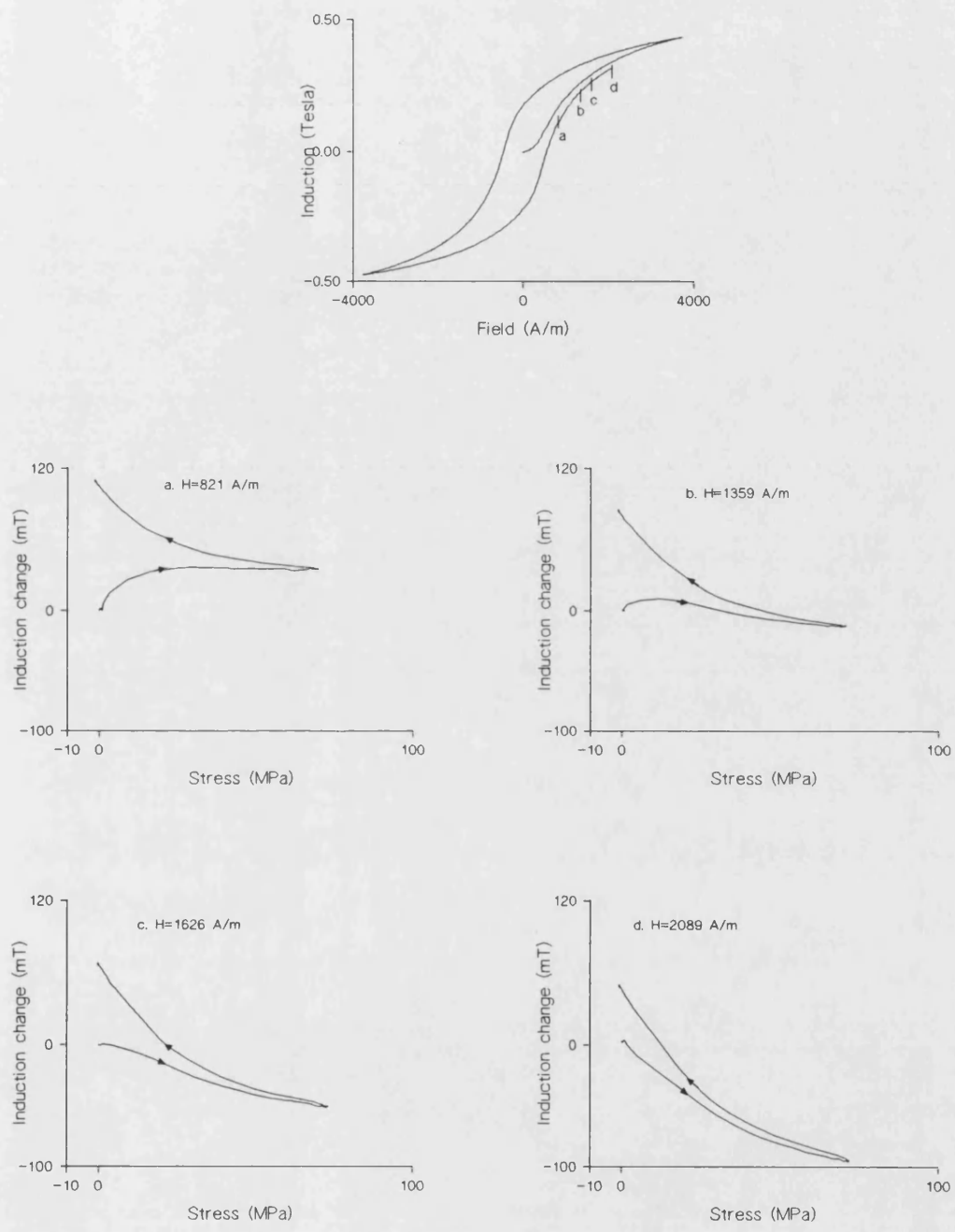6.2.1.2.1 Nickel at major loop points.

To start with, the relatively simple magneto-elastic characteristics of nickel subjected to tensile cycles around its major loop are examined. In figures 6.14 nickel induction changes from a point close to 'positive' remanence are shown. The specimen is relatively quickly brought to a reproducible cycle (within three tension and release processes) with the third 'reversible' stage shown artificially displaced on the induction axis for clarity. This rapid approach to a stable condition is in keeping with the reported changes on the initial induction curve, but the magneto-elastic characteristic differs from that of the initial curve in the important aspect that on this branch of the hysteresis loop, the net irreversible and reversible components of change are now acting to both produce a decrease in the overall induction value. This means that the profile is not distorted by the inversion processes observed on the initial curve and is in fact, more similar in shape to the positive magnetostrictive polycrystalline materials on their initial branches. This behaviour provides a clear example of a fundamental aspect common to all specimens subjected to iso-field stress in this study, that is the dependence of the sense of the irreversible component on the immediate field sweep direction. An appreciation of this is essential for a fuller understanding of stress-induced induction changes.
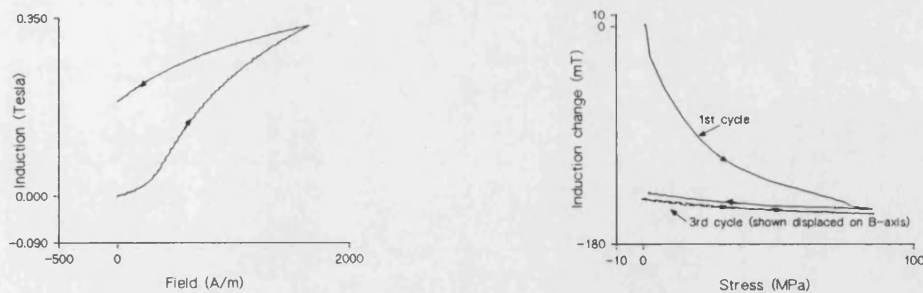
Figures 6.14: Left; arrival at a remanent condition. Right; subsequent tensile induced change. The third cycle induction change is displaced on the induction axis for clarity, (on this scale it would overlap the induction profile of the initial cycle release stage).

In contrast to this, figures 6.15 show how the changes observed during tension and release stress cycles from points on the major loop in the final portion of the hysteresis loop closely mirror those observed of the initial curve. In this case the field sweep previous to the stress process is seen to steadily increase the induction value irreversibly towards 'positive' saturation. At the four points indicated in the first figure the field is held constant for a single tension and release cycle. The induction-stress (B/σ) profiles are characterised by those processes of the earlier section, namely net irreversible changes which are greatest where the specimen permeability is high, and reversible contributions (not shown explicitly) which reduce the induction during the application of tension. At the lower permeability points (c & d), this negative-going trend is seen to dominate the upward-going, irreversible one

112

during stress application. The dependence of the sense of the irreversible change on the immediate field sweep history should again be appreciated.

Figures 6.15: Top; arrival at major loop points above 'positive' coercivity. (a-d): tensile-induced induction changes from indicated points.

113

These profiles suggest a consistency of magneto-elastic behaviour when the start conditions are similar, but markedly different behaviour at points characterised by quite different immediate magnetic history.

That the iron-based materials obey similar ground rules in their stress-induced induction changes has been demonstrated in section 6.2.1.1. Qualitative differences in their magneto-elastic performance stem from the complexity which arises from the dissimilarity of the magnetostriction constants along the three principle crystallographic axes. The irreversible changes can be expected to show the same dependence on the immediate field sweep history, with the comparative magnitudes of the changes dependent on the domain wall motion restrictions presented by lattice imperfections, which will be relatively high in the carbon steel specimens. This may go some way towards an explanation as to why nickel generally attains a reversible B/σ profile within a much lower number of stress cycles.

6.2.1.2.2 Biaxial HY80 specimen from major loop points.

In figure 6.16, points from which the biaxial specimen is subjected to compression and tension cycles are shown. Figures 6.16a show the results of multiple tensile and compressive cycles taken from a point above positive coercivity, as indicated in the hysteresis loop figure (point a). It can be clearly seen that the behaviour closely resembles that reported of the initial curve stress-induced induction changes of the previous section. The increased permeability correspondes to a greater magnitude of irreversible change compared to the changes observed from the initial curve. For this

114

particular field history, compression causes a greater irreversible increase in induction with the reversible 'inverse-magnetostrictive' components showing their expected senses in the adjacent figure given on an expanded scale. (The reader is asked to recall that for this specimen the rôles of tension and compression are reversed compared to their rôles in uniaxial positively magnetostrictive materials). Some indication that small but measureable irreversible changes are occuring at the fourth cycle stages is consistent with other observations from high permeability points.
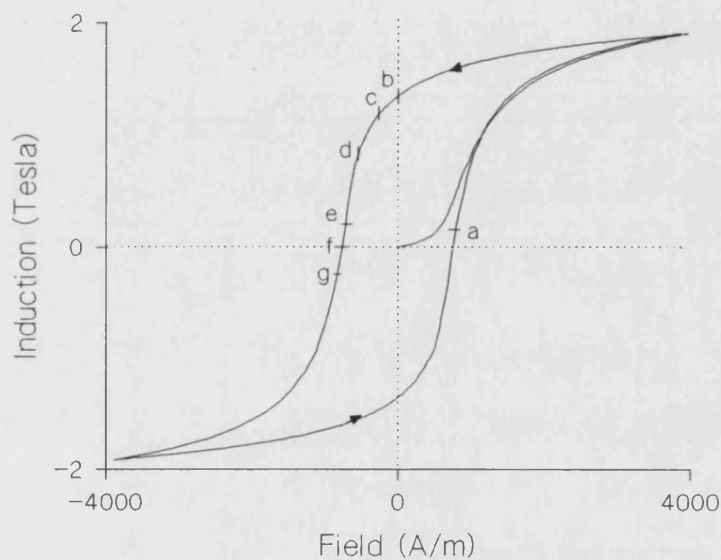

Figure 6.16: Hysteresis loop for biaxial HY80, indicating points at which stresses are induced.
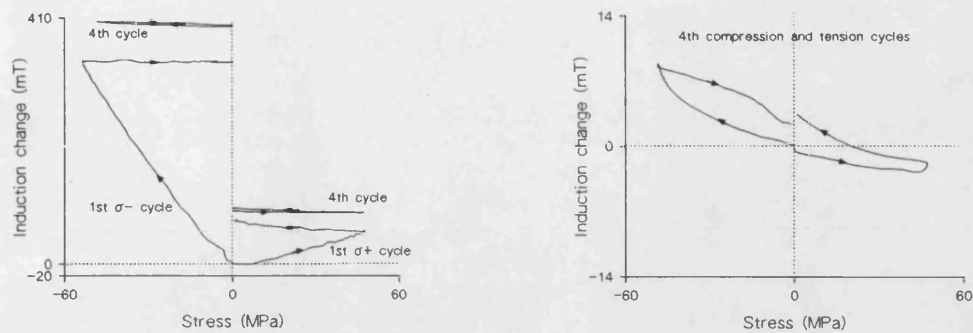
Figures 6.16 (continued). a. Left: first and fourth cycle changes shown on the same induction axes for compression and tension cycles from point (a) of the hysteresis loop shown. Right: Fourth cycles on expanded scales.

In figures 6.16b-g, the induction changes observed for single tensile and compressive cycles from the points indicated on the hysteresis loop are shown. The data show how the senses of the irreversible induction changes are reversed compared to changes on the initial curve and on the major loop above positive coercivity. In this case, on the demagnetization quadrant, over most of the field range, it is tension that gives rise to the greater irreversible induction changes. However, as the coercive field is approached, the irreversible change induced in compression sharply increases beyond that of tension, reaching its peak very close to the coercive field.
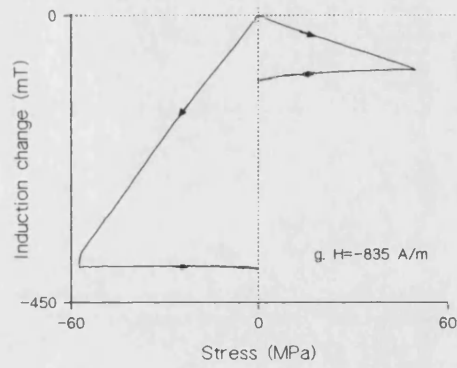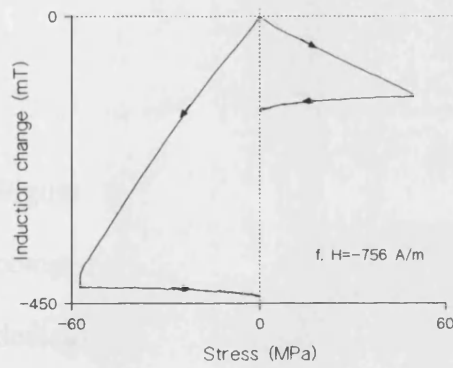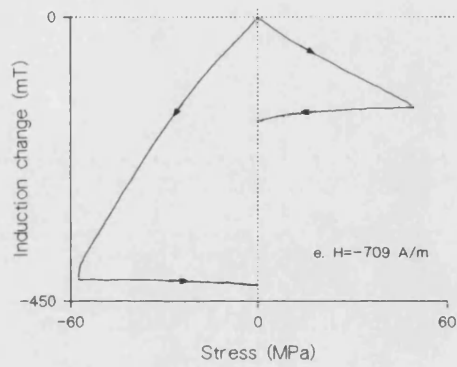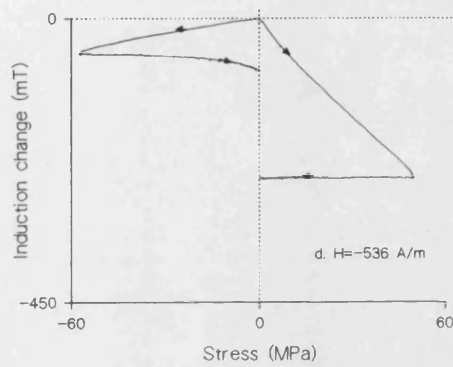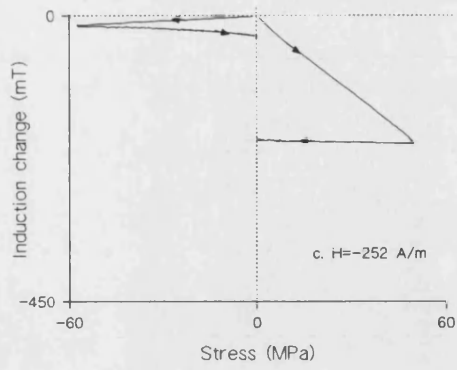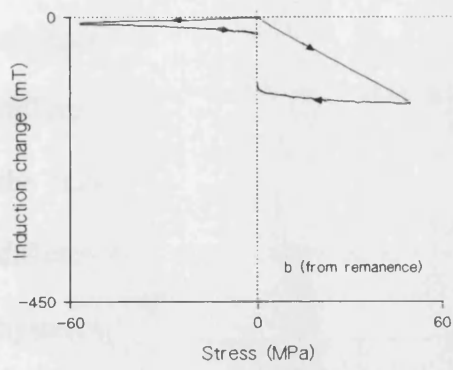
Figures 6.16 (continued). b-g. First cycle tensile and compressive induced induction changes for biaxial HY80 at points on the major loop (as indicated in figure 6.16).

Inspecting figure 6.17 it can be seen that the peak in the stress-induced induction changes for tension and is shifted laterally along the field axis with respect to the differential permeability profile. Compressive loads induce peak changes close to the peak permeability, but tension at some point at lower fields. In this figure the differential permeabilities along the initial and demagnetizing portions of the hysteresis loop are plotted against the stress-induced induction changes of the single tensile and compressive cycles for a consistent stress range of 50 MPa.
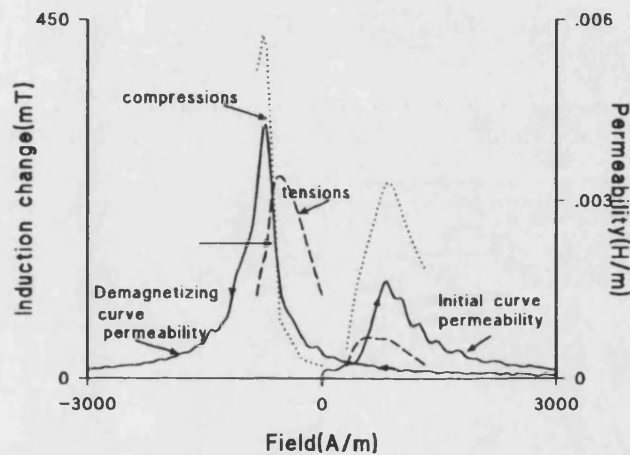

Figure 6.17: Net changes in induction caused by single tension (dashed) and compression (dotted) cycles to 50 MPa on biaxial HY80 at points on the initial and demagnetizing curves. These profiles are compared to the differential permeability.

Closer examination of this trend reveals some interesting departures from expectation. In figure 6.18a, the induction changes measured in single tension or compression cycles over a range of stress and field values are plotted. A clear monotonic shift in the magnitudes of the stress-induced induction changes along the field axis is observed

118

both in tension and compression. At the lowest compressive values the peak in the induction change occurs slightly below the coercive field, whilst in tension, slightly above. In each case a measurable shift in the peak induction location towards lower field values is observed. This same data set is expressed differently in figure 6.18b, where the location of the peak induction for each stress value used is shown with respect to the zero stress coercive field value.
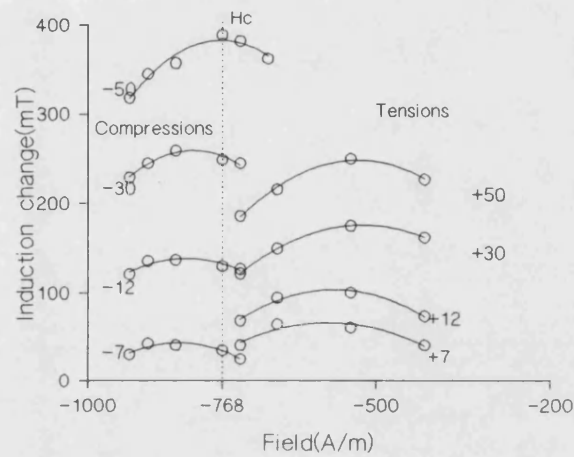

Figure 6.18a. Induction changes with tension and compression over a range of field and stress values between remanence and coercivity.
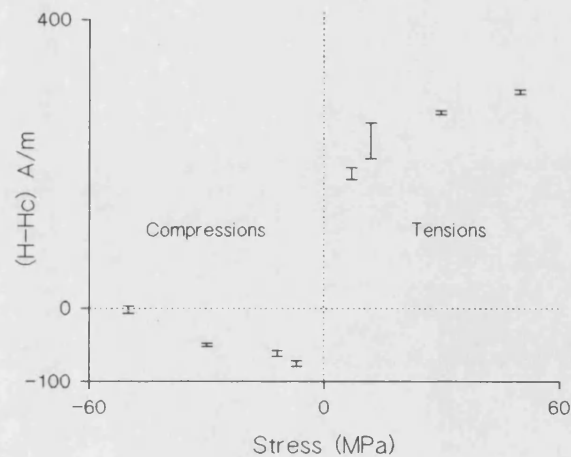

Figure 6.18b. Location of peak induction changes with respect to zero stress coercivity.

119

It is interesting to compare this observation of a lateral shift in the peak induction change with the expected behaviour as predicted by existing models. In earlier work, Schneider, (1985), has suggested the use of the field-dependent irreversible component of the specimen differential permeability as a 'response function' which could aid prediction of subsequent stress-induced induction changes. This quantity is seen to represent the rate at which irreversible induction changes are initiated by the applied field. As such, it possesses a similar profile to the specimen Barkhausen signature, shown as a function of stress in figure 6.19a along with the full iso-stress differential permeabilities in figure 6.19b. A study of the reversible component of this quantity, obtained by small field reversals, indicates that the full permeability profiles are perturbed significantly by subtraction of the reversible component only at very high and very low fields. For the purposes of the discussion presented here, the full profile comprises predominantly the irreversible component (in the range of interest of this work). Both differential permeability and Barkhausen signature are a reflection of the numbers of discrete induction changes occurring through domain wall motion or moment rotation in the bulk of the material. As such it has previously seemed reasonable to conclude that where field changes initiate greatest induction change, so will stress, acting as an additional pressure on domain walls as Brown postulated (1949). Whilst it is evident that peak induction changes are occurring in the vicinity of the peak differential permeabilities and Barkhausen signatures, the shifts in the peak inductions in this field region suggests an additional complexity beyond that indicated by Schneiders' model. It is worth noting that the observed shifts cannot be interpreted in terms of the lateral shifts in the stress-dependent permeabilities, as these are observed to translate in the opposite sense to the stress-induced induction changes.
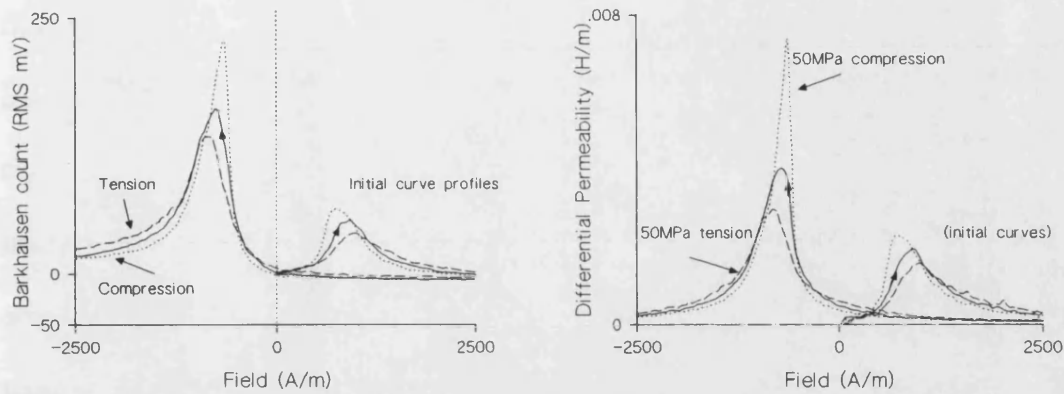
Figures 6.19a. Iso-stress (0 MPa, ±50 MPa) Barkhausen signatures for biaxial HY80 shown over the initial induction and demagnetizing curves, (field sweep rate = 330 A/m/s, frequency range = 100Hz to 100 kHz). b. Iso-stress differential permeability profiles over the same field and stress conditions. Stresses are 0 and ±50 MPa.

The empirical model of Jiles and Atherton, (1984), presents a picture of an irreversible change in induction towards 'equilibrium' when a specimen is acted upon by stress. The model represents a significant step towards an understanding of magneto-elastic processes. In figure 6.20a the biaxial HY80 specimen zero stress hysteresis loop is shown with its corresponding anhysteretic profile. The model predicts that greatest irreversible changes in induction value will occur at those locations where the distances between the anhysteretic and the original induction values are greatest. In figure 6.20b the induction interval between the zero stress anhysteretic and the corresponding values located on the initial and demagnetizing

portions of the hysteresis loop are shown. The magnitude of this interval at negative fields is seen to peak at some point between positive remanence and negative coercivity, in contrast to the permeability and Barkhausen signatures which are centred around the coercive point. Second, as figures c and d show, no shift in the interval along the field axis is observed when the difference between the stress-dependent anhysteretics and the corresponding zero stress induction values are plotted. These plots indicate that attempts to model stress-induced induction changes from discrete point on the B/H plane by using the anhysteretic as a 'moving target' problem will fail in the aspect of being unable to accommodate the lateral shifts in peak induction values. It is evident then that the shifts presented in the experimental data are not directly explicable in terms of existing representations of magneto-elastic processes.
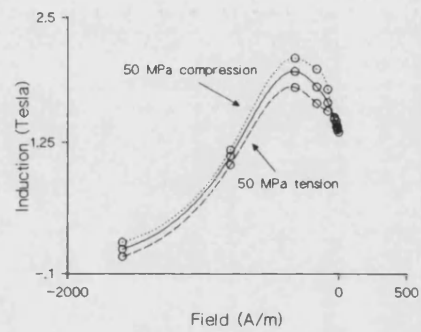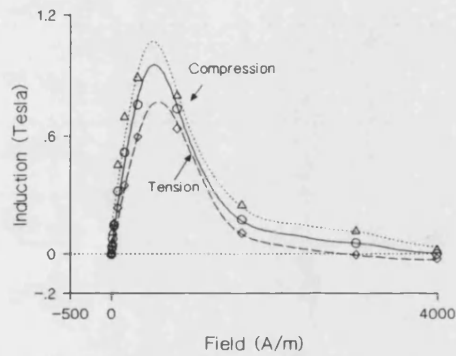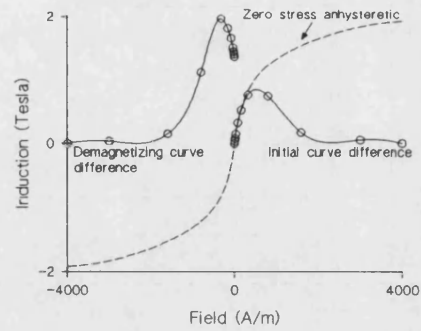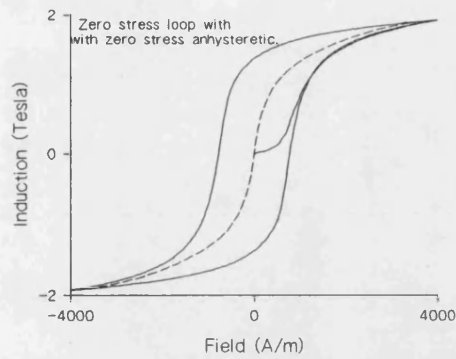
Figures 6.20 a. (Top left): zero stress hysteresis loop for HY80 with corresponding anhysteretic. b. (Top right): Difference between the anhysteretic and corresponding initial and demagnetizing curves (all at zero stress). c.(Bottom left): Difference between zero stress initial curve and anhysteretics at 0 and ±50 MPa. d. Difference between zero stress demagnetizing curve and anhysteretics at 0 and ±50 MPa.

The major loop data for the nickel and biaxial steel specimens readily demonstrate

many of the key features of the magneto-elastic behaviour of these materials. Studies of the characteristics of the other polycrystalline specimens provide confirmation of these trends, along with additional information that can be gained from the more varied stress intervals that can be applied because of differing cross-sectional areas.

6.2.1.2.3 HY80(2) from points on the major loop.

HY80(2) allows the effects of application of uniaxial field and stress on the steel specimen to be investigated over a wider range of loads. Increased sensitivity of induction measurement is available from the co-axially wound search coils compared to those mounted on the biaxial specimen. In figure 6.21a the results of compressive and tensile stress cycles applied from a (positive) remanent condition are shown in the usual manner. For clarity, the ninth stage induction changes are shown as the broken lines at their correct relative location. The specimen demonstrates behaviour similar to the biaxial specimen. The roles of tension and compression are consistent with those expected of a positively magnetostrictive polycrystalline material. At the low stress values uses, the Villari effect does not complicate the profile in tension. These points are demonstrated in figure 6.21b where the ninth cycle induction changes are shown in more detail.

In figure 6.21c the total changes in induction caused by tension and compression for the two data sets are plotted against stress cycle number. Whilst the initial changes induced with the first stress cycles are of significantly different magnitudes, the trend in the approach to a stable condition is similar for the two stress modes. This

suggests that the same mechanism may be at hand during the asymptotic fall to an equilibrium condition for both tension and compression.
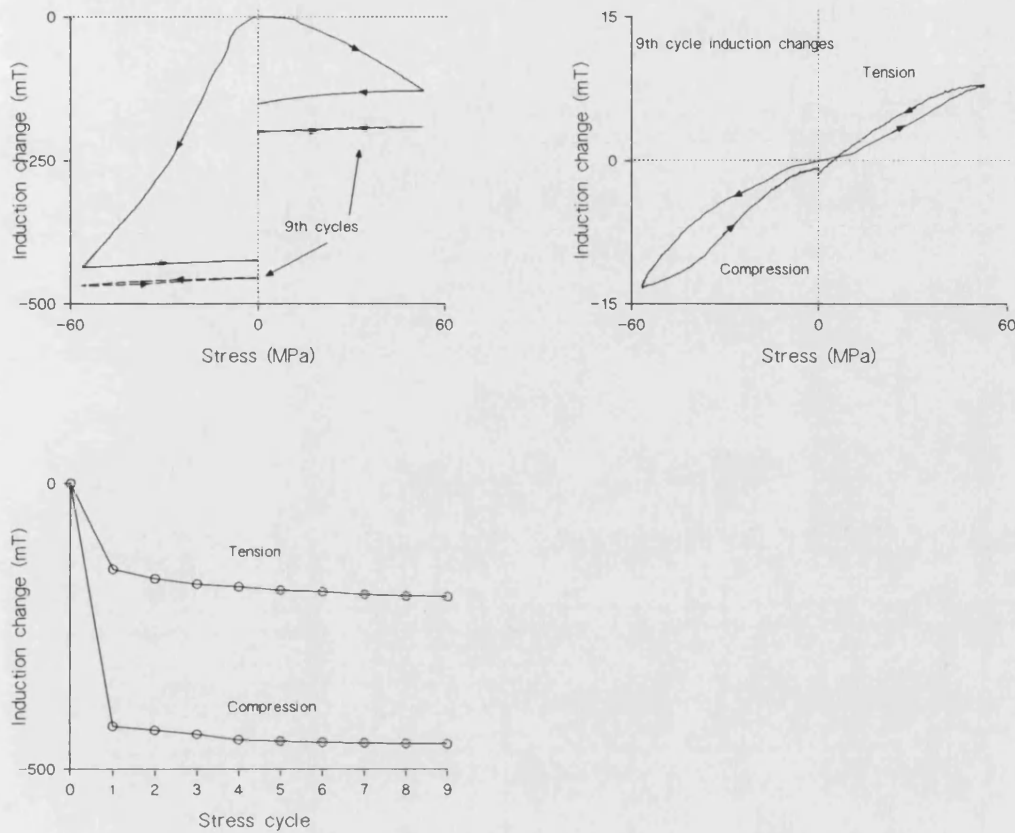
Figures 6.21a. (Top left). Induction changes from remanence (first and ninth cycles. b. (Above) ninth cycles on expanded scale. c. Induction change against stress cycle number from the remanent condition.

In the Jiles-Atherton model of ferromagnetic hysteresis, this equilibrium condition is the anhysteretic induction value at the corresponding field and stress levels. The cyclic stress processes undertaken in the above measurements are expected to be characterised by an approach to a stable induction value, stability being indicated by a closed or reversible induction loop. Although the ninth cycle changes suggest that

125

small irreversible induction changes approaching the resolution of the measuring system are still taking place, it is clear that a stable magnetic condition is being approached.

Data upon which the empirical law is based are shown in figures 6.22 to 6.24. In 6.22 the reduction in absolute induction from a condition close to positive remanence with a tension cycle is shown with respect to the corresponding anhysteretic curve. To clarify the discussion presented here, the field-induction profiles in all these figures have been corrected for demagnetizing fields using tabulated demagnetizing factor data for specimens of similar geometry (Bozorth, 1951). The induction change induced by the change in load is shown on the same induction scale and on a horizontal axis representative of stress but not related to the field axis. An irreversible change in net induction towards the tensile anhysteretic is observed with a minimal induction change with stress release.
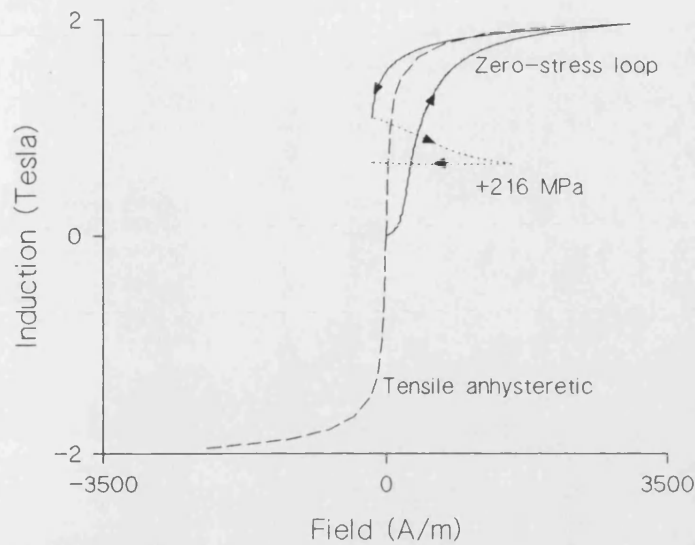
Figure 6.22: Tension and release for uniaxial HY80(2) with respect to tensile anhysteretic.

In figure 6.23a, a similar process is observed for tension cycles to the same level from a point on the major loop above positive coercivity. The first and fifth induction changes are shown at their correct relative locations and demonstrate a gradual increase in induction towards the equilibrium condition. In the inset, the fifth stress cycle, shown fifty times induction scale for clarity, demonstrates the behaviour expected of a positively magnetostrictive material over this field and stress range. Close examination of this profile reveals the complications in magneto-elastic profiles that arise at high fields and tensile loads due to the reduction in length along the <111> direction. Such behaviour is broadly categorized as the 'Villari effect'. In figure 6.23b the asymptotic approach to equilibrium is shown to have a similar profile to those presented in figure 6.21c.

127
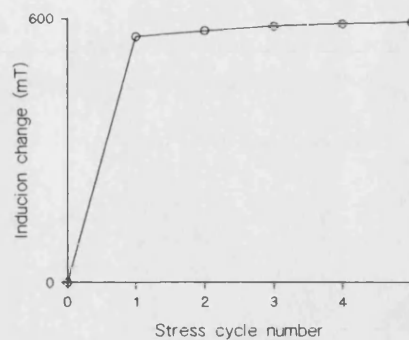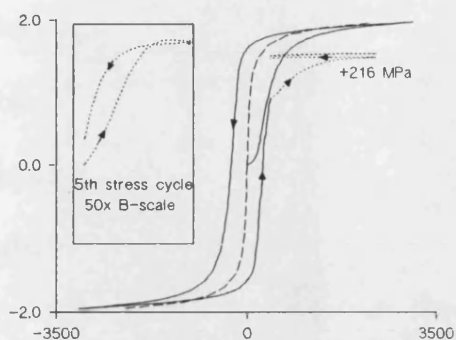
Figures 6.23 a. (Left): Induction changes with tension cycles above positive coercivity compared to the location of the tensile anhysteretic. b. Asymptotic approach to equilibrium.

In figures 6.24a and b, measurement of the induction changes induced by compressive loads from slightly different locations on the major loop of the HY80(2) specimen are shown. These serve to demonstrate more complex operation of the equilibrium principle. In 6.24a, the induction value is observed to initially rise with the application of compression, although some indication of a reduction at higher stress levels is present. This is shown more clearly in the inset. This behaviour, along with the observed increase in induction during stress release is explained by the Jiles-Atherton model in terms of the induction value 'tracking' its anhysteretic condition. The close proximity of the initial location on the B/H plane and the distortion of the anhysteretic as a function of load leads to a condition where the induction value originally climbs and eventually meets the 'downward'-moving anhysteretic value. The validity of this explanation is confirmed in figure 6.24b.

128

From a start condition appreciably above the compressive anhysteretic value the increase in induction with applied load is quickly dominated by the negative-going trend. That the net irreversible induction change was positive in this measurement is confirmation that the final location of the zero-stress anhysteretic lies somewhere above the original specimen induction value.
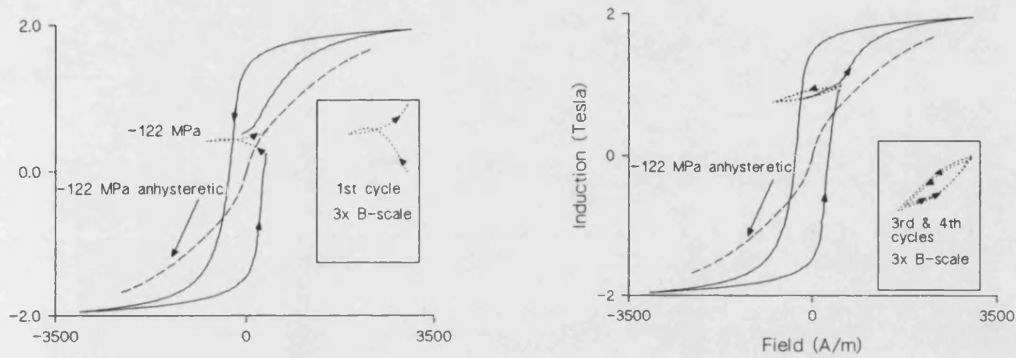
Figures 6.24 a. (Left): Compressive induction change from point below equivalent (compressive) anhysteretic. b. The same measurement from a point above the compressive anhysteretic. Such data has suggested the validity of the concept of the specimen induction value 'tracking' its corresponding anhysteretic point.

6.2.1.2.4 Fe(2) from major loop points.

The universal nature of the processes operating in stress-induced induction changes is demonstrated through similar measurements on other materials. The uniaxial iron specimen, Fe(2) has been subjected to tensile cycles at various points on its major hysteresis loop. In figure 6.25, the induction changes with several stress cycles from

129

a point on the major loop in the positive quadrant is shown. The loop has not been corrected for demagnetizing fields. The profiles for the total and reversible induction changes show the expected behaviour for a positively magnetostrictive material. The peculiarity in the shape of the reversible component of induction change, as measured in the fourth stress cycle shown on expanded scale in the inset, during the release of stress is difficult to explain. On the basis that a similar profile has been observed for the tubular iron specimen in compression it is plausible that this may be another manifestation of texture caused by the sheet rolling process.
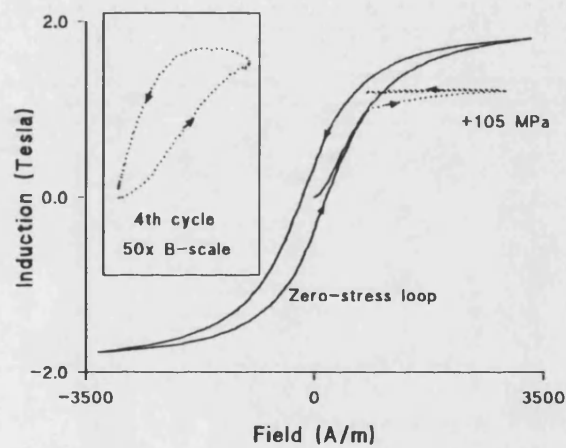
Figure 6.25: First and fourth cycle induction changes from a major loop point for Fe(2).

The magnetostriction of this specimen has been measured by the strain gauge technique to produce the curve shown in figure 6.26a. Of particular interest is the marked (relative) contraction in specimen length observed at the high field values,

130

characteristic of iron specimens with modest levels of residual (compressive) strain. This allows a deeper assessment of the validity of effective field formulae based on the induction dependent differential magnetostriction dλ/dB.

In figure 6.26b, the magnetostriction and its induction differential are shown as functions of absolute induction from peak negative to peak positive induction values. It is the shape of the latter profile, shown as the non-fitted data points, which is expected to predict the form of the reversible component of stress induced induction changes, as discussed earlier for HY80(2) on its initial induction curve.
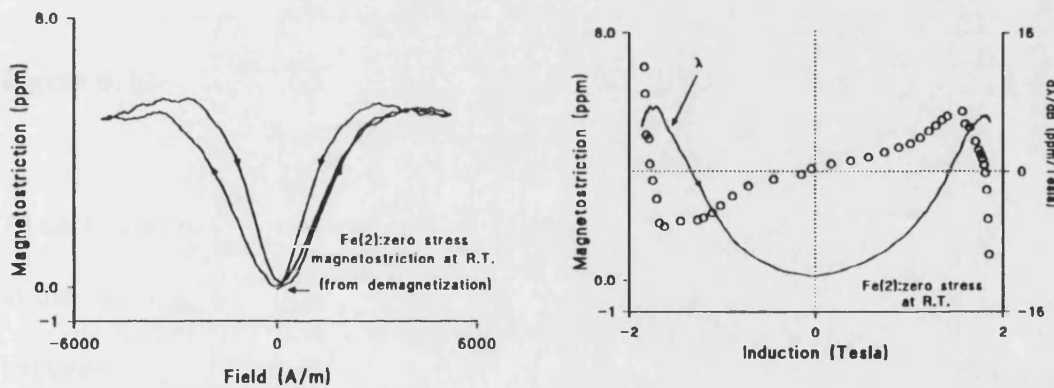
Figures 6.26   a. (Left): Fe(2) magnetostriction taken by strain gauge.   b. Magnetostriction and differential magnetostriction induction-dependence.

Tension intervals to 63 MPa were undertaken on this specimen from the points indicated in figure 6.27. Typical profiles, representative of the changing trends are shown in figure 6.28a-d.
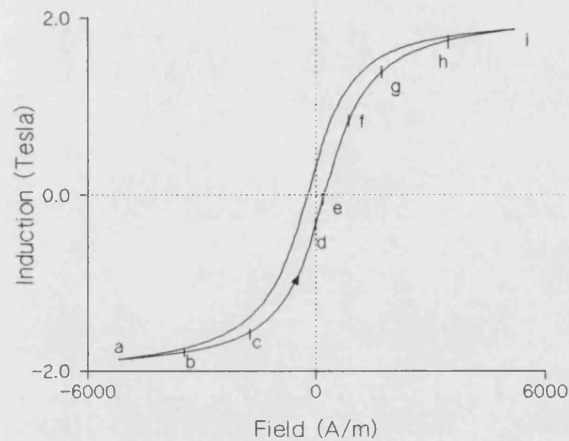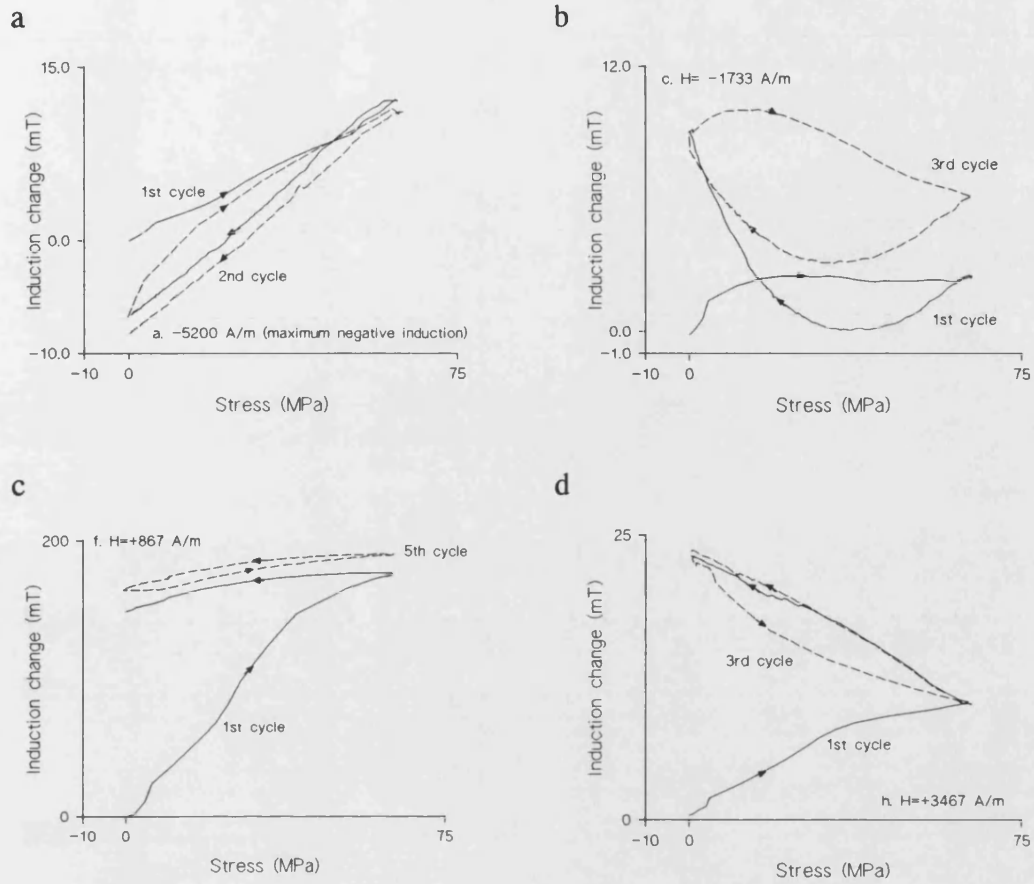

Figure 6.27: Locations from which Fe(2) has been subjected to tensile cycles.

At each indicated point the reversible component of the induction change is measured at the last stress cycle stage consistent with providing a closed induction loop. The irreversible induction change instigated in the earlier stress cycles is added to the initial induction value to compute the absolute induction from which the reversible component is measured. The reader's attention is drawn to the fact that because of the large differences in induction changes measured, the data of figure 6.28 have been plotted on different induction scales.

The magnitudes of the reversible component induction changes are shown with the corresponding magnetostriction data in figure 6.29. Correspondence between the trends in the differential magnetostriction and the reversible component of induction

132

change is evident. However, whilst it is clear that an effective field formula involving the differential magnetostriction would give a more satisfying result than those which solely employ the saturation magnetostriction value, some lack of parallelism in the profiles, along with the non-coincidence of their zero locations, is indicative of increased complexity in the magneto-elastic processes. It can be argued that this complexity arises through the stress-sensitivity of the sample bulk magnetostriction. Moving from negative to positive saturation, as in the conditions of this data collection, the act of tension below positive coercivity will serve to drive the magnetostriction to negative values. This will have the effect of shifting the induction change peak to the left in the figure. A more thorough examination using smaller tensile cycles would, on the basis of this argument, show a stronger relationship between the two quantities.

a

15.0

Induction change (mT)

0.0

-10.0

1st cycle

2nd cycle

a. -5200 A/m (maximum negative induction)

-10   0   75

Stress (MPa)

b

12.0

c. H= -1733 A/m

Induction change (mT)

3rd cycle

1st cycle

0.0

-1.0

-10   0   75

Stress (MPa)

c

200

f. H=+867 A/m

Induction change (mT)

5th cycle

1st cycle

0

-10   0   75

Stress (MPa)

d

25

Induction change (mT)

3rd cycle

1st cycle

h. H=+3467 A/m

0

-10   0   75

Stress (MPa)

Figures 6.28 a-d. The changing tension-induced stress profiles from peak negative to peak positive induction for Fe(2), indicated by their field locations.
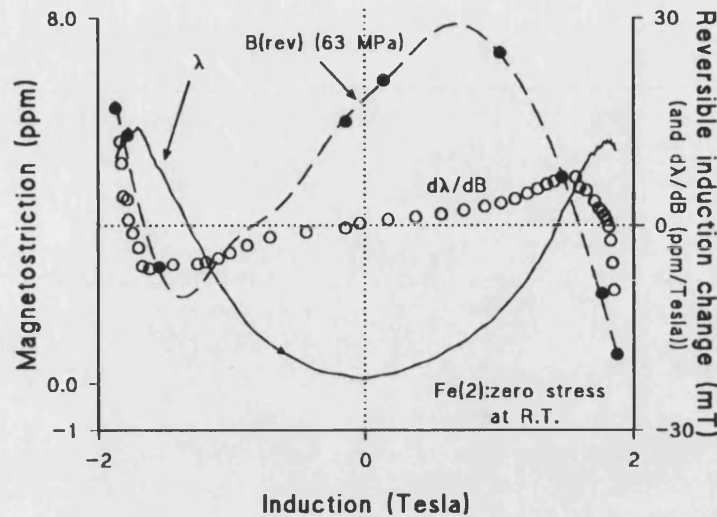
134

Figure 6.29: The reversible component of induction change for Fe(2) in tension to 63 MPa is compared to the induction-dependent magnetostriction profiles.

The tubular iron specimen has been examined in as-received (drawn) and vacuum annealed conditions. In the as-received condition, avoidance of any subsequent treatments allows a determination of the properties of an 'off-the-shelf' specimen, whilst an inspection of its properties after heat treatment allows some conclusions to be drawn concerning those properties which are dependent on treatment history. Of particular interest with this specimen is its demonstration of properties which can be directly linked to specimen texture, as shown from points on its initial induction curve on the previous section. In figure 6.30a the compression-induced induction changes from a point above positive coercivity for the as-received specimen are shown with respect to the compressive anhysteretic. The B/H profiles presented in this discussion have been corrected for demagnetizing fields. The general performance is as expected with an irreversible shift towards the equilibrium condition evident. The reversible

135

component of the induction change shows the anticipated overall reduction in induction with the application of load but with the same peculiarity in shape, namely the small but measurable increase in induction at low stress, as that observed from the initial curve. It should be stated that this peculiarity is characteristic of the reversible induction change from other locations on the major loop. In figure 6.30b the trend in approach to a closed induction loop with stress cycles is as expected.
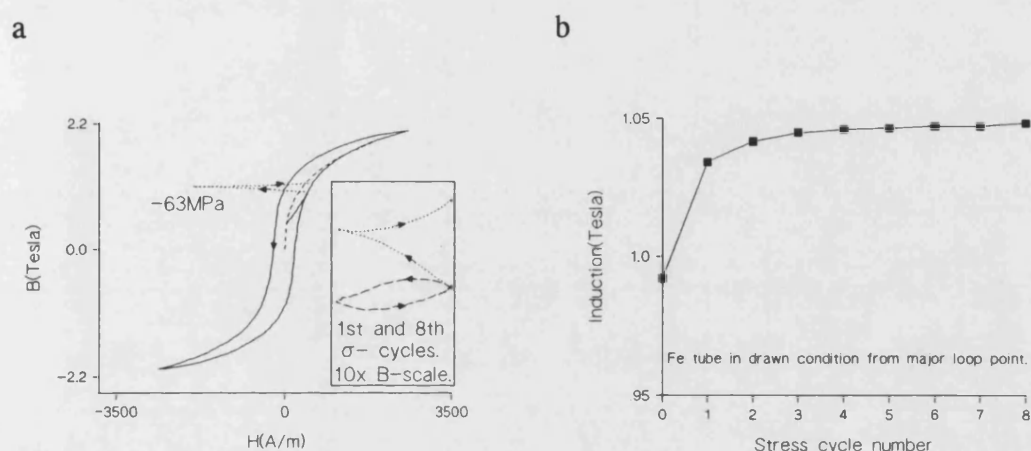
a   b

Figure 6.30 a. (Left). As received Fe tube in compression from major loop point. The first and eighth compression-induced cycles are shown in the inset.b. Trend in approach to a stable condition.

Figure 6.31a compares the hysteresis loop of the as-received specimen to its profile after a vacuum anneal (650°C for 3 hours). The reduction in the coercive field and the overall increase in specimen permeability, as indicated by the more easily obtainable higher induction values, is consistent with the reduction of residual compressive strains caused by the drawing process. By comparison with the

136

specimen in as-received state, it was found that, the anneal also lead to increased magneto-elastic sensitivity of the hysteresis loop profile compared to that observed of the as-received condition. The iso-stress loop performance is shown in figure 6.31b.
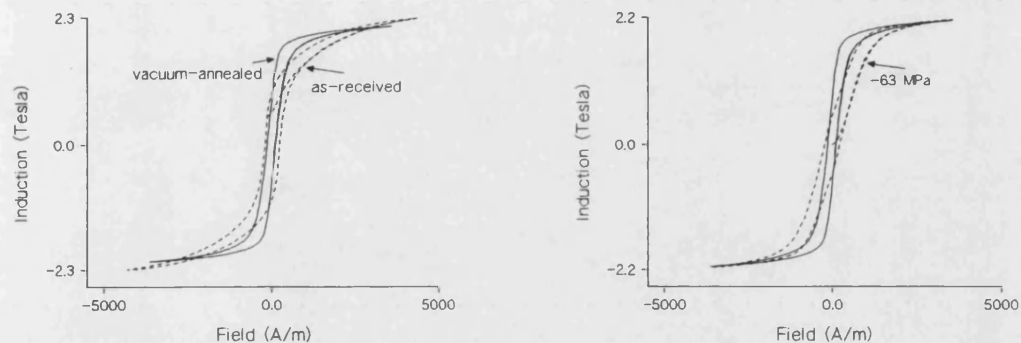
Figures 6.31 a. (Left). Comparison of the zero stress loops for drawn and annealed Fe tube. b. Annealed Fe tube at zero and -63 MPa.

In figure 6.32 the iso-field induction changes from a point above positive coercivity are shown relative to the location of the compressive anhysteretic. The specimen in the annealed condition shows the same qualitative behaviour as in the as-received state, the magnitude of the irreversible change was observed to be maximized close to maximum differential permeability. Of particular interest though is the absence of the rise in induction at the low stress values in the reversible component of induction change, as seen by the closed loop third cycle. This is the clearest indication of the complications that can arise from material texture. Such complexity is enhanced by

137

the particularly complicated magnetostriction of iron in the <111> direction. It should also be noted that in the annealed condition the specimen arrives at a stable magnetic condition within three cycles in contrast to the greater number of stress cycles required for the as-received specimen.
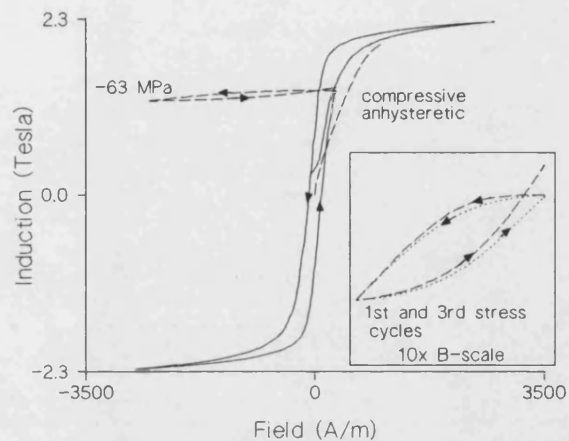

Figure 6.32. Annealed Fe tube. First and third compression cycles from point above coercivity. The absence of additional complexity in the third cycle is evidence of reduction in texture caused by the annealing process.

6.2.1.2.5 Silicon-Iron from major loop points.

Finally, the magneto-elastic performance of Silicon-Iron has been examined. The results obtained demonstrate a wider range of performance amongst the iron-based materials. In figure 6.33 the main hysteresis profile, not corrected for demagnetizing fields, is shown. The specimen has been subjected to tension cycles from the indicated points, a and b. The results of these experiments are shown in figures 6.34.

138

In 6.34a, induction changes observed from a point significantly above coercivity are seen to have an irreversible component of change in the same sense as that caused by the previous field sweep, yet a reversible component tending to reduce the absolute induction value during the application of tension. The profile is in fact, reminiscent of a positively magnetostrictive material in compression. This behaviour comes about because of the high sensitivity of the bulk magnetostriction to stress as shown in the work of Eadie (1982). In the iron based materials examined before, the importance of processes associated with the Villari effect has been discussed. Confirmation that the Silicon-Iron specimen under investigation here can exhibit behaviour typical of predominantly positively magnetostrictive material comes from figure 6.34b. In this measurement the tension-induced induction changes observed from a point further along the B/H profile are not characterized by a negative reversible component. The explanation for this lies in the fact that the initial condition is 'high' enough on the λ/H profile not to move into the negative region with the onset of tension. It is reasonably clear though, that a higher level of load would have eventually forced this inversion behaviour.

Consistent with other measurements made on the relatively soft magnetic specimens in this study, the rapid approach to a stable magnetic condition with the application of cyclic stress should be noted.
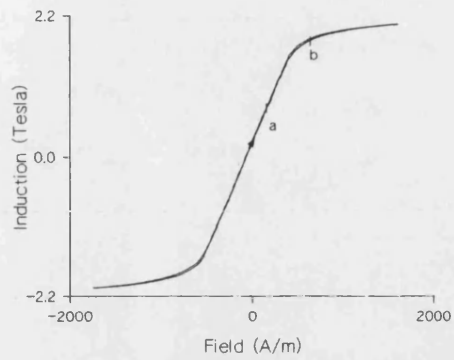
Figure 6.33: Points from which Silicon-Iron has been subjected to tensile stress cycling.
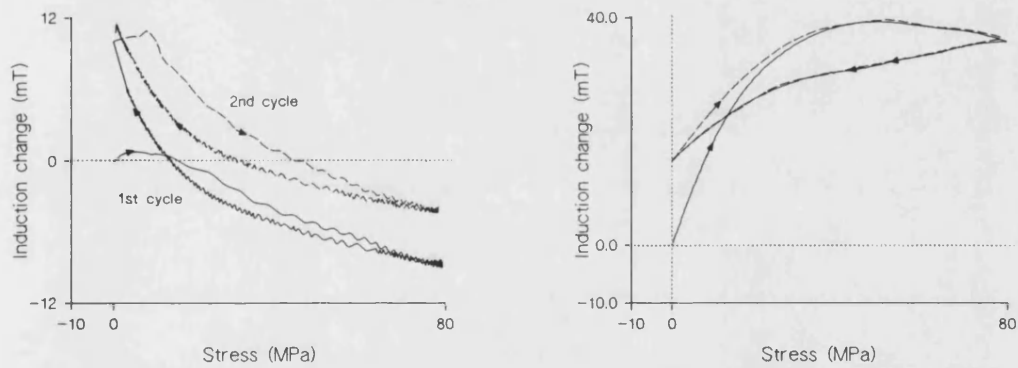

Figure 6.34 a. (Left). Tension induced change from point (a) in 6.33. b. Tension induced change from point b.

6.2.2 *Induction changes from complex magnetic histories - minor hysteresis loop points*

So far results presented have been extracted from specimens in well-defined magnetic conditions. This has allowed an examination of the fundamental processes active in several polycrystalline specimens. By establishing well-defined domain configurations at major and initial loop points, the iso-field B/σ profiles have been simple enough to interpret in terms of these processes. It will be shown in this section that the magneto-elastic performance from minor loop points involves an increased level of complexity. This has not been highlighted in the available literature to date. It is not immediately apparent how this increased level of complexity will be accommodated in existing models.

By again starting with the relatively simple example of polycrystalline nickel, some aspects of minor loop complexity can be readily observed. As reported in the earlier sections the magneto-elastic behaviour of nickel and that of the iron-based specimens can be interpreted on the grounds of similar mechanisms. Results for the latter along their minor loops will also be presented.

6.2.2.1 Nickel from minor loop points.

In figure 6.35a the hysteresis loop for nickel is shown, wherein it is forced to describe the indicated minor loop profile by the appropriate field sweeps. At the

major loop turn-around point and at the points (a) and (b), the specimen has been subjected to a single tension and release cycle with the field held constant. The results of these experiments are shown in figures 6.35 b-d. At the major loop point the specimen shows the characteristic irreversible increase in its induction value as reported in the previous section. The net reduction of induction with stress applied is as expected for the negative magnetostriction of the material. However, as the specimen moves along the minor loop leg to point (a), this irreversible induction change with the application of a load cycle is reduced. At point (b), at the end of the described minor leg, this has transformed to a net irreversible reduction in the absolute induction value. At some stage between these two locations, the irreversible induction change for this level of externally applied load must have gone through a null point. Previous arguments presented here would suggest that no change in the induction with stress cycling implies that the specimen has achieved an equilibrium condition. It is of great interest to determine if such a condition shares its location on the B/H plane with the equilibrium for induction changes from major loop and initial induction curves. If it does not, then specimen history, as opposed to location on the B/H plane, must feature in any attempt to predict irreversible induction changes with stress.
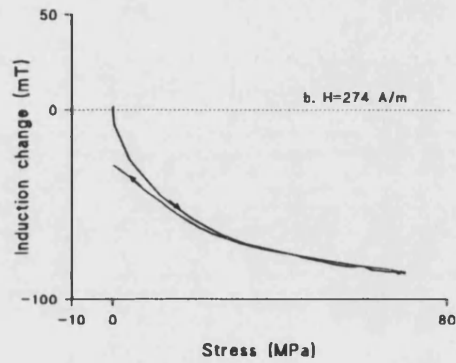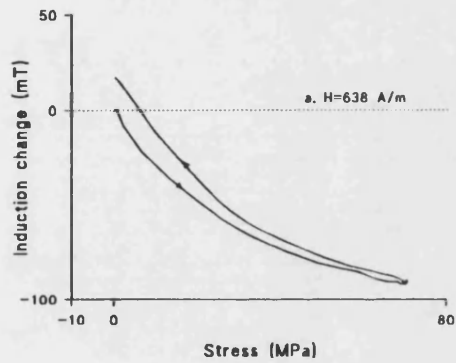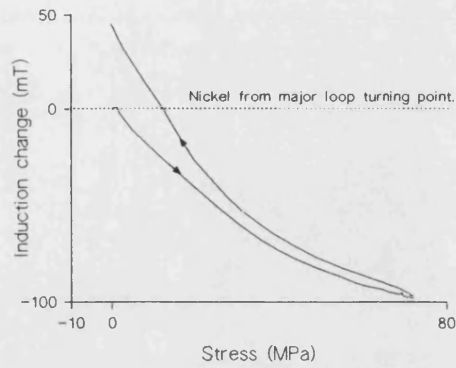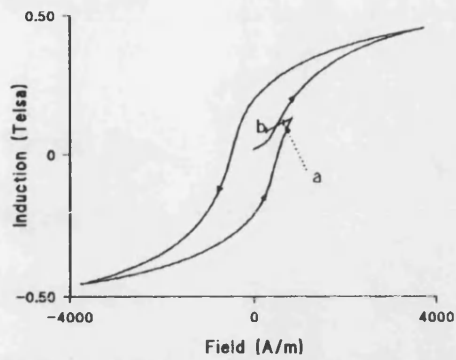
Figures 6.35 a-d. a. (Top left). Nickel taken along a minor loop trajectory. A single tension cycle has been applied from the turn-around point and points (a) and (b) as indicated. b. (Top right). Induction change at turning point. c. (Bottom left). Induction change at (a). d. Induction change at b. At some stage between (a) and (b) a null in the irreversible induction change with stress should be encountered.

6.2.2.2 Fe(2) from minor loop points

Similar trends along minor legs can also be observed in the iron-based materials. In figure 6.36a the main hysteresis loop for the uniaxial iron specimen Fe(2) is shown from a demagnetized condition. The loop has not been corrected for demagnetizing effects. An excursion along the minor loop interval is shown. At the indicated points, the specimen has been subjected to a tension cycle at constant field, the results for which are shown in the subsequent figures indicated (a)-(e). At the major loop turning point the specimen shows the previously reported comparatively large irreversible increase in induction with the stress cycle as indicated in figure (a). At the minor loop points the B/σ profiles become increasingly complex. At point (b) shown in figure 6.36b, the irreversible increase in induction is considerably reduced and the general shape of the profile somewhat distorted. This trend continues through points (c) and (d) to the stage where at (e), the end of the minor loop path, the specimen exhibits a monotonic decrease in its absolute induction value at all stages of the stress cycle. Of particular interest here is the manner in which the transformation occurs, shown most vividly in figures 6.36c and d. An initial reduction in induction during the application of load is eventually overcome at higher stress levels by effects which tend to raise the induction value, as seen more clearly by the expanded scale profiles. As the specimen progresses along the minor leg the induction-reducing effects increase to the point where they eventually dominate. At some stage between points (b) and (c) on the minor leg, a null point should have been encountered, corresponding to an equilibrium condition for these field and stress

144

magnitudes. In this way the behaviour is almost identical to the nickel described earlier. The important point to be be drawn from this data set though, is that on the minor loop paths, there are two conflicting processes which appear to cause either a reduction or increase in the induction value. The magnitudes of these effects are dependent on the level of applied stress. As will be shown later, this observation is an important factor which aids interpretation of minor loop stress-induced induction changes.
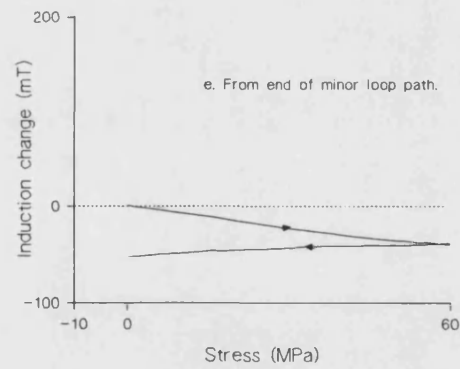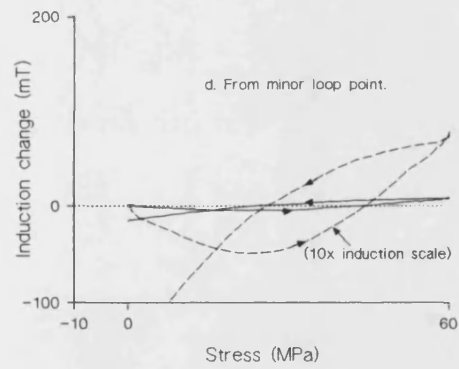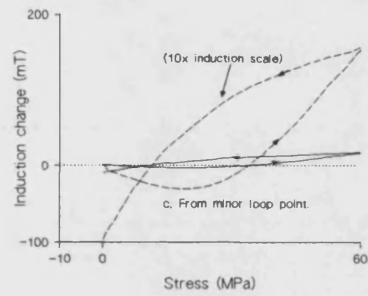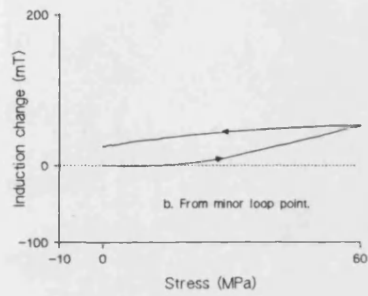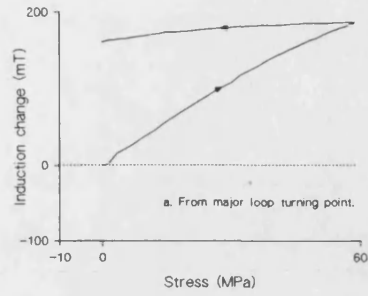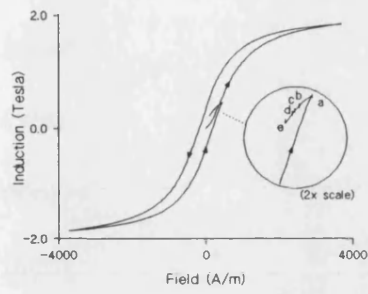
Figures 6.36. (Top left) Fe(2) loop with minor loop path. a-e: Induction changes with tension from indicated points.

6.2.2.3 HY80(2) at minor loop points.

In order to gain an increased understanding of the transformation of behaviour along minor loop paths, the prime material of this investigation, HY80, has been extensively studied in its uniaxial form, (specimen HY80(2)). Despite the complications presented by demagnetizing factors, the advantage of maximized induction sensitivity allows a clearer analysis of such changes compared to the biaxial specimen.

In figure 6.37a the method of arrival along a minor loop path from an initial demagnetized condition is shown. In (b) the points at which the field is held constant whilst the specimen is subjected to a single tension cycle are indicated on an expanded scale, showing their positions with respect to the 150 MPa tensile principal anhysteretic. The B/H profiles presented here have been corrected for demagnetizing fields.
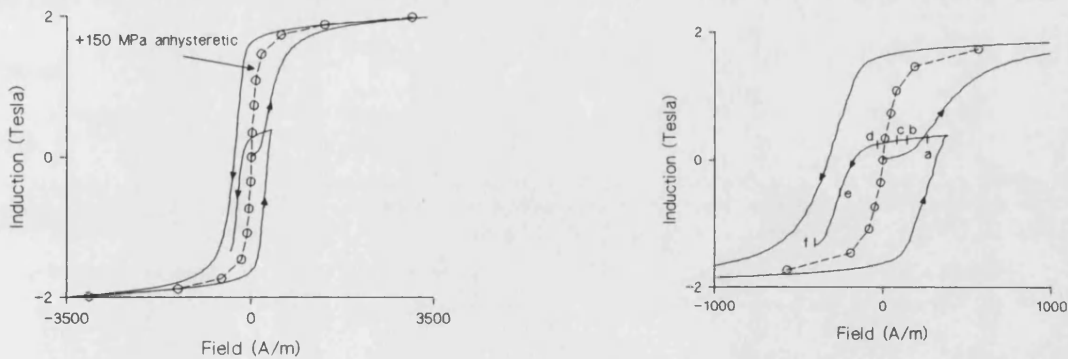
Figures 6.37 a. (Left). Method of arrival at minor loop leg for HY80(2). b. Locations from which tensile stress-induced induction changes are measured, (expanded field scale, 150 MPa tensile anhysteretic also shown).

145

The results of the stress-induced induction changes are shown in figures 6.38a-f. At the early stage along the minor leg, (a and b) a large irreversible increase in specimen induction is observed, similar to the expected trend at the major loop turning point. The growth of induction-reducing effects at low stresses is noticeable in (b). At point (c), the conflicting processes combine to produce zero net induction change characterized by a complicated form with stress. It is significant that this null does not coincide with the location of the principal anhysteretic. Paraphrased, this result indicates that on the minor loop path described, the equilibrium condition with stress cycling does not appear to correspond to the expected locations of the principal anhysteretic. Even accounting for the known stress-dependence of the anhysteretic curve, it is obvious that at all times in this experiment, the anhysteretic point lies significantly above the minor loop initial location (c). The irreversible stress-induced induction change from point (c) has clearly not moved towards the principal anhysteretic. From points (d-f) further along the minor loop path, the irreversible induction change becomes wholly negative. The magnitude of this negative change is observed to go through a maximum value before falling away at the minor loop end point. This behaviour is consistent with the observation from major loop points that the magnitude of the irreversible change roughly follows the material differential permeability.
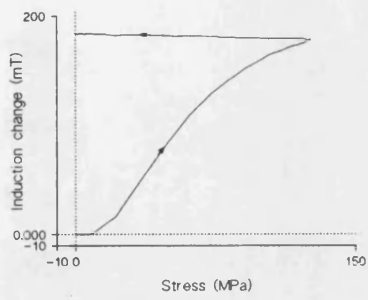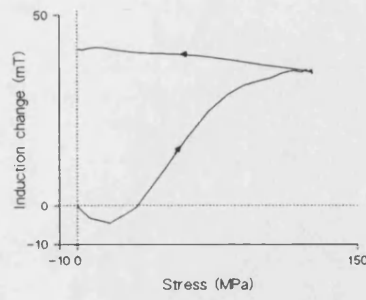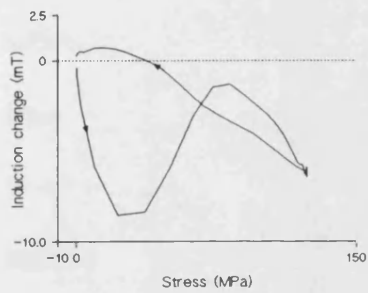
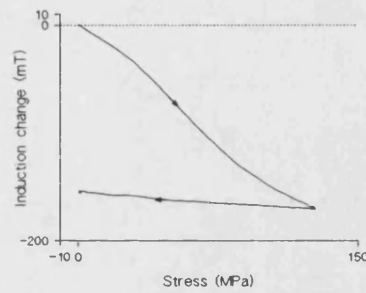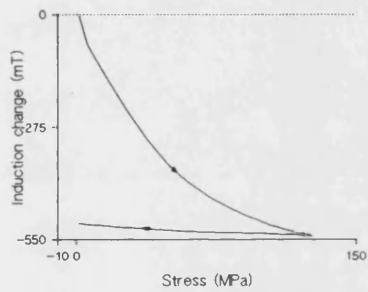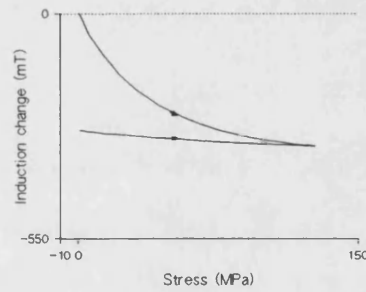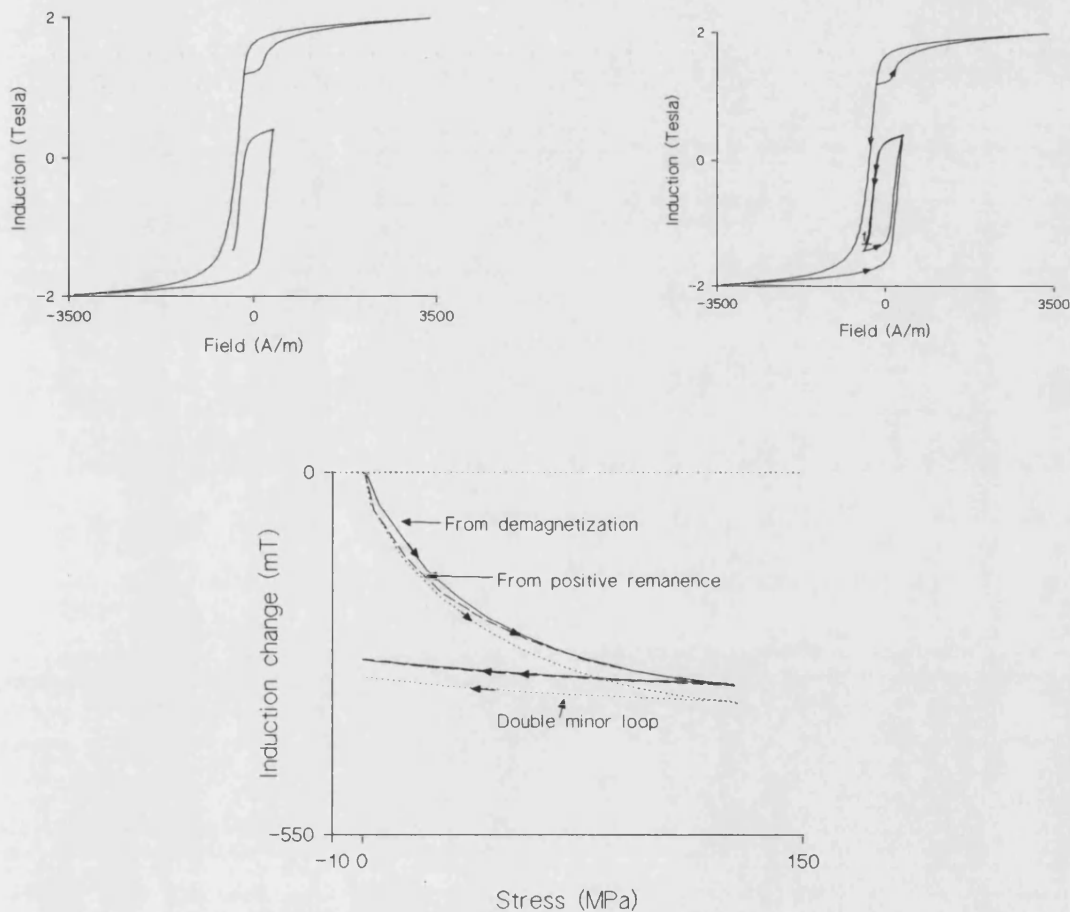Figures 6.38 a. (Top left). Induction change from point (a) of figure 6.37b. b.(Top right). The onset of induction-reducing effects at low stress values is evident. c. The null location is displaced from the equivalent anhysteretic. d-f. The irreversible induction change becomes wholly negative.

The stress-induced induction changes are thus seen to be influenced by magnetic history, contrasting with models predicting dependence on location on the B/H plane. It is of interest to ascertain at what level the previous magnetic history needs to be considered. It could be argued that this may prove to be simply determined by the available measurement resolution. However, it is generally accepted that an efficient demagnetization has the effect of erasing the influence of previous events on the subsequent magnetic performance. For a study of stress-induced induction change from points on initial curves this became the reference condition. A study of stress-induced induction changes from major loop points suggests that approach to technical saturation, negative or positive, has a similar effect. It did not prove necessary to demagnetize the specimen to obtain reproducible behaviour from, for example, major loop points above positive coercivity or near positive remanence. For minor loop points this condition again applies. In figure 6.39a the method of arrival at the end of the minor loop path of the previous figures is from an initial condition near positive remanence. In 6.39b arrival is again from positive remanence but with a double excursion around the minor loop path such that the major loop turn-around point is crossed twice. The subsequent stress-induced induction changes for these two arrival methods are compared in 6.39c along with the data obtained in the original experiment. The B/σ profiles from demagnetization and from remanence are practically coincident, (to a first approximation on this measurement scale), verifying the previously held assumption. The small comparative change in the magnitude of the profile observed from arrival at point (f) through traversing a double minor loop suggests that the repeat loop has an effect on the subsequent stress-induced induction

change. In other words, whilst this data confirms the validity of the assumption that approach to technical saturation removes the effects of previous history, it also suggests that arrival at major loop (turning) points does not. In this way stress-induced induction changes from points within the B/H plane can be expected to gain an increased level of complexity as the magnetic history builds up if they do not at some stage arrive at technical saturation or if they are not efficiently demagnetized. As discussed earlier, determination of the influence of the previous history will depend to a great extent on instrument resolution.

Figures 6.39 a. (Top left): Arrival at minor loop point ((f) of figure 6.37) from remanence. b.(Top right): Arrival by repeat minor loop. c. Stress-induced induction changes by the three different arrival methods.

149

To add weight to the conclusion that the specimen equilibrium condition for minor loops is not necessarily the corresponding principal anhysteretic induction value, the following argument is presented. It is generally accepted that for a specimen demagnetized by an efficient application of a decaying A.C. field, no stress-induced induction change is observed for stress magnitudes within the material elastic limit. This is attributed to the alignment of domain vectors parallel and anti-parallel to the stress axis in equal numbers. Such a technique can be used, as discussed in chapter 5, to confirm the efficiency of demagnetization. In figure 6.40a, arrival at the co-ordinate origin by a different technique is shown. This point, by definition lies on the principal anhysteretic. As such, no irreversible induction change would be predicted if this parameter is truly the equilibrium condition. In the figure inset, the stress-induced induction change observed in the first tension cycle shows a significant irreversible reduction in the absolute value, so contravening the empirical rule of the anhysteretic model.
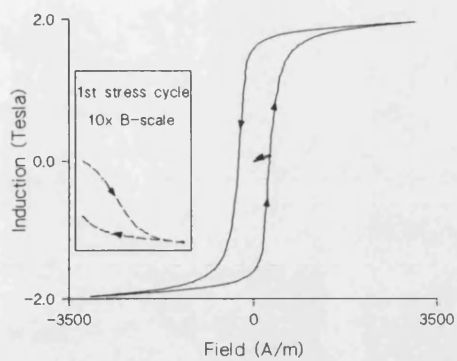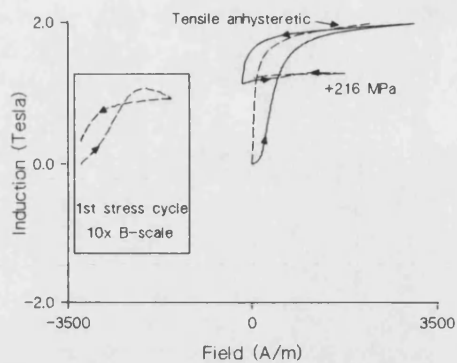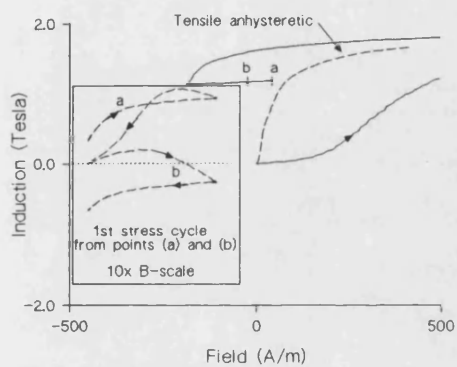
Figures 6.40 a.(Top left). The stress-induced induction change from the co-ordinate origin, arrived at via a minor loop path. b. The stress-induced induction change from a minor loop close to positive remanence. c. Minor loop of b on expanded scale. All three data sets demonstrate a departure from the law of approach to principal anhysteretic.

In figure 6.40b and c, the stress-induced induction changes from minor loop points close to positive remanence are shown relative to the equivalent tensile anhysteretic.

151

At the end of the minor loop path, at point (a) the induction value is measureably above the corresponding tensile (and hence, zero stress) anhysteretic value. The irreversible induction increase with the tension cycle from this point again demonstrates a change away from the supposed equilibrium condition. How the trends in irreversible induction change develop is shown more clearly on the expanded scale of figure 6.40(c). The stress-induced induction change from an intermediate minor loop point is also shown, (point (b)) and demonstrates the nature of the positive-going induction trend. Similar processes are present as for the uniaxial iron specimen on its minor loop above positive coercivity. The transformation of sense for the irreversible induction change from the major loop turning point starts again at the low stress values. An appreciation of this is essential in order to gain insight into the complex magneto-elastic profiles of minor loops.

Analogous behaviour above positive coercivity for the HY80(2) specimen can be demonstrated, (figures 6.41 and 6.42a-f). In figure 6.41 arrival at minor loop co-ordinates relative to the tensile (+216 MPa) anhysteretic is indicated in the expanded scale inset. In 6.42a-f the stress-induced induction changes are shown from the corresponding points. As expected the large irreversible increase in induction observed from the major loop turning point is gradually transformed to a net induction reduction at increasing length of the minor loop from the major loop co-ordinate. Point (e) rests at a point of marginally higher field than that of the intersection between anhysteretic and minor loop path. The net downwards deflection from this point for this stress value, again contravenes the empirical rule of the Jiles-Atherton model. Of particular interest in these figures is the comparison

between the reversible (6th cycle) and first cycle changes from point (d). The comparatively very small irreversible induction change indicates that this point is very close to the 'null' location on the minor loop path for this stress value. One can clearly see how the reversible component serves to modify the overall shape of the stress-induced induction change in the first cycle. As the absolute induction value has not changed significantly in the first five cycles, (to a first approximation), the irreversible component of induction change during the first stress cycle can be obtained by subtraction of the sixth cycle stress-induced induction change from the first. The result of this is shown in figure 6.42g. The first cycle induction change is shown as the solid line, the sixth cycle as the broken one. The irreversible induction change, shown as the dotted line, is observed to consist of a net induction reduction at low stresses and an induction increase at high stress values. This is consistent with measurements from other minor loop points. It should be noted that the shape of the profile during stress release suggests that irreversible induction changes may also be occurring during these release stages.
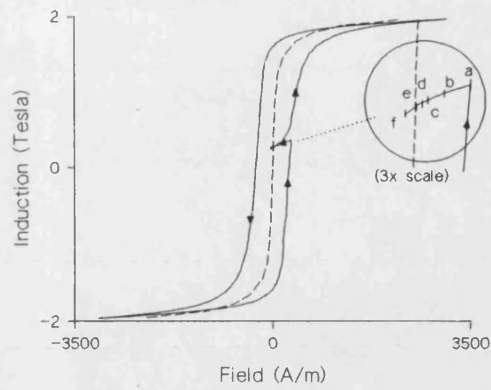
Figure 6.41: Arrival at minor loop co-ordinates for HY80(2). The equivalent tensile anhysteretic is shown.

a. From major loop turning point.

b. H=340 A/m

(5x induction scale)

c. H=181 A/m

6th cycle

d. H=87 A/m

154
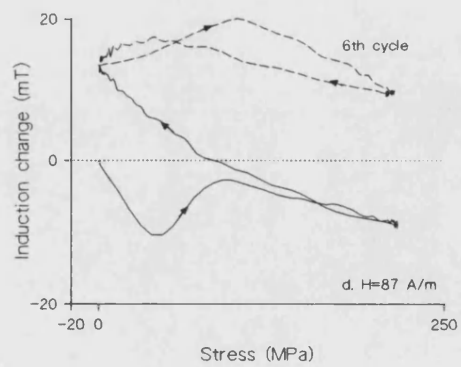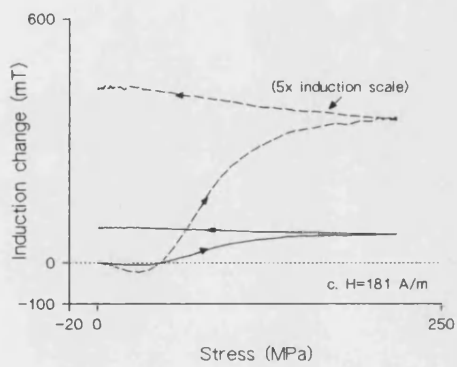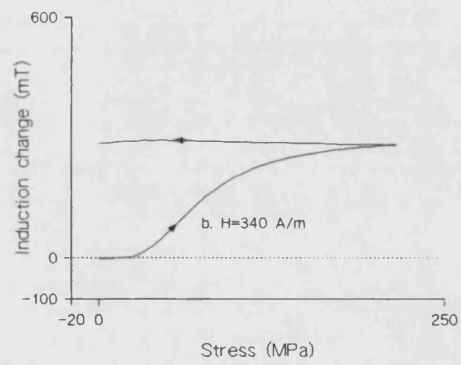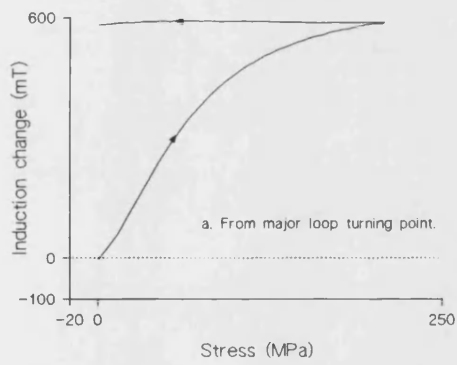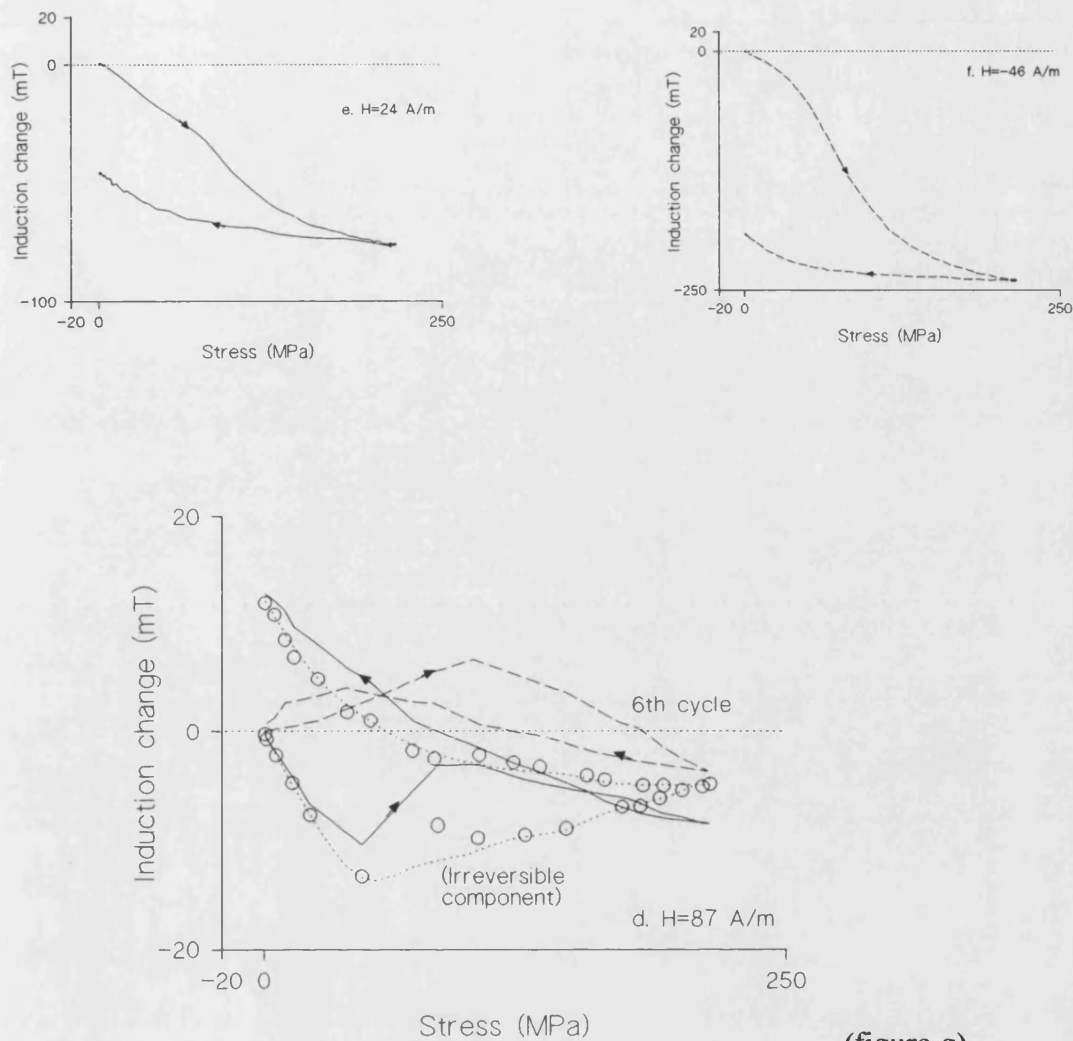
(figure g)

Figure 6.42a-g. Stress-induced induction changes from points indicated in previous figure. The complex reversible profile of figures (d) (and (g), shown as the unbroken line) is thought to be due to the tensile-dependence of the magnetostriction.

The reversible component in figures (d) and (g) is rather complex. The absolute induction values of the minor loop co-ordinates indicate that the specimen is in the 'positive' half of the main magnetic hysteresis profile. As such, tensile stress-induced

155

reversible induction changes should be positive, as the bulk magnetostriction (and its derivative) can be expected to be positive in this region. The low stress regions are indeed characterized by such an increase. In these experiments, however, the absolute induction value is very low. It is known that at low induction values the correspondingly low bulk magnetostriction can be forced negative by the application of sufficient tensile load (Cullity, 1972). It seems likely that this is the mechanism responsible for the peculiar shape of the reversible component. The measurement serves as a good example of the additional complexity in magneto-elastic processes that can arise at low induction values and high tensile load.

Through the use of a close-fitting tufnol support, modest compressive loads can be applied to uniaxial HY80(2) without the risk of buckling. The results of these measurements are shown in figures 6.43 and 6.44 with respect to the equivalent compressive anhysteretic. In figure 6.43 the arrival at minor loop locations is in the usual manner with the equivalent (-122 MPa) compressive anhysteretic shown as the broken line. In figures 6.44a-e the stress-induced induction changes for compressive loads are shown from the corresponding points on the minor loop path. In (a), the major loop turning point, the expected large irreversible increase in induction is again observed. The characteristic loop at high stress levels has been described in an earlier section and has been attributed to the induction value 'meeting' its downwards-moving principal anhysteretic. At points along the minor loop the gradual transformation to a reduction in absolute induction with stress application is again seen to emerge at low stress values. The conflicting processes can give rise to the very complicated profiles from point (c) shown at normal and three-times

induction scale for clarity. The null point for this stress level on this minor loop path was carefully determined, occurring at a point (d), in this case very close to the compressive anhysteretic location. The reversible component is also shown and again demonstrates how it can dominate the shape of the profile at these low induction change levels. As the absolute induction is not changing during the first and fifth stress cycles, the irreversible contribution to the change during the first cycle can be extracted as before. This is shown in (e) as the dotted line. This component is again observed to be characterised by an inversion in the direction of change during stress application similar to the tensile stress-induced induction changes from similar minor loop points.
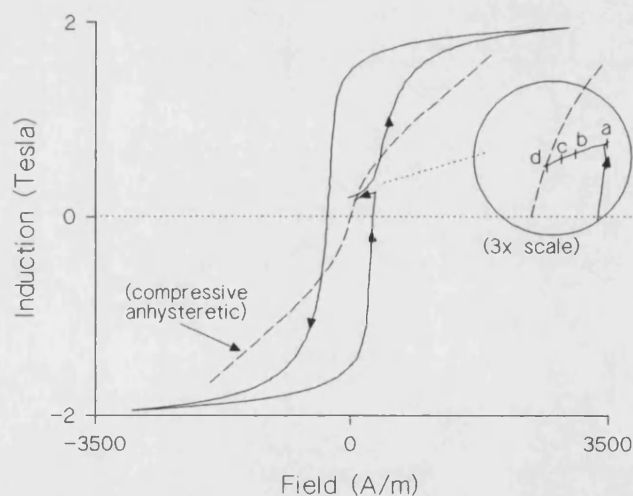
Figure 6.43: Arrival at minor loop points relative to -122 MPa anhysteretic.
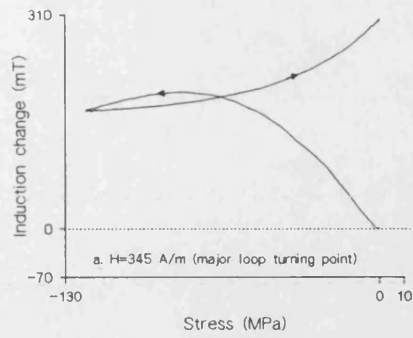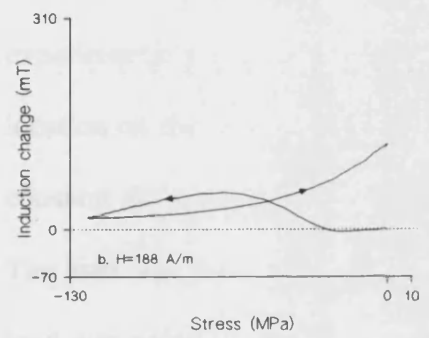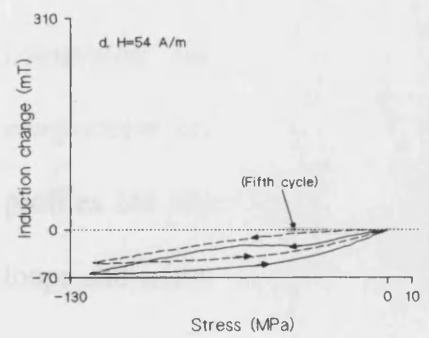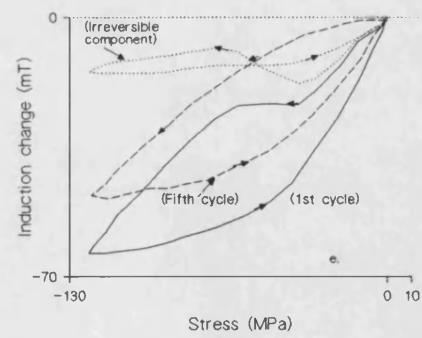
Figures 6.44a-e. Stress-induced induction changes from shown points. In (e) the irreversible component is extracted from the total and reversible changes.

158

The nature of the stress-induced induction changes occurring in the above data sets has been examined more closely through the application of a range of stress values. The indication from results previously shown is that a transformation in the sense of stress-induced induction change develops along the minor loop path. It seems that this transformation originates at the low stress values, although it has not yet been established that these small stresses have caused an irreversible change. The following results demonstrate that this is, in fact, the case. In figures 6.45 the compressive stress-induced induction change from point (c) of the previous figures are shown for several intermediate stress values up to the maximum load. The experimental procedure was as follows. The specimen was brought to the required location on the minor loop through the appropriate field sweeps. With the field held constant the specimen was subjected to low magnitude compressive stress, 20 MPa. The load was then released. The field was then kept constant whilst the compressive load was again applied to a higher value (43 MPa), and again released. This was repeated for two more stress magnitudes, the fourth and fifth cycles possessing the same size of load. The resulting profiles prove conclusively that the *sense of the irreversible induction change is dependent on the magnitude of the applied compressive load*. In this way, stress-induced induction changes on minor loop profiles are essentially different from stress-induced induction changes on major loops and initial induction curves.

For completeness, figure 6.45b shows the results of a similar experiment performed on the steel using tensile loads. The specimen was twice taken to a point on the minor loop shown in figure 6.43 between points (c) and (d). On one occasion it was

159

subjected to a relatively low tensile load (65 MPa), on the other to 216 MPa. The results clearly show again how the sense of the stress-induced induction change is critically dependent on stress magnitude. The results shown in these two figures suggests that the effective mechanism active in irreversible stress-induced induction changes is not overly dependent on the sense of the stress imposed, as both tension and compression are evidently giving similar trends in induction change from minor loop co-ordinates.
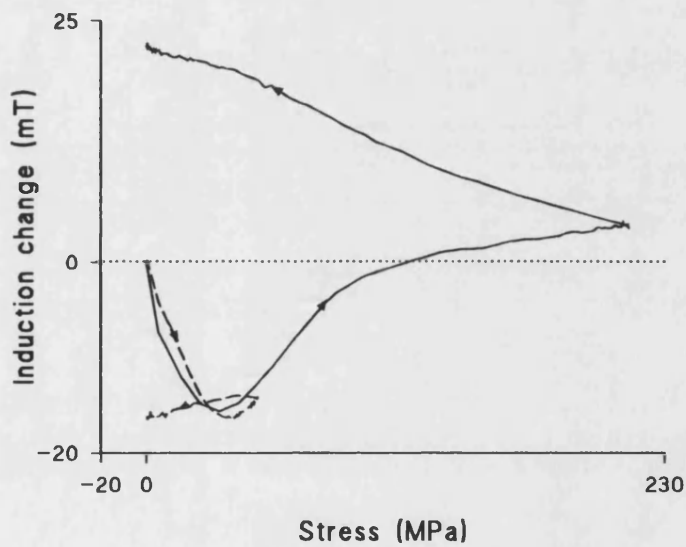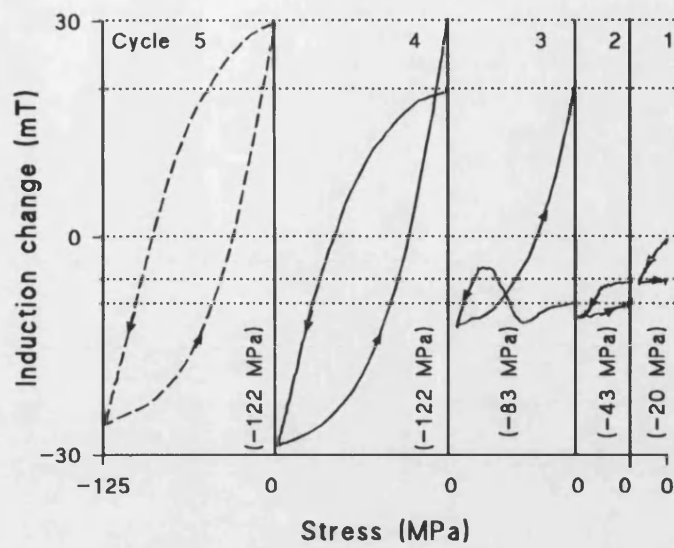
Figure 6.45. a. (Top) Stress-induced induction changes with increasing magnitude of compression from a minor loop point. b. Stress-induced induction changes for low and high tensile loads from a minor loop point. These results prove conclusively that the sense of irreversible induction changes on minor loops is stress-magnitude dependent.

The complexity of minor loop stress-induced induction changes can be explained broadly in terms of the build-up of magnetic history induced largely by external field changes. Earlier in this work, additional complexity associated with double reversals of the field sweep direction was indicated. As a final demon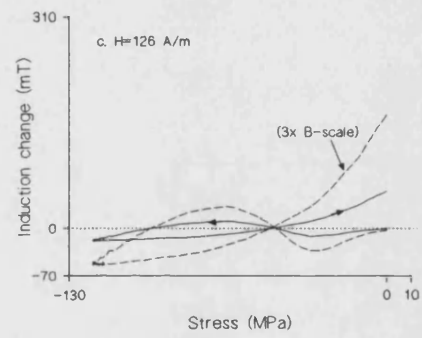stration of HY80 stress-induced induction changes from minor loop points figures 6.46 and 6.47 are included. In figure 6.46 arrival at minor loop locations is shown relative to the corresponding tensile anhysteretic (+216MPa). In 6.47, the stress-induced induction changes from the indicated points are shown. At point (a) a short distance from the second field reversal the induction change is wholly negative, similar to previously observed changes from points distant from the major loop under the same circumstances. As the B/H co-ordinate moves towards increasingly positive values a transformation in the B/σ profile is observed. At point (c) the first cycle induction change is shown with its reversible component. A departure from the law of approach to principal anhysteretic is again demonstrated. The stress-induced induction change profile shows a level of complexity hitherto not observed, showing the full effects of its complicated history. The B/σ profiles eventually transform to a wholly positive induction change at point (f).
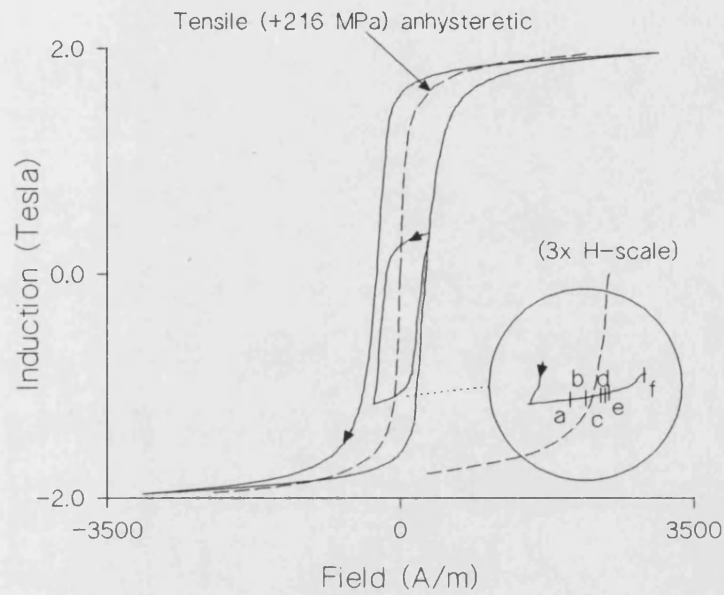
Figure 6.46: HY80(2): Arrival at minor loop locations through double field sweep

reversals relative to tensile anhysteretic.
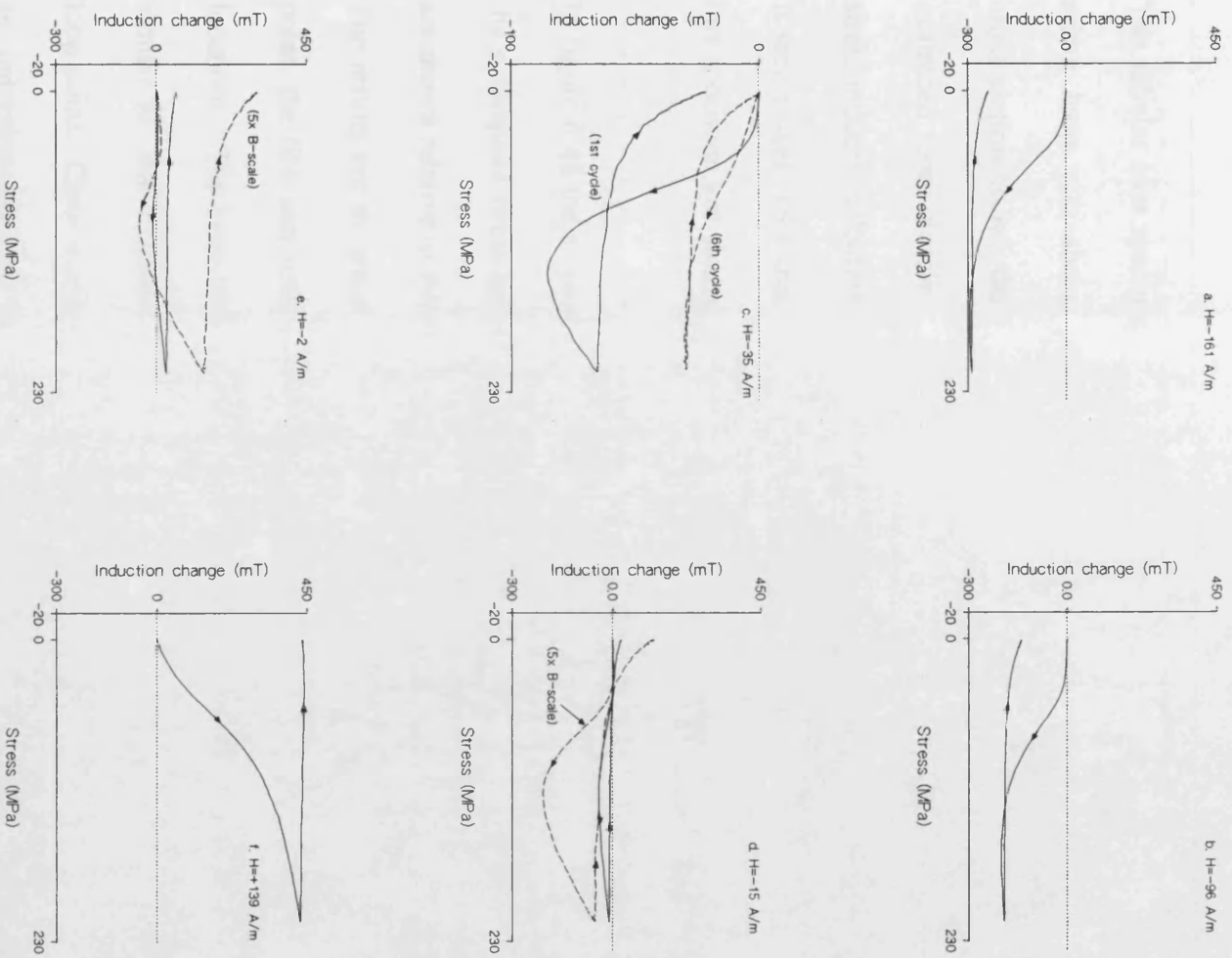
Figures 6.47a-f. Stress-induced induction changes from points indicated in previous figure.

164

6.2.2.4 Tubular Iron specimen at minor loop points.

The tubular iron specimen has been investigated in compression at points along a minor loop path above positive coercivity. The comparatively large specimen cross-section allows the fine details of the induction changes on minor loops to be examined more closely. This specimen has been shown previously to demonstrate stress-induced induction changes similar to those of the other iron-based specimens. It seems likely then that the fine details on the magneto-elastic processes revealed in this specimen are shared with the other polycrystalline specimens.

In figure 6.48 the as-received specimen is taken to points on the minor loop path and the subsequent stress-induced induction changes measured in the usual manner. These are shown relative to the equivalent compressive anhysteretic (-63MPa, in these tests). The results are shown in figure 6.49. For point (a), just off the major loop turning point, the first and sixth cycle induction changes are shown in their correct relative locations. The large irreversible increase in induction observed in the first cycle is similar to that expected of stress-induced induction change from the nearby major loop point. Close examination of the first cycle profile does reveal the emergence of an induction-reducing tendency at low stress levels, a feature demonstrated in previous data sets. The reversible component, as demonstrated by the sixth cycle, does not change noticeably over the range of fields used on this minor loop path. It possesses the peculiar profile at low stress levels which has been reported from initial curve and major loop points, thought most likely to be attributable to texture.

As the distance from the major loop turning point increases, the B/σ profile is complicated by the conflicting mechanisms of induction change. At point (c), the first cycle induction change is zero. However, the increased resolution allowed by use of a larger section specimen, reveals that subsequent stress-induced induction changes from this point are characterized by small but measureable irreversible induction changes as shown in the inset for this figure. A similar deviation from expectation is demonstrated from points (d) and (e). The first cycle induction changes in each case are seen to be significantly negative. For both locations though, the subsequent irreversible induction changes, for stress to the same level, have changed sense. This is a demonstration of complexity on minor loop paths not previously observed, and serves as a vital aid towards an understanding of such processes. At points (f) and (g) the large irreversible induction changes are consistent with previous observations. The demonstration of continued departure from the law of approach to principal anhysteretic is implicit in the above measurements from points (d)-(f).
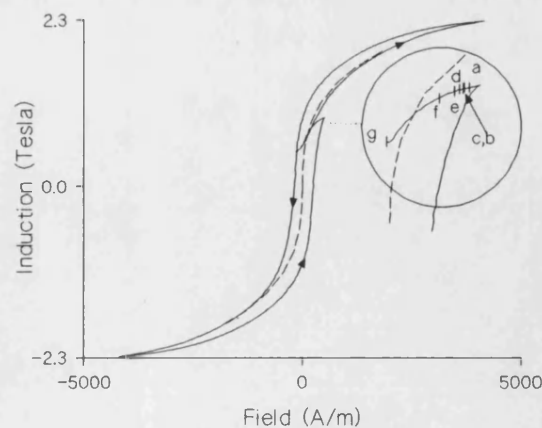
Figure 6.48: Arrival at minor loop co-ordinates for Fe tube with respect to compressive anhysteretic.

166
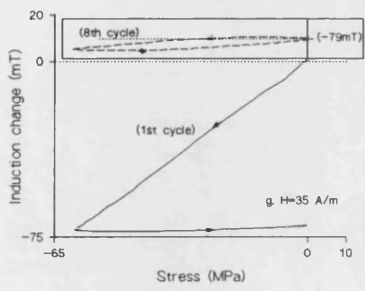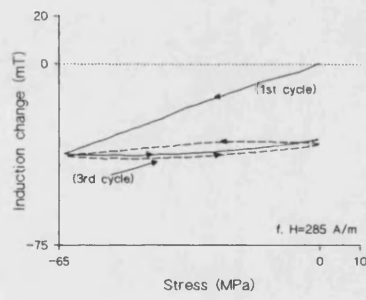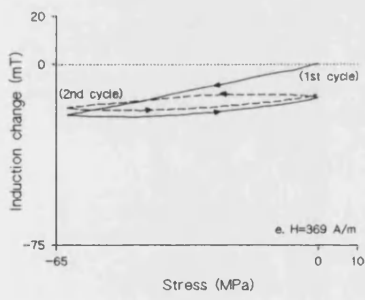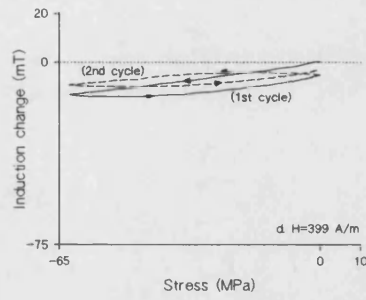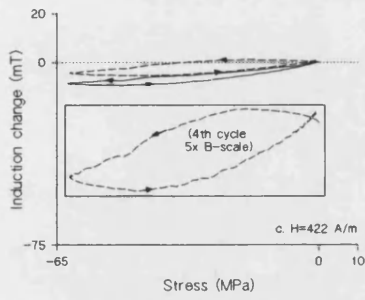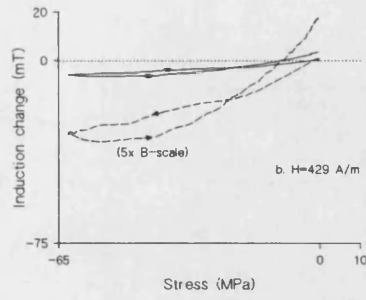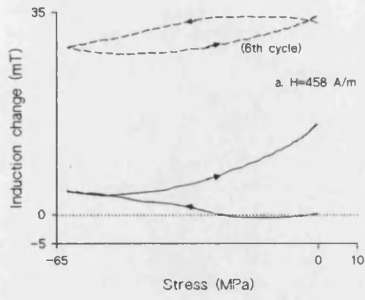
Figures 6.49a-g. Compressive stress-induced induction changes from minor loop points for Fe tube. First cycle is the solid line in each case.

167

The irreversible change in the induction as a function of stress cycle number for points a, d, e and g are shown in figure 6.50. At either extreme of the minor loop path, (points a and g), the induction value shows the asymptotic approach to stability similar to major loop and initial induction curve points. From points d and e, the reversals in the induction change sense after the initial cycle serve to raise the absolute induction towards the start values. In the first case, from point d, this results in a final induction slightly greater than indicated at the minor loop point. At e the reversal is not so dramatic and serves to modify the final induction change in such a way that a net reduction in absolute value is still evident. A consideration of the implications of these trends will be given in a chapter 7, but it is immediately clear that the inversion of the stress-induced induction change sense with stress cycle number indicates a further complexity in the magneto-elastic mechanism.
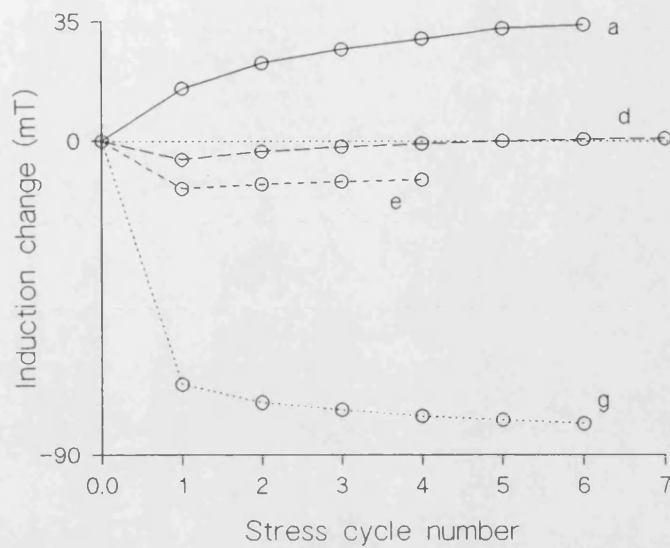
Figure 6.50: The irreversible induction change against number of stress cycles for minor loop points of figure 6.48 in the tubular iron specimen. Reversal in the sense of the irreversible component of change is evident from points d and e.

It is of interest to examine the stress-induced induction changes from minor loop points of the tubular iron specimen in its annealed condition. The results are shown in figures 6.51a and b. In (a), arrival at minor loop co-ordinates relative to the equivalent (-63 MPa) compressive anhysteretic is shown. In figure (b) the stress-induced induction changes from the indicated points demonstrate similar behaviour to the specimen in as-received form. At point (a), at marginally higher field than the compressive principal anhysteretic, an irreversible reduction in induction demonstrates that the annealed specimen shows similar qualitative profiles along minor loop paths to those of the as-received condition. The effective null location (zero irreversible induction change) is at point (b), shown with its third

169

cycle as the dashed line. Comparison of the relative locations of the effective null with respect to the width of the hysteresis loops of the annealed and cold worked specimens indicates that on a proportional basis, the null location for the as-received specimen occurs much closer to the major loop turning point. Paraphrased, the specimen in its as-received condition demonstrates a departure from the law of approach to principal anhysteretic more readily than in its annealed condition. This observation reflects the importance of residual stresses within the specimen acting as pinning sites for domain wall motion. In the annealed condition the reduction in the number of pinning centres for domain walls, allows the specimen to demonstrate reduced coercive fields and attain inductions much closer to the corresponding anhysteretic values. The absence of the peculiarity reported earlier in the shape of the reversible component (third cycle), attributed to texture in the as-received tube, should again be noted.
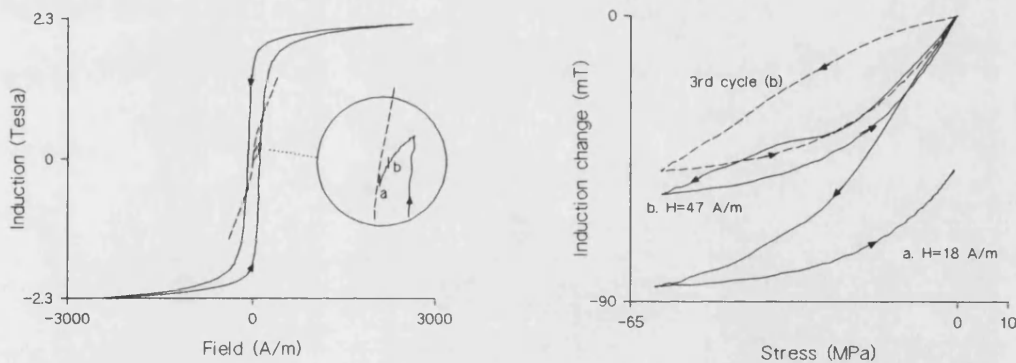
Figure 6.51 a. (Left): Arrival at minor loop co-ordinates for the tubular ironspecimen in annealed condition. b. Induction changes from points (a) and (b). From point (a) a departure from the Jiles-Atherton empirical rule is observed.

6.2.3 *The influence of material temperature changes*

The discussion has hitherto centred on the the magneto-elastic performance of polycrystalline materials at ambient temperatures, typically varying between 18-25 °C. Variation in temperature can provide some insight into the processes active in stress-induced induction changes through its influence on the magnitude of such changes. Furthermore, temperature-induced induction changes at constant field and load can confirm ideas concerning the thermal activation of domain walls held at pinning centres. Such experiments have been reported before, (Cullity, 1972), in which iso-field temperature changes have been shown to induce both reversible and irreversible induction changes in specimens. In this way one can draw an analogy between the effects of stress and temperature from discrete points on specimen B/H profiles, as both serve to release domain walls from their pinned sites through the contribution of additional energy. It should be noted though that the analogy may not be extended too far. Whilst it is considered that stress can influence the position of domain boundaries separating regions where the moments are aligned orthogonally, increasing temperature is likely to influence all wall types, including stress-inactive 180° walls.

Temperature changes have a marked effect on specimen coercivity. In materials of the type investigated in this work, the magnitude of the coercive field relates directly to the density of pinning sites in the form of lattice dislocations, alloying elements or grain boundaries. The dependence on dislocation density was shown for the previously reported tubular iron specimen, in which reduction of residual stress

through annealing served to reduce the coercive field. In figure 6.52a the variation

in the coercive field as a function of temperature for the uniaxial HY80(2) specimen

is shown. Other works (Gaunt 1976, 1984, 1987; Rancourt 1989a and 1989b), have

reported a logarithmic relationship between temperature and coercivity based on the

thermal activation of domain walls. Such reports have often considered larger

temperature intervals than presented here and different material types. The errors in

the coercivity variation measured for the HY80(2) specimen do not allow a detailed

analysis of the exact relationship between temperature and coercivity over this small

temperature range but the trend in the results confirm that increased thermal

activation will allow irreversible induction changes more easily. The mechanism for

this is assumed to be domain walls being more readily freed from their pinned sites.

In 6.52b, the variation in peak induction measured for HY80(2) is shown for

reference. The observed 0.7% decrease is expected, given the known temperature

dependence of the spontaneous magnetization in iron in this temperature interval.
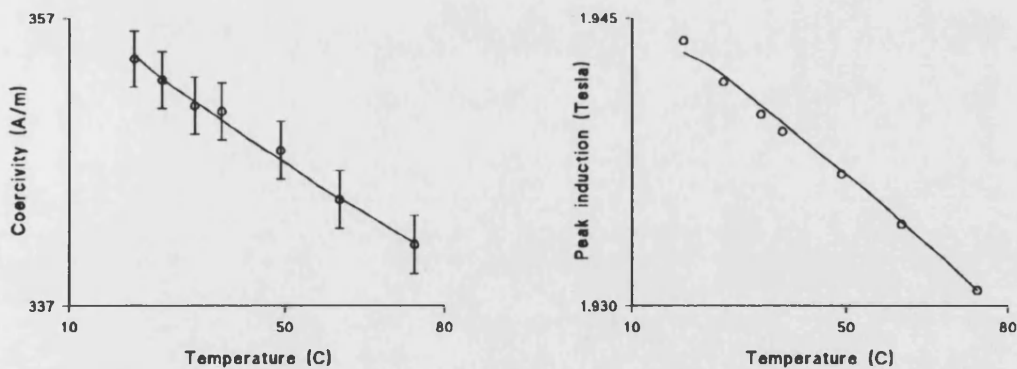
Figures 6.52a-b. Coercivity and peak induction for uniaxial HY80(2) versus

temperature. The variation in coercivity is an indication of the thermal activation of

domain walls at their pinned sites.

172

In figure 6.53a, the hysteresis loops for uniaxial HY80(2) are shown at 20°C and 75°C on an expanded scale for clarity. The increased permeability of the high temperature profile is evident in its greater induction values on the initial induction curve. However, as the peak induction at 75°C is less than that at 20°C, the B/H curves will be seen to cross over at higher fields on both the initial induction and major loop lines. In other words, the low field high temperature permeability is greater, the situation being reversed at higher fields. Indicated in the figure are the field locations from which the specimen has been subjected to a single 140 MPa tensile cycle at 20°C and 75°C. In figure 6.53b, the stress-induced induction changes from point (b) at 298 A/m are shown. An increase in the stress-induced induction change is observed at the higher temperature. In 6.53c, the magnitudes of the irreversible changes induced by single tension cycles at the indicated points are shown for the two extremes of temperature used in the investigation. The results show that the peak in the stress-induced induction change is located 'beyond' the corresponding coercivity. This is consistent with the previously reported experiments on the biaxial HY80 specimen in which the roles of tension and compression are reversed. Also evident is the cross-over in the magnitudes of the stress-induced induction changes at the higher fields (above the coercivities). It has been shown (section 6.2.1) that the relative magnitudes of the stress-induced induction changes are related to the differential permeabilities, and this relationship is evident in these data sets. However, the relationship is distorted by the previously reported lateral shifts in the profile of induction change as a function of stress magnitude relative to the zero stress permeability profiles.
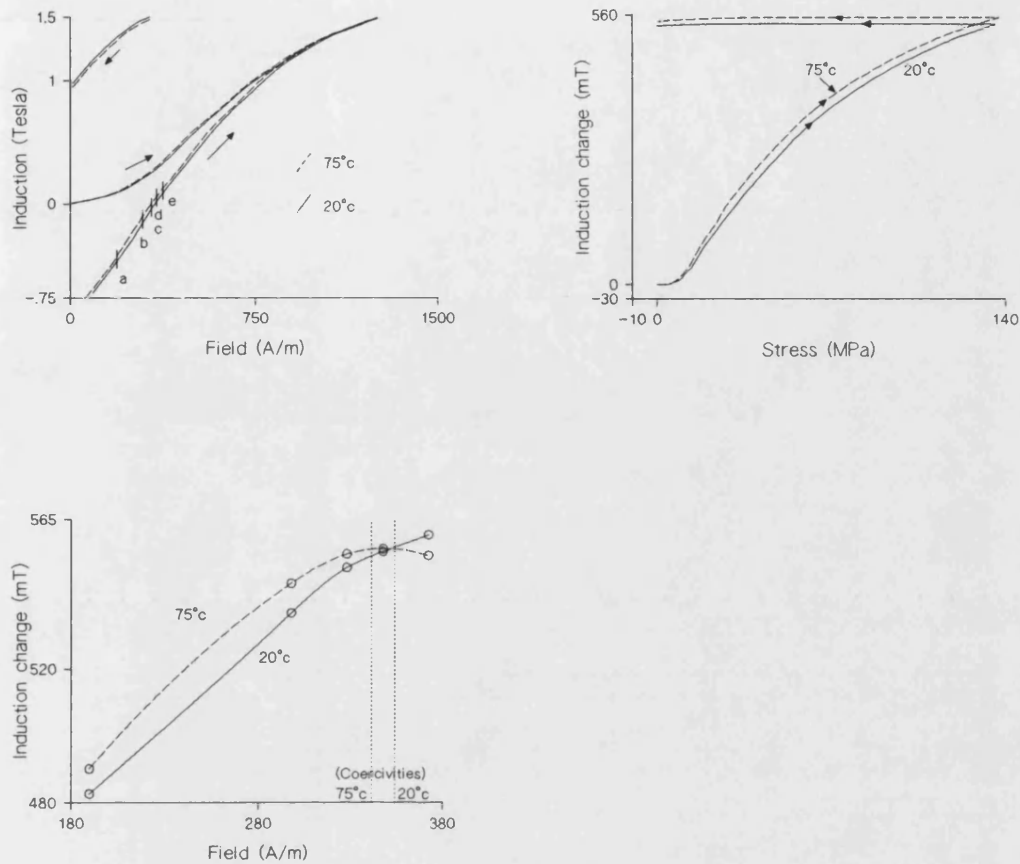
Figures 6.53a-c. a. (Top left). Portions of the hysteresis loops for uniaxial HY80(2) at 20°C and 75°C with points from which stress-induced induction changes are measured. b. Stress-induced induction changes at the two temperatures from point (b). c. How the magnitude of the induction change differs with field.

It has been shown earlier that the reversible component is dependent on the induction-dependent bulk magnetostriction, or more precisely, its induction derivative. The relationship between the magnetostriction constants for iron and temperature has been previously reported, (Tatsumoto and Okamoto, 1959; Williams and Pavlovic,

174

1968), although, apart from electrical steels, there do not appear to be many reports on the temperature dependence of the magnetostriction of polycrystalline iron-based materials. The magnetostriction of the uniaxial specimen HY80(2) has been measured at the high and low temperatures available in these tests by the strain gauge technique, the results for which are shown in figure 6.54. It is evident from these profiles that the increase in temperature over this range leads to larger values of magnetostriction and hence its induction derivative, implying the reversible component of stress-induced induction change may do likewise.
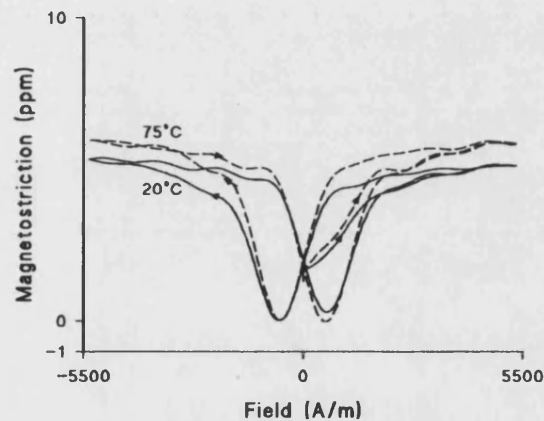
Figure 6.54: Magnetostriction of uniaxial specimen HY80(2) at room temperature and 75°C. The increase in values for the high temperature profile suggests that the reversible component of stress-induced induction changes will increase with temperature in this range.

Finally, the induction changes from discrete points on or within the B/H plane have been measured at constant field and zero load but with varying temperature. This has

been performed for the uniaxial HY80 and iron specimens with closely similar results. For brevity, the results of the uniaxial iron specimen Fe(2) are presented here.

Figure 6.55a shows the specimen taken along a minor loop path from an initial demagnetized condition. At points (a), (b) and (c) shown on the expanded scale inset, the specimen has been subjected to temperature cycles. The results for three temperature cycles at the major loop turning point (a) are shown in figure 6.55b. The initial cycle to nearly 80°C is characterized by a significant increase in the specimen induction, with a minimal induction change during cooling. Subsequent cycles have the effect of causing a further, limiting irreversible increase in specimen induction.

The similarity between induction changes induced by temperature and stress cycling is immediately apparent. Classically, one can view the increase in temperature as providing energy to allow domain walls to overcome their barriers at pinned sites, moving in a way that allows increased induction in a sense consistent with that caused by the previous field sweep. The analogy is extended by the observation of reptation, also evident in stress cycling. It has been reported (Cullity, 1972) that reversible induction changes are also associated with temperature fluctuations at discrete points. One would expect these to be measureable from temperature cycles in excess of the three recorded here.
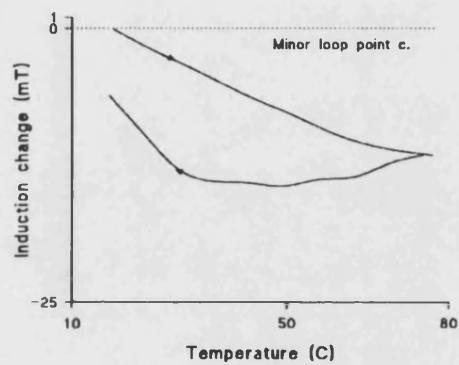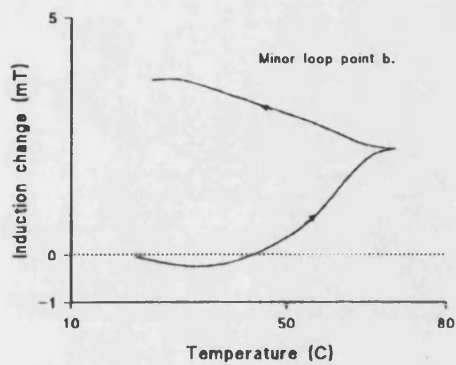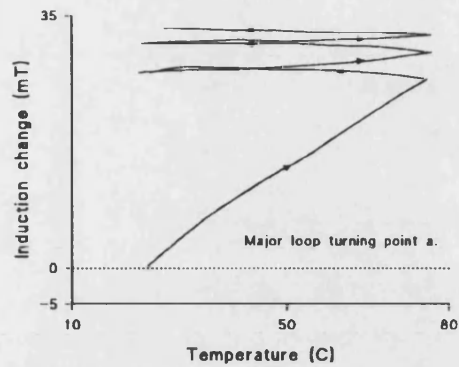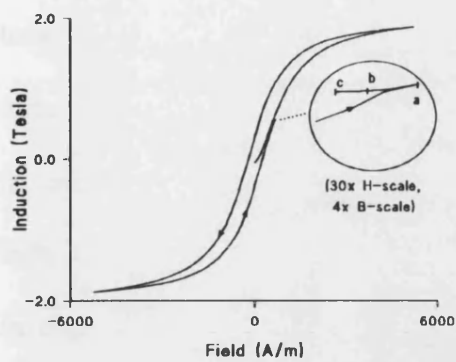
Figures 6.55a-d. a. (Top left): Arrival at minor loop locations for uniaxial Fe(2). b. (Top right). At the major loop turning point temperature cycles affect an irreversible increase in specimen induction. In c and d (bottom left and right), the transformation of the induction change to wholly negative mirrors the trends observed in stress-induced induction changes reported earlier.

At point (b) on the minor loop of the figure, the induction profile with temperature shows some of the characteristics which are present in stress-induced induction changes from similar histories. In particular, the growth of induction-reducing

177

tendencies, at temperatures marginally above ambient, resembles the profiles seen of tension and compression from minor loop points. At point (c), at the end of the minor loop profile, a net irreversible decrease of induction with increased temperature is recorded. The similarity between the temperature-induced and stress-induced induction changes, especially on minor loops (section 6.2.2) suggests that variations in these quantities may be capable of inducing the same mechanisms for induction change in polycrystalline ferromagnets.

Of interest in these figures is the distance from the major loop point at which the irreversible induction change transforms to wholly negative. Compared to the stress-induced induction changes shown in earlier sections, the field difference between point (c) and the major loop turning point (a) is relatively small. The absolute changes in induction for the temperature changes applied are also comparatively small. This implies that, for the temperature range of these experiments, only a small fraction of domain walls are being released from their pinned sites. The temperature variation applied is inducing changes more compatible with those observed in low stress intervals as seen in figure 6.45b. This information is vital in aiding increased understanding of the processes at hand in stress-induced induction changes from discrete points and assists in the description of the simple model suggested in chapter 7.

7   Discussion and conclusions.

The experimental evidence of the preceding chapter, when viewed against the existing models of stress-induced induction changes, suggests a complexity which is not covered by such models. Discrepancies between experimental and modelled behaviour are common to both the steel and iron specimens investigated. The demonstration of similar magneto-elastic processes across a wider range of materials, as demonstrated by the nickel specimen investigated here, suggests that many aspects of stress-induced induction changes in polycrystalline specimens can be explained in terms of characteristics which are not unique to particular specimens or materials. A cursory examination of the archival literature (Craik and Wood, 1970) adds weight to this conclusion.

A significant development is the recognition that, in common with field-induced induction changes, stress-induced induction changes from discrete points on or within a specimen hysteresis loop possess irreversible and reversible components. As Atherton, Rao and Schönbächler state, (1988), it was the inability to distinguish between reversible and irreversible components of stress-induced induction change that confused early attempts to understand (polycrystalline specimen) magneto-elastic performance. Hence, as demonstrated here and elsewhere, the irreversible changes are usually dominant in the first few stress cycles with the reversible component superimposed and contributing to a (usually) relatively small alteration of the overall $\Delta B/\sigma$ profile. The reversible component magnitude, itself a function of the absolute induction, is measurable in the 'closed' loop induction change of later stress cycles

in the same background field. These ideas are consistent with a physical interpretation of domain wall motion considered by Globus and Duplex (1966, 1969, 1970), where the walls are viewed essentially as elastic membranes, possessing surface energy when held between sites under the action of applied field. Irreversible contributions to induction change can then be viewed as motion of domain walls through such sites, reversible ones to changes in the amount of 'bowing' between sites. These processes have already been discussed in chapter 4.

Stress-effective field formulae have usually been expressed in terms of the saturation magnetostriction of the material. For a single domain this takes the common form,

$$H_\sigma = \pm \frac{3}{2} \frac{\lambda_s \sigma}{\mu_0 M_s} \qquad \text{7.1}$$

This has led some workers to assume that the action of stress on polycrystalline ferromagnets can be modelled on the basis of suitable polycrystalline averaging. In this work it has been shown that the reversible component of stress-induced induction changes from discrete points can be interpreted in terms of the induction derivative of the bulk magnetostriction, as suggested by Sablik (1989), as opposed to the single domain saturation value. This approach, predicted by thermodynamics, correctly describes how the reversible component of stress-induced induction changes will suffer an inversion at high fields in iron based materials, as clearly demonstrated in chapter 6, figures 6.26-29. An interpretation of reversible changes in terms of equation 7.1 would predict a constant effective field suffering no inversion, which is clearly not the case. (The polycrystalline saturation of iron at - 7ppm would, in fact,

predict that tensile induction changes should reduce specimen induction for all field values, which is even further departed from experimental observation for induction values below the knee of the hysteresis curve). Whilst it was the approach of early workers to interpret small irreversible stress-induced induction changes in terms of the pressure on $\pm 90°$ walls, (Brown, 1949) such a method appears to be of limited value when considering larger changes. The work of Birss (1971) and Faunce (1970) highlighted the increased complexity in large scale stress-induced induction change, leading them to consider the more significant contribution of other processes. The irreversible component of change is more readily interpreted in terms of the changes in the energies associated with domain wall pinning, according to these authors, associated with the 'opposition' term. Similarly, in the Jiles-Atherton model, application of external load is seen to change the energy associated with pinning sites such that some domain wall areas will be released, others more firmly held, (Jiles and Atherton, 1984). The work of Astie, Degauque, Porteseil and Vergne (1981) highlighted the importance of the dislocations in iron to magneto-elastic processes. Movement of dislocations in a specimen subjected to load, would be seen in an empirical model as supplementary to this 'depinning' process. The empirical model of Jiles and Atherton, describing how the application of stress cycles allows the asymptotic approach to the true equilibrium condition, as depicted by the principal anhysteretic, has been demonstrated to be of value for simple magnetic histories. From points along the initial curve and major loop their model correctly explains how compression and tension give rise to induction changes of the same sense. Differing magnitudes of change are explained in terms of the stress-dependence of the

181

anhysteretic itself. In work presented here departures from the model predictions are further evidence of the increased complexity of stress-induced induction change.

Most striking in the magneto-elastic performance of polycrystalline ferromagnets is the behaviour from complex magnetic histories along minor loops, demonstrated in section 6.2.2. As a consequence of the build up of magnetic history, stress-induced induction changes from points within the B/H plane are seen to show a level of complexity not described by existing formulae. This is indicative of the importance of magnetic history as opposed to the relative location on the B/H plane of the initial and anhysteretic conditions. Above all, the sense of the irreversible component of induction change has been demonstrated to be a function of stress magnitude, for minor loop points. This manifests itself in conflicting directions of change for high and low stress, as demonstrated, for example, in figures 6.45. Implicit in this behaviour is that departures from the 'law' of approach to the principal anhysteretic can be readily demonstrated on minor loops. As large structures comprising significant quantities of polycrystalline ferromagnetic material will be subjected to similar complex field (and stress) histories, the performance of irons and steel from minor loops more accurately describes the *in-situ* performance of such structures, as opposed to the simpler behaviour from carefully controlled histories.

An attempt to describe how such complicated behaviour can arise is given in figures 7.1. In these figures no attempt is made to represent the differing magnitudes of induction change which characterize the two stress senses. Rather, a qualitative picture of how the conflicting processes on minor loops could emerge is presented.

In each figure, two regions of the same ferromagnetic specimen are shown. In the upper region, a domain wall is seen to move through a volume containing sites at which it is heavily pinned. In the lower, a similar wall is seen to progress through a region of material in which the sites retard the wall motion less efficiently.

In figure (a), a schematic domain wall configuration consistent with hypotheses of domain walls acting as membranes is depicted. Such a configuration may result from the specimen being subjected to a demagnetization, (which would result in planar domain walls), followed by an excursion along the initial induction curve. Alternatively, such a configuration may arise at points on a major loop after an excursion towards positive or negative saturation, as it has been demonstrated in chapter 6, that such a process also has the effect of erasing magnetic history. In either case, one observes that domain walls for both heavily and lightly pinned regions are 'bowed' in the same sense consistent with a direction which would allow them to approach their equilibrium condition in the absence of such pinning sites. The application of stress is seen to allow both domain walls to progress irreversibly towards their equilibrium location, the lightly pinned wall moving through a greater distance, consistent with the co-operative release mechanisms described in works by Gaunt (1984). If the stress sense is chosen as tensile, for example, and the specimen is at an absolute induction level where $d\lambda/dB$ is positive, then the inverse magnetostrictive or reversible component can be represented by moment canting along the domain boundary, (a perturbation to the level of bow), in such a way that further increases the absolute induction value, when stress is applied. With the release of stress this addition to the induction level is subtracted.

In figure (b) we consider a possible domain configuration on a minor loop. Such a configuration may arise from the previous case in figure (a) but then the field sweep direction has been reversed i.e. the field reduced a small amount relative to the magnitude of the initial field sweep. The field reduction can be shown to instigate a reversible and irreversible decrease in specimen induction. It seems reasonable to suggest that in the region where the domain walls are less heavily pinned, motion in the reverse direction under the influence of the field reduction will be initiated more readily. As such, domain walls in such regions will more easily become bowed in a sense opposite to that previously developed in the simpler magnetic history of case (a). In the heavily pinned region, it is reasonable to suggest that the field reduction has caused a reduction in the amount of bow, i.e. the surface energy, but because this energy was previously large in case (a), the bow sense has not been reversed, merely its magnitude reduced. The action of stress can be examined through application of large or small stresses. At low levels of external load, the change in energy associated with the pinned sites is enough to allow continued motion of the domain wall through the low energy region in a way that reduces the absolute induction level. At high applied stress levels, the heavily pinned domain wall can still be released to move in a direction dictated by its wall surface energy or bow. In this way one observes the conflicting directions of stress-induced induction changes on minor loop points. The reversible component of change, again represented by moment canting remains largely unchanged in this field interval. This is consistent with experimental observation contained here and in other works, (Atherton and V Ton, 1990).

184
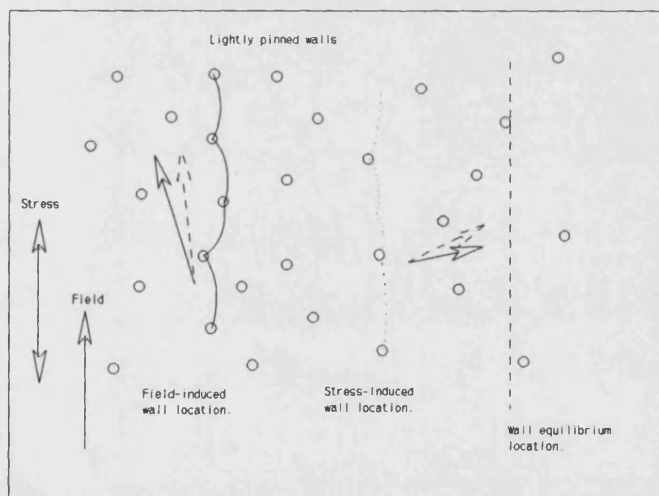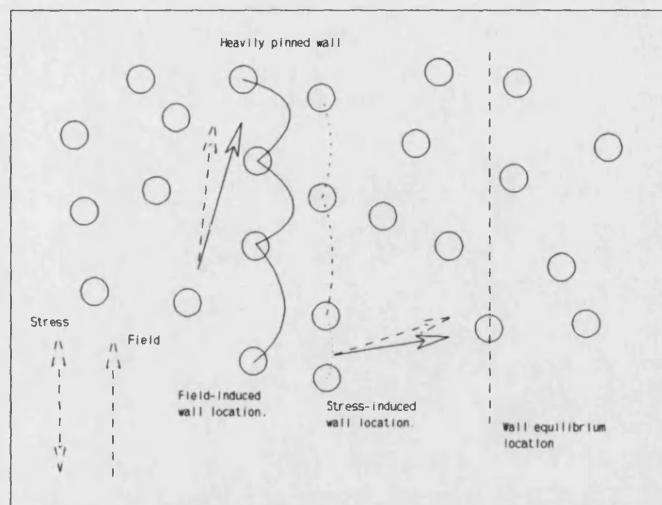
Figure 7.1a: A major loop domain configuration. In the upper portion of the figure a domain boundary moves through sites which heavily retard its motion. This results in increased boundary curvature. In the lower portion of the figure, a similar domain wall moves through a region in which it is lightly pinned. The application of stress allows both boundaries to progress in the same sense.

185
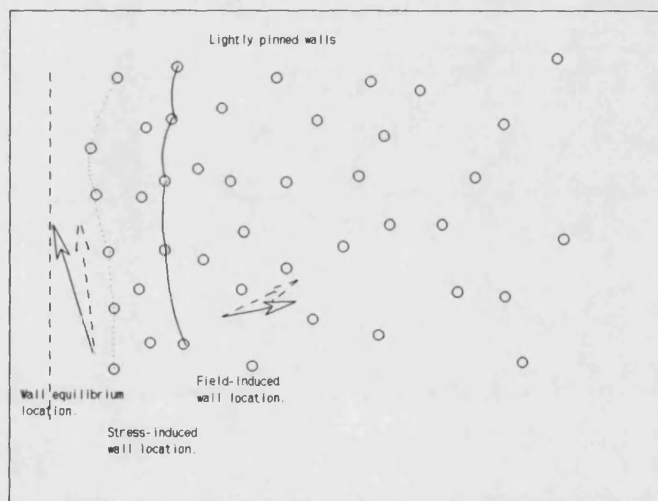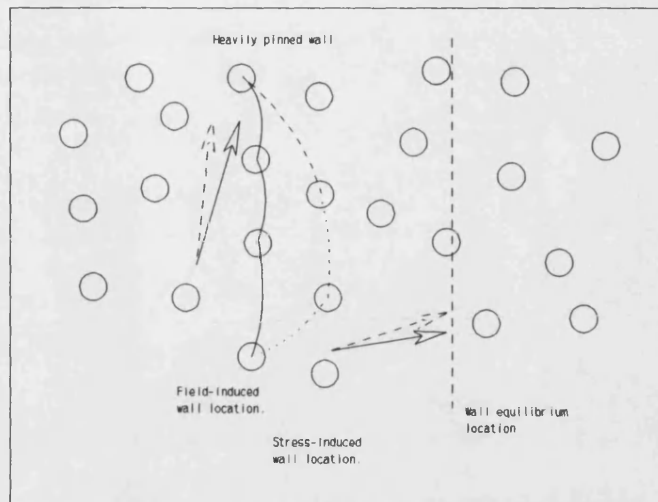
Figure 7.1b: Proposed minor loop domain configuration. The reduction in field strength has reversed the direction of motion of the wall in the lightly pinned region. With the application of low stresses these walls continue to move in this reverse sense. The previously highly pinned wall of the upper region again travels in its original direction with stress.

This schematic representation of stress-induced induction change is capable of explaining the main qualitative results of minor loop B/σ profiles. Fundamental to its correctness is an assumption of a spread of pinning site energies within the polycrystalline specimens investigated. This seems a reasonable assumption, and it is worth noting that any existing models which assume a mean pinning site energy would have to be modified to include this analysis. The mechanisms evident on minor loops conclusively prove that the concept of a 'stress-effective' field cannot meaningfully be applied to large irreversible induction changes, as this concept could not accommodate the dependence of induction change sense on stress magnitude. An alternative mechanism of stress-induced induction change must be more dominant than that suggested in an analysis of the opposing pressures on $\pm 90°$ walls. According to Birss (1971), confirmation of the effects of changes to the opposition to domain wall motion is derived from the induction-temperature work of Yamada (1960). This has been expanded upon in the work presented here, especially with respect to the performance on minor loops. Increases in temperature have been used as an additional tool to probe the irreversible component of the induction-stress interaction, as demonstrated in section 6.2.3. It has been clearly demonstrated that an analogy exists between the effects of application of stress and increase in temperature in that similar irreversible induction changes can be initiated by either process. This leads to the possibility that both stress and temperature act through an activation process whereby domain boundaries will be freed from their pinned sites if supplied with sufficient energy, provided thermally or elastically. Inhomogeneous media have a large contribution to their coercivity from obstructions to domain wall motion. The reduction of coercivity with increased temperature, as demonstrated in

figure 6.52a adds weight to the argument that release from pinned sites is an activation process. In this way, increased temperature at discrete points on a specimen B/H plane can initiate induction changes. Whilst Yamada has recorded both reversible and irreversible processes, it is the latter which have been highlighted in this work. From major loop points, a heat and cool cycle is seen to cause a significant, monotonic change in the induction in the same sense as that initiated by the previous field sweep, as demonstrated in figure 6.53(b) and 6.55(b). For the range of temperatures used in these cases the induction changes are comparable to those caused by very small stresses. (Use of temperatures above the ranges reported in this work is considered inappropriate, as the effects of microstructural changes associated with annealing or diffusion processes in the specimen would complicate the analysis of magnetic performance). In keeping with previous arguments presented here, this would suggest that this temperature range is capable of influencing domain boundaries pinned predominantly at sites of relatively low energies. This is confirmed by inspection of the irreversible induction changes induced by heating at minor loop points. One observes again the shared trends between the stress-induced and heat-induced induction changes. As the field is gradually reduced from a major loop turning point, small increases in temperature are seen to initiate a reduction in the level of induction, whereas this trend is capable of being reversed at higher temperatures, as shown in figure 6.55c. In figure 6.55d, one observes that, similar to stress-induced induction changes from points along a well-developed minor loop, temperature increases induce a wholly negative induction change. The fact that for the temperature-induced induction change, the position on the minor loop path is only slightly removed from the major loop turning point compared to the corresponding

typical stress-induced induction profiles, is evidence of the lower spectrum of pinning energies that this temperature range is influencing, compared to those influenced in typical stress-induced induction changes involving loads of tens of mega Pascals. The analogy between temperature and stress can, of course, only be carried so far. It is only the irreversible component of induction change to which these arguments can be applied. Street and Woolley (1949), demonstrated the relationship between temperature and magnetic viscosity. This latter quantity is found to be a maximum at the peak irreversible permeability locations on the specimen B/H plane (Street and Woolley (1949), Wohlfarth (1984)). It could be expected that thermal energy would instigate the largest irreversible induction changes at such points. Whilst Schneider (1984) has demonstrated a close relationship between the magnitudes of irreversible stress-induced induction changes and the irreversible component of the differential susceptibility, results presented in this work show that a direct proportionality between the two quantities is perturbed by more complex magneto-elastic processes as demonstrated in figures 6.17-6.20. It does however, seem reasonable to conclude that the concurrence of experimental induction changes induced by changes in temperature and stress implies that a significant factor in stress-induced induction changes involves the enhancement of the normal temperature-time dependence of the field-induced change. This is in keeping with the general idea of stress allowing an approach to an equilibrium condition, although, as has been shown here, this condition is not defined, at fixed field, by a singularity on the B/H plane but is acutely dependent on history.

It can be concluded that the action of tensile or compressive stress imposed at

189

discrete points on a specimen B/H plane manifests itself as two recognizably separate mechanisms. The relationship of the reversible component and the specimen bulk magnetostriction has been demonstrated. This lends itself easily to a mathematical description and can be readily modelled. The application of stress also instigates an irreversible component of induction change. The consequence of this is that the specimen induction approaches an equilibrium condition. Unfortunately, the complexity of the hysteretic state does not allow the precise form of this change to be predicted, as the 'localised' equilibria or metastable states are history dependent. At present no adequate quantitative description of the irreversible process is available. It is likely that a successful description will need to incorporate the spectrum of hysteretic processes present in inhomogeneous media.

8   Ideas for future work

The duration of this research has not allowed examination of several physical aspects relevant to this work. It is hoped that the following brief list of technical points may prove useful for others considering investigation in this subject area.

1.   No attempt has been made in this work to account for the large differences in induction changes caused by the stresses of opposite sense. The reversal in the relative magnitudes of magnetization change caused by each sense on different parts of the hysteresis major loop points needs examination. Whilst a hypothesis central to much of the work contained here has been the separation of stress-induced induction changes into reversible and irreversible components, the reversal in the effects of tension and compression at various points around a major loop may suggest that at the very least an interaction may exist between the two components. Alternatively, in the future, a mechanism for stress-induced induction change may be proposed which unifies these processes. An inspection of the effects of the two stress senses on specimen dislocation density could be central to this work.

2.   Domain imaging under stress, with carefully controlled field histories could serve to clarify some of the conclusions drawn from this work. As it has been shown that similar performance is demonstrated by a range of specimens, the difficulties associated with an examination of the fine martensitic structure of HY80 may not be necessary, although some work on structural steels has been done (Beale, Jokubovics,

Hetherington, Scruby and Lewis, 1992). Amorphous or grain-oriented materials may prove to be useful for study.

3.   A close examination of the pinning energies of the specimens is required. In particular, the temperature dependence of the coercive field, which is used to analyse the pinning energies of other, quite different materials in the works of Gaunt (1976, 1984, 1987) needs closer examination. For example, it has not been possible to interpret the measured temperature dependence of the coercive field for HY80 in terms of known formulae from the limited data given here.

4.   The presence of demagnetizing fields acting on some specimens of this study has not allowed a detailed quantitative analysis of the magnitudes stress-induced induction changes. Furthermore, the Jiles-Atherton model, would suggest that if the elastic energy were sufficient, anhysteretic conditions should be achieved by specimens subjected to stress. There has been some indication in the results contained here that this may not be the case. This aspect needs closer examination.

9   References

Astié B., J. Degauque, J.L. Porteseil and R. Vergne, "Influence of the dislocation structures on the magnetic and magnetomechanical properties of high-purity iron", *IEEE Trans. Magn.* Mag-17 (1981) 2929.

Atherton D.L. and D.C. Jiles, "Effects of stress on the magnetization of steel", *IEEE Trans Magn.* MAG-19 (1983) 2021.

Atherton D.L. and J.A Szupunar, "Effect of stress on magnetization and magnetostriction in pipeline steel", *IEEE Trans. Magn.* MAG-22 (1986) 514.

Atherton D.L., T.S. Rao and M. Schönbächler, "Magnetization changes induced by stress under constant applied field in 2% Mn pipeline steel", *IEEE Trans. Magn.* MAG-24 (1988) 2029.

Atherton D.L., T.S. Rao, V. De Sa, and M. Schönbächler, "Thermodynamic correlation tests between magnetostrictive and magnetomechanical effects in 2% pipeline steel", *IEEE Trans. Magn.* MAG-24 (1988) 2177.

Atherton D.L., T.S. Rao and M. Schönbächler, "Effect of applied stress on the reversible and irreversible differential permeabilities in 2% Mn pipeline steel", *IEEE Trans. Magn.* MAG-24 (1988) 2033.

Atherton D.L. and V. Ton, "The effects of stress on a ferromagnet on a minor hysteresis loop", *IEEE Trans. Magn.* MAG-26 (1990) 1153.

Atherton D.L. and V. Ton, "Effect of order of stress and field application on changes in anhysteretic magnetization", *IEEE Trans. Magn.* MAG-26 (1990) 1157.

Beale A.D., J.P. Jakubovics, M.G. Hetherington, C.B. Scruby, B.A. Lewis and K.J. Davies, "TEM studies of domains and micromagnetic processes in structural steels", *J. Magn. Mat.* 104-107 (1992) 365.

Becker R. and W. Doring, Ferromagnetismus (Springer, Berlin 1939).

Birss R.R., "Magnetomechanical effects in the Rayleigh region", *IEEE Trans. Magn.* MAG-7 (1971) 113.

Birss R.R., C.A. Faunce and E.D. Isaac, " Magnetomechanical effects in iron and iron-carbon alloys" *J. Phys. D*, 4 (1971) 1040.

Bozorth R.M. Ferromagnetism (Van Nostrand, 1951).

Bozorth R.M. and H.J. Williams "Effects of small stresses on magnetic properties", *Rev. Mod. Phys.* 17 (1945) 72.

Brown W.F., "Irreversible magnetic effects of stress", Phys. Rev. 75 (1949) 147.

Brugel L. and G. Rimet, "Interprétation des effets irréversibles descontraintes au moyene d'un modele d'hystérésis dans l'espace", *J. Phys. Rad.* 27 (1966) 589.

Brugel L. and G. Rimet, "Effets les tractions sur l'aimantation de quelques aciers", *C.R. Acad. Sci. (Paris)*, 261 (1965) 5342.

Callen H.B. and N. Goldberg,"Magnetostriction of polycrystalline aggregates", *J. Appl. Phys.*, 36 (1965) 976.

Callen E. and H.B.Callen, "Static magnetoelastic coupling in cubic crystals", *Phys.Rev.B,129* (1963) 578; Magnetostriction, forced magnetostriction, and anomalous thermal expansion in ferromagnets", *Phys.Rev.A,139* (1965) 455.

Chen C.-W., Magnetism and Metallurgy of Soft Magnetic Materials, (Dover Publications, New York, 1986).

Corner W.D. and J.J. Mason, "The effect of stress on the domain structure of Goss-textured silicon iron", *Brit. J. Appl. Phys.* 15 (1964) 709.

Craik D.J. and M.J. Wood, "Magnetization changes induced by stress in a constant applied field", *J. Phys. D,* 3 (1970) 1009.

Cullity B.D., Introduction to Magnetic Materials (Addison-Wesley, Reading, MA, USA, 1972).

Dijkstra L.J. and U.M Martius, "Domain patterns in silicon iron under stress", *Rev. Mod. Phys.* 25(1) (1953) 146.

Eadie G.C., "The effects of stress and temperature on the magnetostriction of commercial 3.25% silicon-iron grain-oriented electrotechnical steel strip", *J. Magn. Magn.* Mat. 26 (1982) 43.

Ewing J.A., "Magnetic induction in iron and other metals", The Electrician Press (1891).

Faunce C.A., Ph.D. Thesis, University of Salford (1970).

Garshelis I.J., "Force transducers based on the stress dependence of coercive force", *J.Appl.Phys.* 73 (1993) 5629.

Gaunt P., "Magnetic viscosity in ferromagnets. I. Phenomenological theory", *Phil. Mag.* 34(5) (1976) 775.

Gaunt P., "Scaling theory applied to strong and weak pinning in ferromagnets", *Phil. Mag. B*, 50 (1984) L45-L48.

Gaunt P., "Magnetic coercivity", *Can. J. Phys.*, 65 (1987) 1194.

Gerlach Von W., "Die abhängigkeit der ferromagnetischen eigenschaften von der temperatur als grundlage für metall-physikalische forschungen", Metallforshung 2 (1947) 275.

Globus A. and P. Duplex, "Initial susceptibility and topography of domain walls in polycrystalline materials", *IEEE Trans. Magn.* MAG-2 (1966) 441.

Globus A. and P. Duplex, "Initial susceptibility of ferrimagnetic materials and topography of domain walls", *Phys. Stat. Sol.*(a) 31 (1969) 765.

Globus A. and P. Duplex, " Size of Bloch walls and parameters of the magnetic susceptibility in ferrimagnetic spinels and garnets", *Phys. Stat. Sol.* (a) 3 (1970) 53.

Jagadish C., L. Clapham and D.L. Atherton, "Influence of uniaxial stress on power spectrum and pulse height distribution of surface Barkhausen noise in pipeline steel", *IEEE Trans. Magn.* MAG-26 (1990) 1160.

Jiles D.C., Introduction to magnetism and magnetic materials (Chapman and Hall, London 1991).

Jiles D.C., "Integrated on-line instrumentation for simultaneous automated measurement of magnetic field, induction, Barkhausen effect, magnetoacoustic emission and magnetostriction", *J. Appl. Phys.* 63 (1988) 3946.

Jiles D.C., "Magnetic properties and microstructure of AISI 1000 series carbon steels, *J. Phys. D*, 21 (1988) 1186.

Jiles D.C., "The effect of compressive plastic deformation on the magnetic properties of AISI 4130 steels with various microstructures", *J. Phys. D*, 21 (1988) 1196.

Jiles D.C., "Variation of the magnetic properties of AISI 4140 steels with plastic strain", *Phys. Stat. Sol. A*, 108(1) (1988) 417.

Jiles D.C., "The effect of stress on magnetic Barkhausen activity in ferromagnetic steels", *IEEE Trans. Magn.* MAG-25 (1989) 3455.

Jiles D.C. and D.L. Atherton, "Ferromagnetic hysteresis", *IEEE Trans. Magn.* MAG-19 (1983) 2183.

Jiles D.C and D.L. Atherton, "Theory of the magnetization process in ferromagnets and its application to the magnetomechanical effect", *J. Phys. D*, 17 (1984) 1265.

Jiles D.C. and D.L Atherton, "Theory of ferromagnetic hysteresis", *J. Appl. Phys.*, 55 (1984) 2115.

Jiles D.C. and D.L Atherton, "Theory of ferromagnetic hysteresis", *J. Magn. Magn. Mat.*, 61 (1986) 48.

Jiles D.C., J.B. Thoelke and M.K. Devine, "Numerical determination of hysteresis parameters for the modeling of magnetic properties using the theory of ferromagnetic hysteresis", *IEEE Trans. Magn.*, MAG-28 (1992) 27.

Joule J.P., "On the effects of magnetism upon iron and steel bars", Sturgeon's annals of electricity, (1842) 219.

Kaminski D.A., D.C. Jiles, S.B.Biner and M.J.Sablik, "Angular dependence of the magnetic properties of polycrystalline iron under the action of uniaxial stress", *J. Magn. Magn. Mat.* 104-107 (1992) 382.

Kashiwaya K., "Magnetoelastic effect of 3.25% Si-Fe single srystal under low magnetic field", *Jpn. J. Appl. Phys.* 31 (1992) 237.

Kittel C., "Theory of long period magnetic relaxation", *Phys. Rev.* 69 (1946) 640.

Kittel C., "Physical Theory of ferromagnetic domains", *Rev. Mod. Phys.*, 21 (1949) 541.

Kondorsky E., "On the theory of magnetization and hysteresis curves of polycrystalline ferromagnetics", *J. Phys. (USSR)*, vol 6, Nov. 1941, pp 93-110.

Langman R., "Measurements of the mechanical stress in mild steel by means of rotation of magnetic field strength-part 3: practical applications", NDT Int. (April 1983) 59.

Langman R., "Magnetic properties of mild steel under conditions of biaxial stress", *IEEE Trans. Magn.* MAG-26 (1990) 1246.

Lliboutry L. Ann. Phys. (France), 6 (1951) 731.

Moses A.J., "Effects of applied stress on the magnetic properties of high permeability silicon-iron", *IEEE Trans. Magn.* MAG-15 (1979) 1575.

Néel L., "Basis of a new general theory of coercive field", Ann. Univ. Grenoble, vol. 22, (1946) 299.

Ng D. and P. Gaunt, "Domain wall pinning transition in iron-rich FeCu alloy", *J. Appl. Phys.* 67 (1990) 4598.

Osborn J.A., "Demagnetizing factors of the general ellipsoid", *Phys. Rev* 67 (1945) 351.

Pitman K.C., "The influence of stress on ferromagnetic hysteresis", *IEEE Trans. Magn.* MAG-26 (1990) 1978.

Rancourt D.G., S.Chehab, and G. Lamarche, "Reentrant magnetism, antiferromagnetism and domain wall pinning in nominallly ferromagnetic Fe-Ni Invar", *J. Magn. Magn.* 78 (1989) 129.

Rancourt D.G., "Phenomenology of domain wall pinning in ferromagnets and application to Fe-Ni Invar", *J. Magn. Magn.* 78 (1989) 153.

Rhodes P., "Thermal changes in irreversible magnetization", *Proc. Leeds Phil. and Lit. Soc.* 5 (1949) 116.

Ruuskanen P. and P. Kettunen, "Reversible component ΔBr of the stress-induced change in magnetization as a function of magnetic field strength and stress amplitude", *J. Magn. Magn. Mat.* 98 (1991) 349.

Sablik M.J., "Modeling stress dependence of magnetic properties for NDE of steels", Nondestr. Test. Eval., Vol 5 (1989), pp49-65.

Sablik M.J., H.Kwun, G.L. Burkhardt and D.C. Jiles, "Model for the effect of tensile and compressive stress on ferromagnetic hysteresis", *J. Appl. Phys.*, 61 (1987) 3799.

Sablik M.J. and D.C. Jiles, "A model for hysteresis in magnetostriction", *J. Appl. Phys.* 64 (1988) 5402.

Sablik M.J., H.Kwun, G.L. Burkhardt and D.C. Jiles, "A model for the effect of stress on the low-frequency harmonic content of the magnetic induction in ferromagnetic materials", *J. Appl. Phys.*, 63 (1988) 3930.

Saito A., K-i. Yamamoto and S. Ueda, "Reversible and irreversible magnetization changes of amorphous ribbon due to stress", *J.Magn. Magn. Mat.* 112 (1991) 41.

Schneider C.S. and E.A. Semcken, "Vibration induced magnetization", *J. Appl. Phys.*, 52 (1981) 2425.

Schneider C.S. and J.M. Richardson, "Biaxial magnetoelasticity in steels", *J. App. Phys.* 53 (1982) 8136.

Schneider C.S. and M. Charlesworth, "Magnetoelastic processes in steel", *J. Appl. Phys.* 57 (1985) 4198.

Schneider C. S., P. Y. Cannell and K. T. Watts, "Magnetoelasticity for large stresses" *IEEE Trans. Magn.* MAG-28 (1992) 2626.

Schönbächler M. and D.L Atherton, "Pneumatic stressing mechanism for magnetomechanical studies", *Rev. Sci. Instr.* 59 (1988) 619.

Shirkoohi G.H. and A.J. Moses, "Effects of stress on magnetostrictive properties of low silicon non-oriented electrical steel", *J. Magn. Magn. Mat.* 83 (1990) 177.

Smithells, Metals reference handbook, 5th edition, 1982.

Spano M.L., K.B. Hathaway and H.T. Savage, "Magnetostriction and magnetic anisotropy of field annealed METGLAS 2605 alloys via dc M-H loop measurements under stress", *J. Appl. Phys.*, 53 (1982) 2667.

Squire P.T. and M.R.J. Gibbs, "Fibre-optic dilatometer for measuring magnetostriction in ribbon samples", *J. Phys. E*, 20 (1987) 499.

Squire P.T., S.M. Sheard, C.H. Carter and M.R.J. Gibbs, "Digital M-H plotter for low-coercivity metallic glasses", *J. Phys. E*, 21 (1988) 1167.

Stanbury H.J., "Magnetostriction effects at angles to the rolling direction in grain oriented 3¼% silicon steel", *J. Magn. Magn. Mat.* 26 (1982) 47.

Stanbury H.J., "The dependence of magnetostriction of grain oriented silicon steel on angle to the rolling direction", *Phys. Script.* 39 (1989) 538.

Stoner E.C. and E.P. Wohlfarth, "A mechanism of magnetic hysteresis in heterogeneous alloys", *IEEE Trans. Magn.* MAG-27 (1991) 3475.

Street R. and J.C Woolley, "A study of magnetic viscosity", *Proc. Phys. Soc. A*, 62 (1949) 562.

Tanner B.K., "The magnetic properties of high strength steels", Nondestr. Test. Eval., Vol 5 (1989), pp 9-15.

Tebble R.S. Magnetic Domains, (Methuens, London) (1969) 15.

Tegart W.J.McG., The Electrolytic and Chemical Polishing of Metals in Resarch and Industry (London, Pergamon 1959).

Thompson S.M. and B.K. Tanner, "The magnetic properties of plastically deformed steels", *J. Magn. Magn. Mat.* 83 (1990) 221.

Veksar N.A., A.S. Smirnov, A.Yu. Fadeev, M.M. Shel', V.F. Tokunov, and V.A. Gudyrya, "Study of the magnetoelastic effect in rail steel", Ukrainian Scientific Research Institute of Metals, Khar'kov. Translated from Defektokopiya, No.2, pp69-74 March-April 1975.

Williams H.J., R.M Bozorth and W. Shockley, "Magnetic domain patterns on single crystals of silicon iron", *Phys. Rev.*75(1) (1949) 155.

Willcock S.N.M., B.K. Tanner and P.A. Mundell, "The magnetic properties of seamless steel pipe", *J. Magn. Magn. Mat.*, 66 (1987) 153-157.

Wohlfarth E.P., "The coefficient of magnetic viscosity", *J. Phys. F*, 14   (1984) L155-L159.

Yamada O., "Sur les variations d'aimantation dues a des échauffements ou des refroidissements, dans le domaine de Rayleigh", *C.R. Acad. Sci.* 250 (1960) 4313.

Zijlstra H., Experimental Methods in Magnetism II (North Holland, Amsterdam. 1967).

10 Appendices

10.1 *A: HY80 metallurgy*

The general magnetic characteristics of steels are largely dictated by their iron-carbon ratio, (Bozorth 1951). The other alloying elements contribute to a dilution of the iron moment, so enhancing the reduction in the saturation magnetization for the whole volume of material. Through their function as domain wall 'pinning' sites caused by the lattice strain at a local level, they also contribute towards an increase in the material coercivity, although this parameter may be dominated by other factors, for example the degree of overall strain resulting from the quench or cold-working processes. For completeness, it is worth considering the metallurgical motives for the presence of the various constituents present in HY80. Manganese is always used in steel manufacture as it combines with sulphur to inhibit the formation of FeS_2 which forms at grain boundaries and embrittles the final product. Silicon prevents the formation of 'blow-holes' by combining with excess oxygen to form silicates which rise to the surface of the molten material to form slag. Typically, in a low alloy steel other constituents would be added to act as substitutional solutes, thereby increasing the strength without causing embrittlement. However, in HY80, the strength of the quenched and tempered product is largely dependent on the carbon content. It seems that the additions are required for the more subtle effects they have during the heat treatment process. The allowable tolerances on the cooling rate during quench are increased by the presence of nickel and chromium which delay the onset of equilibrium phases. This ensures homogeneity of thick sections where the interior of the product cools more slowly. Such steels suffer from an effect called

'temper-brittleness' whereby slow cooling through 250-450°c, or post-processing elevation to these temperatures can embrittle the product as chromium carbides precipitate at grain boundaries. Molybdenum is added to negate this effect, forming its own carbide which is small and stable. It also serves to delay the onset of equilibrium phases. Vanadium is often associated with carbide formation, which evenly distributes itself so enhancing grain refinement. Its presence in some HY80 designations is possibly due to its rôle as a powerful de-oxidizer. Copper acts as a corrosion inhibitor and improves the adhesion of paint films. It should be noted though, that small amounts of copper and vanadium revealed during the SEDS were within the claimed tolerances for the process. Only MIL-S-16216 claims the presence of both copper and vanadium.

10.2   B: Induction measurements by the ballistic technique

The induction measurements made in this study are by the 'ballistic' technique. By this method, absolute induction values are not measured at fixed fields. Rather, the absolute induction is calculated by measurement of the induction change, measured from a demagnetized condition. The system used in this study is a derivative of one developed by Squire, Sheard, Carter and Gibbs (1988). Two search coils of closely matching numbers of turns (around 10,000) are mounted within the solenoid. The voltages generated by each in the absence of a specimen are carefully counterbalanced (by potential division of the larger) so that the field-induced voltage term does not need to be corrected for in analysis of the specimen induction. Strictly then, it is the magnetic polarization '$\mu_0 M$' that is being measured directly in much of the work in this thesis, although occasionally, as in the case of the biaxial specimen in which the field term cannot be subtracted, magnetic induction is directly measured. For the sake of consistency throughout the thesis, the specimen magnetism has invariably been expressed as induction in Tesla.

As stated in the main text, a departure from the original design (of Squire and co-workers) in this system concerns the method of data acquisition. In their original set up, the above workers used a software control method which acquired each field and induction data point and plotted them 'real-time' at the controlling computer V.D.U. The integrator was reset at the end of each data point acquisition sequence. Due to the necessity of occasionally acquiring data at a faster rate, this technique has not been used, with field (or stress) data acquired with the data station operating in

fast-acquisition mode. Visual observation of the (drift-corrected) data is then carried out at the end of each experimental stage. Absolute induction values are calculated based on a knowledge of the specimen cross-sectional area and the number of search coil turns. As a relative reference, the induction of nickel, a material recognised as a standard, has been examined in this thesis. The documented approach to a saturation value near 0.5 to 0.6 Tesla suggests an absolute accuracy of measurement to within 10% for these shaped specimens. All induction values given in this study are calculated, not measured with respect to a relative standard.

10.3   C. Rayleigh's law

In 1887 Rayleigh described the shape of ferromagnetic initial magnetization curves in terms of linear, (reversible) and parabolic (irreversible) terms:

$$M = \chi_0 H + \frac{1}{2}RH^2 \qquad (1)$$

where χ_0 is the initial susceptibility and R is the Rayleigh constant. Small hysteresis loops as shown below (figure 10.1) could then be described as a combination of such curves with,

$$M + M_1 = \chi_0(H + H_1) + \frac{1}{2}R(H + H_1)^2 \qquad (2)$$

and

$$M - M_1 = \chi_0(H - H_1) - \frac{1}{2}R(H - H_1)^2 \qquad (3)$$

describing the upward and downward portions of the shown loop. For a loop contained within the limits M_1 and H_1,
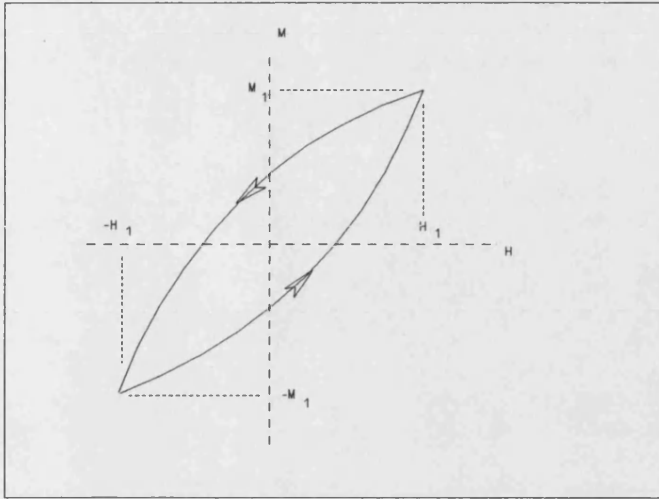
$$M_1 = \chi_0 H_1 + RH_1^2 \qquad (4)$$

Figure 10.1 A Rayleigh loop.

In Brown's analogy, pressure on domain walls supplied by either field or stress is equivalent to magnetizing force.

211